INFLUENCE OF LOW-FREQUENCY ATMOSPHERIC TELECONNECTIONS ON ARCTIC BLOCKING PATTERNS

by

HAYLIE NICOLE MIKULAK

(Under the Direction of Thomas L. Mote)

ABSTRACT

Atmospheric blocking is a large-scale pattern of nearly stationary atmospheric pressure and geopotential height. Blocking patterns play a major role in the transportation of moisture and heat from the mid-latitudes to the high latitudes. Low-frequency atmospheric teleconnections, including the Arctic Oscillation (AO) and the North Atlantic Oscillation (NAO), influence blocking patterns. Two methods of blocking identification are utilized to develop a climatology of blocking across the Arctic for 1980–2017. Exploratory data and statistical analyses quantify the relationship between teleconnection phases and blocking frequency during the four seasons on annual, seasonal and monthly time scales. Results show distinct differences in blocking frequency based on the method, but no significant trends in blocking were identified by season or quadrant, contrary to previous studies. Similar to previous studies, increased blocking frequency is related to the negative phases of both the AO and NAO.

INDEX WORDS: Blocking Patterns, Atmospheric Teleconnections, Arctic

INFLUENCE OF LOW-FREQUENCY ATMOSPHERIC TELECONNECTIONS ON ARCTIC BLOCKING PATTERNS

by

HAYLIE NICOLE MIKULAK

B.S., University of Nebraska-Lincoln, 2017

A Thesis Submitted to the Graduate Faculty of The University of Georgia in Partial Fulfillment of the Requirements for the Degree

MASTER OF SCIENCE

ATHENS, GEORGIA

2019

INFLUENCE OF LOW-FREQUENCY TELECONNECTIONS ON ARCTIC BLOCKING PATTERNS

by

HAYLIE NICOLE MIKULAK

Major Professor:	Thomas L. Mote
Committee:	Andrew Grundstein Gina Henderson

Electronic Version Approved:

Ron Walcott
Interim Dean of the Graduate School
The University of Georgia
December 2019

ACKNOWLEDGEMENTS

This project is partially supported by SERDP Project RC18-1658 subaward from the U.S. Navy to the University of Georgia.

First, I would like to take a moment to thank my advisor, Dr. Thomas Mote, for his guidance and insight in assisting me in my thesis work and my graduate school experience. I would also like to acknowledge my committee members, Drs. Andrew Grundstein and Gina Henderson, for their support and feedback allowing for completion of this project. I would also like to thank Dr. Lynne Seymour for her assistance on some of the statistical analyses included in this thesis.

Additionally, I am eternally grateful to the Department of Geography staff, faculty, and students for providing me with immense support and assistance to allow me to continue to grow in my academic career as well as personal life. I especially would like to thank the members of the Climate Research Laboratory for their emotional support and guidance.

Finally, last but certainly not least I would like to thank my family and friends for their abundant amount of love and support. Thank you for always believing in me even when I did not believe in myself, I do not know what I would do without you.

TABLE OF CONTENTS

Page

LIST OF TABLES

Page

LIST OF FIGURES

Page

CHAPTER 1

INTRODUCTION AND LITERATURE REVIEW

1.1 Atmospheric Blocking Overview

Blocking patterns are defined as quasi-stationary, large-scale circulation patterns that can persist for weeks (Rex 1950; Dole and Gordon 1983; Diao et al. 2006). Blocks normally occur when a low-vorticity subtropical airmass advects poleward, leading to the development of an anticyclonic circulation (Rex 1950). Rex (1950) defined the presence of a blocking pattern when a double-jet, also called a split jet, is detectable over more than 45° in longitude and persisting a minimum of 10 days. However, other studies, including Trieidl et al. (1981) and Geb (1966), stated this was too restrictive, defining a blocking event duration as a minimum of five days or three days, respectively. Even today, there is no concrete definition for the minimum duration to be considered a blocking event (Woolings et al. 2018).

Blocking patterns are often associated with a temperature dipole with a cold anomaly at the midlatitudes and a warm anomaly at the poles (Luo et al. 2016a). In regions where blocking typically occurs, the warmth in the winter and chill in the summer are provided by the prevailing oceanic westerly flow (Woolings et al. 2018). However, when the winds are disrupted due to blocking, it results in a seasonal extreme of warming in the summer and cooling in the winter (Woolings et al. 2018). Similarly, reduced cloud cover in the region of the blocking anticyclone acts to warm the surface in the summer and cool in the winter (Woolings et al. 2018). Atmospheric blocking frequently occurs over the Arctic as a result of persisting areas of high pressure that result in higher-than-average surface temperatures west of the high-pressure center

(McLeod and Mote 2016). The onset of a block is associated with rapid poleward movement of subtropical air, which develops into a large-scale ridge within one to three days (Woolings et al. 2018). Pfahl et al. (2015) found that 30–45% of the air parcels located in the low potential vorticity (PV) anomaly of blocking patterns experience heating during the last three days of the event. This suggests the importance of latent heat release in building and maintaining a block (Pfahl et al. 2015). Additionally, there is a correlation between the deepening rate of the upstream cyclone and the intensity of the block (Lupo and Smith 1995).

Blocking events in oceanic regions and during the cold season are stronger than warm season or continental blocking events (Lupo and Smith 1995; Cheung et al. 2012; Lupo et al. 2019). In the Northern Hemisphere, the most persistent and strongest blocks occurred during the cold season in the Atlantic region (Wiedenmann et al. 2002; Cheung et al. 2013a; Cheung et al. 2013b). Oceanic blocking patterns are also more active in the cold seasons when the ocean is warmer than the continent, while continental blocking is more active in the warm seasons when the continent is warmer than the ocean (Cheung et al. 2013a; Cheung et al. 2013b). Blocking events in the western Atlantic (0–20°E, 40–50°N) are initially formed by the transport of PV by high- and low-frequency transient flows while the transport of low-frequency PV works to maintain the block once it has formed (Drouard and Woolings 2018). Blocking events located in the eastern Atlantic (35–55°E, 45–55°N) are developed and maintained by the low-frequency transient flow and are often preceded by a large-scale low-frequency Rossby wave train (Drouard and Woolings 2018). Blocks located in the central Atlantic (20–40°E, 50–60°N) are normally located at the end of storm tracks and appear to be influenced by a mix of the dynamical factors associated with blocking in the western and eastern areas (Drouard and Woolings 2018).

Several types of atmospheric blocking patterns exist, including the Omega-block and the split-flow/dipole block (Figure 1.1) (Pelly and Hoskins 2002; Barriopedro et al. 2006; Woolings et al. 2018). The split-flow/dipole pattern consists of a stationary ridge in a large amplitude Rossby wave. These types of blocks advect low PV from the subtropics to the poles resulting in the area becoming anomalously anticyclonic relative to the surroundings (Hoskins et al. 1985). Omega blocks are named as such due to geopotential height contours that appear similar to the Greek letter omega, and are similar to the stationary ridge, but with a larger amplitude (Sumner 1954).

Other blocking patterns are associated with Rossby wave breaking in which an extended ridge is folded over in either a cyclonic or anticyclonic sense (Gabriel and Peters 2008; Masato et al. 2012). These types of blocking events are typically associated with a reversal of the meridional PV gradient. As a result, PV anomalies are able to form a "dipole block" or a "Rex Block" with an anticyclonic PV anomaly poleward of the cyclonic anomaly (Berggren et al. 1949; Rex 1950; Woolings et al. 2018).

Numerous methodological approaches are used to identify atmospheric blocking patterns; some are based on meridional height gradients used to calculate zonal flow indices (Lejenäs and Øakland 1983; Tibaldi and Molteni 1990; Tibaldi et al. 1997; Trigo et al. 2004). Other approaches detect blocking events using normalized indices that are based on daily geopotential height projections over mean blocking patterns, which compares the blocked conditions to the climatological mean (Liu 1994; Renwick and Wallace 1996) or positive height anomalies at the mid-troposphere that persist for several days (Charney et al. 1981; Dole and Gordon 1983). Specifically, the Greenland Blocking Index (GBI) is a measure used to identify the occurrence and intensity of blocking highs over Greenland (Fang 2004; Hanna et al. 2013; Hanna et al.

2014; Hanna et al. 2015; Hanna et al. 2016; Woolings et al. 2010). The GBI is typically defined as the mean 500hPa geopotential height for the region of 60–80°N and 20–80°W (Fang 2004; Hanna et al. 2013; Hanna et al. 2014; Hanna et al. 2015; Hanna et al. 2016; Woolings et al. 2010). Additionally, some studies like Pelly and Hoskins (2003, hereafter PH03) use the meridional potential temperature gradient on a constant PV surface to calculate blocking. Schwierz et al. (2004) use another dynamical approach using negative anomalies of vertically integrated PV with in the 500–150hPa layer. Woolings et al. (2018) discuss the variety of blocking pattern indices; however, they state no single index is able to effectively describe all stages of the blocking pattern life cycle.

Atmospheric blocking patterns form and persist across the entire Arctic (e.g., Tibaldi and Molteni 1990, hereafter TM90; PH03). The TM90 and PH03 indices capture blocking slightly differently with the PH03 method identifying more blocking events compared to the TM90 method (Figure 1.2). Both blocking identification methods identify two peaks of annual blocking frequency, one located between 30°E and 45°W longitude and one located between 180° and 90°W longitude (Figure 1.2). The Arctic can be divided into four main regions for blocking based on areas where the highest blocking activity occurs, the North Pacific, Greenland, Europe, and Ural-Siberian (Shukla and Mo 1983; Kim and Ha 2014). The North Pacific and European/Atlantic regions coincide with the downstream regions of their respective storm track cores (Croci-Maspoli et al. 2007; Kim and Ha 2014).

1.2 Motivation and Research Objectives

Atmospheric blocking patterns develop along the Pacific and Atlantic jet streams and significantly influence the weather conditions across Europe, including cold spells in winter and heat waves in summer (Trigo et al. 2004; Sillmann and Croci-Maspoli 2009; Buehler et al. 2011;

Sillmann et al. 2011). Ural-Siberian blocking patterns promote a cold East Asian winter monsoon (Cheung et al. 2012). A block positioned upstream of Siberia during the winter is associated with enhanced northerly cold air advection that increases mass convergence in the upper troposphere, which intensifies the surface Siberian high and leads to a cold air outbreak in East Asia (Ding 1990; Cheung et al. 2012).

The key role that blocking patterns play in the Arctic is the transport of moisture and energy from the midlatitudes to the high latitudes, which in turn influences the weather and climate of the Arctic (Rex 1950; Benedict et al 2004; Barriopedro et al. 2006; Diao et al 2006; Scherrer et al. 2006; Woolings et al. 2008; Luo et al. 2018). Blocking events interrupt the westerlies across the midlatitudes, which steer midlatitude cyclones further poleward, resulting in anomalous weather in the Arctic (Berggren et al. 1949; Diao et al. 2006). Overland et al. (2012) found an increase in blocking since 2007; while the cause of increased blocking is not completely understood, they stated that it may be related to an earlier seasonal snowmelt and Arctic sea ice loss. Previous studies have found that the decline in sea ice has led to an increase in atmospheric blocking frequency for North America and Europe in winter, summer, and fall (Liu et al. 2012; Francis and Vavrus 2012; Tang et al. 2013).

Warm, moist airmasses are advected toward the poles, become cut off from the polar jet stream, and can remain for several weeks (Benedict et al 2004; Barriopedro et al. 2006; Woolings et al. 2008). Greenland blocks, specifically, last roughly six to nine days and develop from a strong retrograded Atlantic ridge and sometimes follow European blocks (Davini et al. 2012a). Rajewicz and Marshall (2014) found that 38–49% of Greenland's summer air temperature and melt extent variability and 13–27% of lower tropospheric background warming can be attributed to circulation anomalies. As Greenland continues to warm, the warm air

expands further raising geopotential heights, which increases high pressure intensity and frequency on average (e.g. Francis and Vavrus 2012; Overland et al. 2012; Hanna et al. 2013; Hanna et al. 2014). Increased Greenland blocking frequency in the fall since 1979 is a possible explanation for enhanced poleward transport of relatively warmer air, reduced sea ice in Baffin Bay, and increasing coastal air temperatures (Ballinger et al. 2018). McLeod and Mote (2015) found a link between extreme Greenland blocking pattern intensity and cyclones that form west of Greenland prior to the peak of the blocking event. Strong winter Greenland blocking events are linked to positive sea surface temperature anomalies, negative sea ice anomalies, and freeze delays that extend into autumn (Hanna et al. 2018a).

Atmospheric blocking has broad implications in regard to increased rates of surface melt and runoff for places like the Greenland Ice Sheet (GrIS) (McLeod and Mote 2016; Välisuo et al. 2018; Hofer et al. 2019). The advection of relatively warm subtropical airmasses as a result of increased blocking are contributing to further acceleration of GrIS surface melt (Fettweis et al. 2013; Hanna et al. 2014; Delhasse et al. 2018; Hofer et al. 2019). Diabatic latent heat release associated with extreme moisture transport may develop and strengthen blocking patterns (Pfahl et al. 2015; Grams and Archambault 2016; O'Reilly et al. 2016; Mattingly et al. 2018). The physical mechanisms associated with moisture transport, such as the formation of low-level clouds and an enhanced water vapor greenhouse effect, influence the melt of the ice sheet as well as sea ice (Luo et al. 2016a; Binder et al. 2017; Mattingly et al. 2018). Atmospheric blocking can also have hydrological impacts including droughts associated with the dry conditions in the anticyclonic region and extreme rainfall for areas adjacent to the block due to changes in storm tracks (Sousa et al. 2017).

While most recent work on blocking in the Arctic has focused on Greenland, this thesis examines the Arctic as a whole. In addition to examining the different regions of the Arctic, all four seasons are assessed due to the lack of scholarship including the transitional seasons of autumn and spring. Furthermore, previous research involving the relationship of low-frequency atmospheric teleconnections and Arctic blocking patterns focuses primarily on areas like Greenland or Ural-Siberia in winter. This thesis strives to provide an overarching understanding of the relationship between phases of North Atlantic Oscillation (NAO) and Arctic Oscillation (AO) have on the Arctic. Specifically, this thesis addresses the following questions:

1. How do different measures of blocking compare at identifying atmospheric blocking frequency?
2. How is the frequency of atmospheric blocking changing across the Arctic during the past four decades?
3. How do varying phases of low-frequency Arctic teleconnection patterns (i.e., NAO and AO) influence the frequency of blocking patterns in the Arctic?
4. How do varying phases of these teleconnections influence the seasonality and location of blocking patterns in the Arctic?

1.3 Background

1.3.1 Arctic Blocking Pattern Climatology

Atmospheric blocks can occur at any time during the year, however Trigo et al. (2004) found that they most typically occur in winter and spring. Atmospheric blocking activity is most frequent over Europe and the eastern Atlantic Ocean in the winter, and eastern Europe and central Asia during the summer (Tyrlis and Hoskins 2008). Diao et al. (2006) identified more blocking events for the Atlantic/Europe region compared to the Pacific region in winter, spring,

and autumn. Blocks identified in the Atlantic/Europe region lasted longer than Pacific region during all seasons (Diao et al. 2006). Figure 1.3 depicts the centers of action for atmospheric blocking over the Atlantic and Pacific regions identified by Kim and Ha (2014). This varies slightly from the findings of PH03, which determined Euro-Atlantic blocking activity is high in the summer before peaking in autumn, followed by significantly lower activity in winter and spring. In the Pacific, autumn is the least active season while blocking frequency remains approximately constant in the winter and spring before peaking in the summer over the central Pacific and decreasing along the west coast of North America (PH03). Kim and Ha (2014) and PH03 findings differ slightly likely due to the differences in blocking identification. Kim and Ha (2014) used a hybrid index combining the Dole and Gordon (1983) index with the TM90 index; an approach that combines the Dole and Gordon (1983) and the TM90 is more comprehensive due to its ability to minimize misidentification of "quasi-stationary" ridges as blocking highs. On the other hand, PH03 use a dynamical index based on the relationship between potential vorticity and potential temperature. PH03, found that during the summer, Pacific blocking shifts into the western central Pacific due to a change in the stationary wave pattern; however, a small sample size of only five years was used, so due to the short time period the influence of teleconnections like the El Niño Southern Oscillation could not be examined. The dynamical approach of PH03 provides a more complete picture of Arctic blocking than the TM90 method especially for Omega blocks in the Pacific (PH03). The PV approach shows synoptic scale features associated with the block more clearly than the geopotential height fields (PH03).

Models have consistently struggled to present and capture blocking events (Scaife et al. 2011; Masato et al. 2013; Davini and D'Andrea 2016; Pithan et al. 2016; Hanna et al. 2018b; Woolings et al. 2018). Atlantic-European blocking frequency is underestimated 30–50% of the

time in winter and 10–30% of the time in summer (Woolings et al. 2018). When comparing the Institute Pierre-Simone Laplace Climate 5 Model with Medium Resolution general circulation model with NCEP/NCAR reanalysis data, winter blocking frequency was underestimated by 11% by the models (Mokhov et al. 2014). There is low confidence in model projections of atmospheric blocking, despite good agreement among models on an overall decline in blocking in the future (Woolings et al. 2018). Hanna et al. (2018b), found that models predict a decrease in atmospheric blocking frequency in the future possibly associated with an increase in NAO. Before research can examine possible future changes in blocking, a better understanding of past and present blocking frequency is necessary.

1.3.2 Arctic Blocking Patterns and Atmospheric Teleconnections

Low-frequency teleconnection patterns like the North Atlantic Oscillation (NAO) and the Arctic Oscillation (AO) influence the circulation patterns in the Arctic. NAO and AO are closely associated, so much so that Thompson and Wallace (1998) consider the NAO to be a "regional manifestation" of the AO, which further amplifies the importance of how these two patterns influence the Arctic individually as well as together. By examining each teleconnection separately, the relationships between each teleconnection and blocking frequency can be compared in order to see if this "regional manifestation" of the AO holds true or if there are differences in the manner in which AO and NAO influence Arctic blocking frequency. Two aspects of the relationship between low-frequency teleconnection patterns and blocking in the Arctic explored in this thesis are the seasonal and spatial differences, specifically how positive, negative, and neutral phases of each teleconnection is associated with the frequency of blocking events across the Arctic throughout the year. Previous studies focused on one location in the Arctic and specific seasons, while this project examines the Arctic as a whole across the entire

year to gain a better understanding of the relationship between teleconnection phase and blocking pattern frequency.

1.3.2.1 Arctic Oscillation

The AO is a meridional seesaw pattern in sea level pressure between the midlatitudes and the Arctic, which results in changes in weather conditions across the globe (Higgins et al 2000; Higgins et al. 2002). During the positive phase of the AO, stronger winds, located at the poles, confine colder air to the Arctic, which in turn keeps storm tracks further north leading to warmer and wetter conditions over Europe. During the negative phase, the opposite occurs (Figure 1.4). A positive phase AO is associated with weakened meridional flow across East Asia, which creates unfavorable conditions for the formation of blocking highs, while the opposite occurs during negative phase AO (Davini et al. 2012b). The relationship between Ural-Siberian blocking and the East Asian Monsoon is stronger when the El Niño Southern Oscillation (ENSO) and the AO are in phase (i.e. when both teleconnections are in either the positive phase or negative phase) (Figure 1.5) (Cheung et al. 2012). Overall, the negative phase of the AO is correlated with increased blocking conditions across the Arctic (Hassanzadeh and Kuang 2015). When AO and the North Pacific Oscillation (NPO) are in phase, Northern Hemisphere blocking is further enhanced resulting in higher frequency of blocking over the Pacific and the northwestern Atlantic (Figure 1.6) (Kim and Ha 2014).

1.3.2.2 North Atlantic Oscillation

The NAO influences the formation, lifespan, and frequency of Arctic blocking, especially during the winter (Shabbar et al. 2000; Ogi et al. 2003; Davini et al. 2012b). This teleconnection pattern is associated with centers of action in Iceland (i.e., Icelandic Low) and the Azores (i.e., Bermuda-Azores High), and the strength of these pressure centers influences the strength of the

westerlies of the Northern Hemisphere (Barnston and Livezey 1987; van den Dool et al. 2000, Chen & van den Dool 2003). The positive phase of the NAO is associated with lower than normal sea-level pressure near Iceland and higher than normal near the Azores, resulting in a stronger and more zonal jet stream, which leads to colder conditions over Greenland and warmer and wetter conditions over Europe; during negative phase, the opposite occurs (Figure 1.7).

During the negative phase of the NAO, 67% more blocking days are observed in the winter. Additionally, the average length of blocking events during the negative phase of NAO is around 11 days, which is almost double the six days during positive NAO (Shabbar et al. 2001). During periods of high Greenland blocking years (> 30 blocking days per winter), the negative NAO signal is strengthened and shifts further west (Davini et al. 2012b). This leads to an increase in the number of observed southward jet displacements (Davini et al. 2012b). The opposite appears to occur during low Greenland blocking years (< 15 blocking days per winter), which is associated with positive NAO, and this southward displacement of the jet no longer exists (Davini et al. 2012b). During the 1980s and the 1990s, the NAO pattern displaced eastward about 30°, during this time Greenland blocking frequency reached a minimum. This suggests a possible link between the eastward shift of the NAO to variability in Greenland blocking frequency (Davini et al. 2012b). Woolings et al. (2010) found a higher frequency of Greenland blocking events with more negative winter NAO events.

Shabbar et al. (2001) demonstrated that NAO alone accounts for approximately 30% of the variation in wintertime North Atlantic blocking events. Decreases in summer NAO are associated with increasing trends in the GBI (Hanna et al. 2015; Hanna et al. 2016), while increases in winter NAO are associated with more variable trends in the GBI (Hanna et al. 2015; Hanna et al. 2016). Ogi et al. (2003) found a correlation between the winter NAO index and the

mean zonal wind, such that during positive NAO winters, a split jet structure is present in the subsequent summer, which is closely related to atmospheric blocking. Meanwhile, Shabbar et al. (2001) and Rimbu and Lohmann (2011) found that negative NAO leads to the formation of atmospheric blocking and extends the lifespan of pre-existing blocks in the North Atlantic. A negative NAO phase sets up a distribution of surface temperature anomalies with a distinct pattern of "warm ocean/cold land," which creates an environment that is favorable for blocks to form and persist. During positive NAO phases, temperature anomalies switch, leading to a "cold ocean/warm land" scenario, which is unfavorable for blocks to remain or even develop over the area (Shabbar et al. 2001; Cheung et al. 2013a; Cheung et al. 2013b; He et al. 2014; He et al. 2018). North Pacific and North Atlantic blocking are most commonly associated with a negative NAO pattern (Kim and Ha 2014). During positive NAO winters, blocking is intensified over Europe, but significantly reduced around Greenland (Sherrer et al. 2006). However, during negative NAO winters, blocking is more frequent over the western North Atlantic and the Davis Strait, but reduced over Europe (Sherrer et al. 2006). Blocking frequency in the North Atlantic is significantly higher (~10 more blocking days per season) during the negative phase of the NAO (Croci-Maspoli et al. 2007).

Due to the NAO's influence on Arctic blocking, NAO in turn effects the atmospheric conditions over the Arctic. Ogi et al. (2003), found that summer Arctic climate is influenced by the NAO pattern of the previous winter; as a result, sea surface temperature and sea ice anomalies over the North Atlantic Ocean and Arctic Ocean remain from summer to winter. Spring snow cover anomalies over western Eurasia and central Asia as well as over eastern Siberia during the summer appear to be significant as well (Ogi et al. 2003; García-Herrera and Barriopedro 2006; Matsumura et al. 2010; Xiaoge et al. 2010). Blocking and the positive phase

of the NAO creates optimal conditions to significantly increase water vapor over the Barents and Kara Seas, which plays a vital role in the warming of the seas and a reduction in sea ice, while sensible and latent heat flux increases play a smaller secondary role (Figure 1.8) (Luo et al. 2016a; Luo et al. 2017). Warming of the Barents and Kara Seas is related to a decrease in sea ice concentration, which has been paired with an increase in Ural blocking duration (Luo et al. 2017; Luo et al. 2018). Winter Ural blocking plays an important role in winter Eurasian cooling; the relationship between blocking and Arctic warming/sea ice concentration decline is important to understand because as the Arctic continues to warm and sea ice decreases in places like the Barents and Kara Seas, blocking could continue to persist and result in more cold anomalies for Eurasia (Luo et al. 2018). Understanding the influences of blocking patterns across the Arctic can help improve knowledge on the impact blocking has on the Arctic cryosphere, including sea ice and snow cover (e.g. Ogi et al. 2003; Luo et al. 2018).

1.3.2.3 Rossby Wave Breaking

Rossby wave breaking (RWB) is a result of large-scale overturning of potential vorticity contours on an isentropic surface and can be measured when the potential vorticity gradient at the tropopause level (two potential vorticity unit surface) reverses (Thorncroft et al. 1993; Peters and Waugh 1996). There are two types of RWB, cyclonic and anticyclonic wave breaking. Cyclonic wave breaking is characterized as a northwest tilted trough and a southeast tilted ridge advected cyclonically, while an anticyclonic RWB pattern is characterized by a southwest tilted trough and a northeast tilted ridge advected anticyclonically (Thorncroft et al. 1993; Peters and Waugh 1996). The onset of a blocking pattern in the Atlantic is associated with a "coherent precursor" Rossby wave train approximately 110° upstream of the block and approximately five days prior to the onset of the event (Altenhoff et al. 2008). Comparatively, in the Pacific, an "in

situ positive" Rossby wave signal is present three days prior to blocking event onset (Altenhoff et al. 2008). During the decay of an atmospheric blocking pattern, Rossby wave patterns are detected downstream of the event in the Atlantic, these waves are more persistent and larger in amplitude in the Pacific (Altenhoff et al. 2008). RWB associated with atmospheric blocking events over Greenland are strongly anticorrelated with the NAO (Woolings et al. 2008). RWB is influenced by teleconnection patterns like the NAO both in regard to seasonality and frequency. During the winter, RWB-transport is strongly influenced by NAO. During positive phase NAO, anticyclonic wave breaking transports more moisture through the Norwegian Sea and cyclonic wave breaking transports less along the west coast of Greenland. During the negative phase of NAO, the opposite occurs (Liu and Barnes 2015). Understanding RWB is vital due to the association between RWB and extreme moisture transport into the Arctic (Masato et al. 2012; Liu and Barnes 2015).

1.4 Summary

Due to the impact of atmospheric blocking patterns on the Arctic climate system, including increased rates of surface ice sheet melt and sea ice loss, a better understanding of blocking in the Arctic is necessary (McLeod and Mote 2016; Luo et al. 2016a; Luo et al. 2017). This thesis examines the Arctic as a whole as blocking is common across the Atlantic and Pacific sectors. Additionally, a climatology of atmospheric blocking frequency for all seasons is completed to address the paucity of research on the transitional seasons. The seasonal and spatial differences in Arctic blocking patterns frequency are also examined. In order for possible future changes in blocking to be accurately captured in climate models, a better understanding of past and present Arctic blocking pattern frequency is critical.

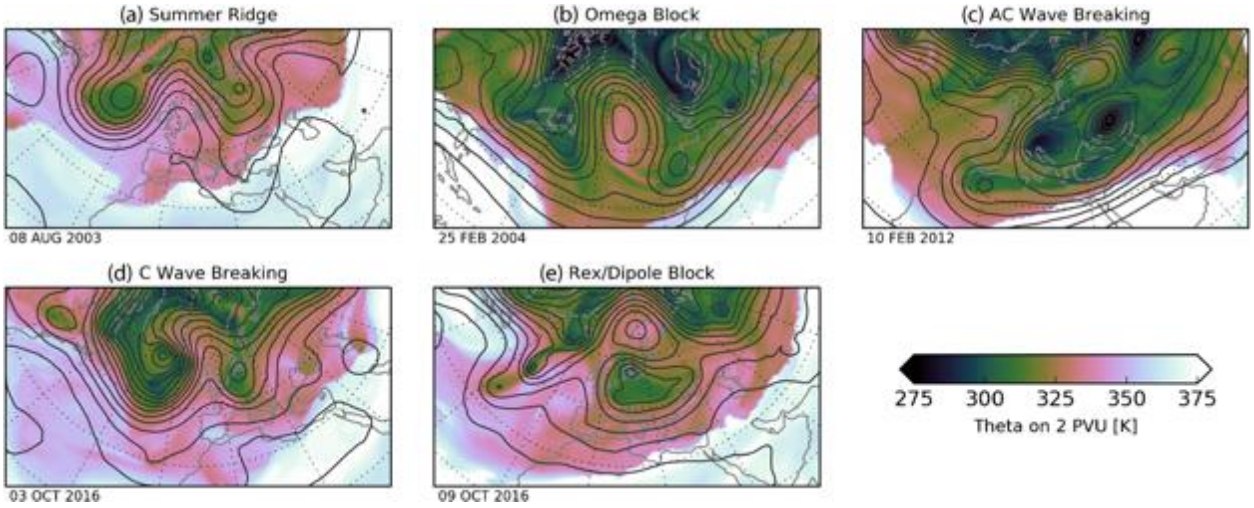

Figure 1.1. Examples of North Atlantic blocking patterns with potential temperature at the dynamical tropopause (shading) and 500hPa geopotential height fields (contours) for the dates indicated (from Woolings et al. 2018).

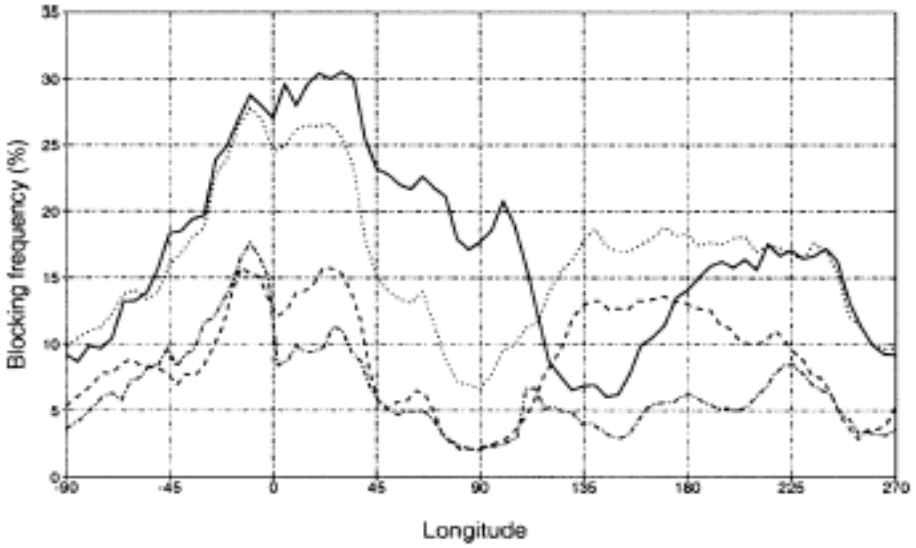

Figure 1.2. Annual mean, local instantaneous blocking frequency with respect to longitude between June 1996 and May 2001 using the PH03 method (solid curve), using the TM90 method (dashed curve), using the PH03 method with a constant blocking latitude (ϕ_0 = 50°N) (dotted curve), and using the TM90 method with a variable blocking latitude (dot-dashed curve) (from Pelly and Hoskins 2003).

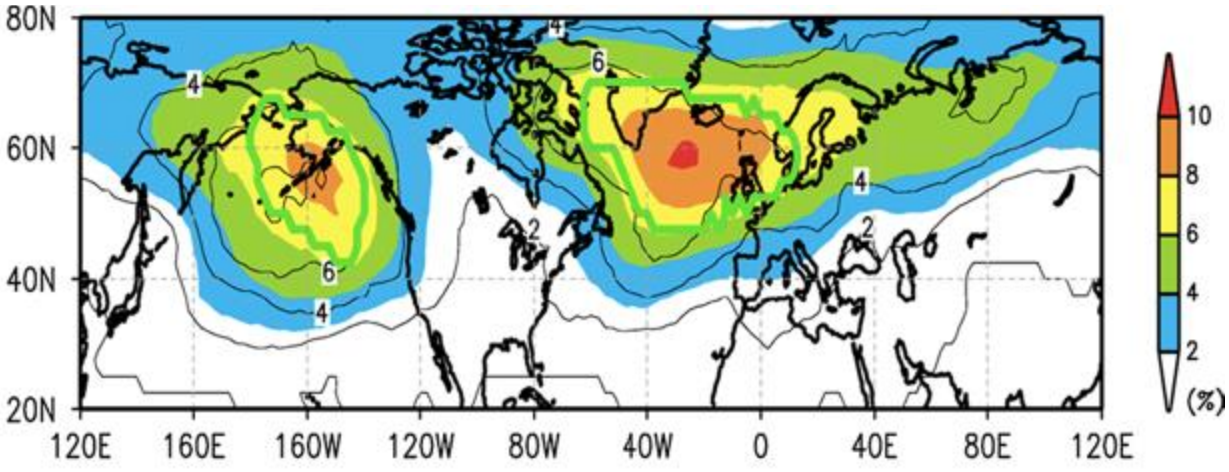

Figure 1.3. DJF climatology (shading) and standard deviation (contour) of Northern Hemisphere blocking frequency using the National Centers for Environmental Prediction reanalysis data from 1948/1949–2011/2012 (from Kim and Ha 2014).

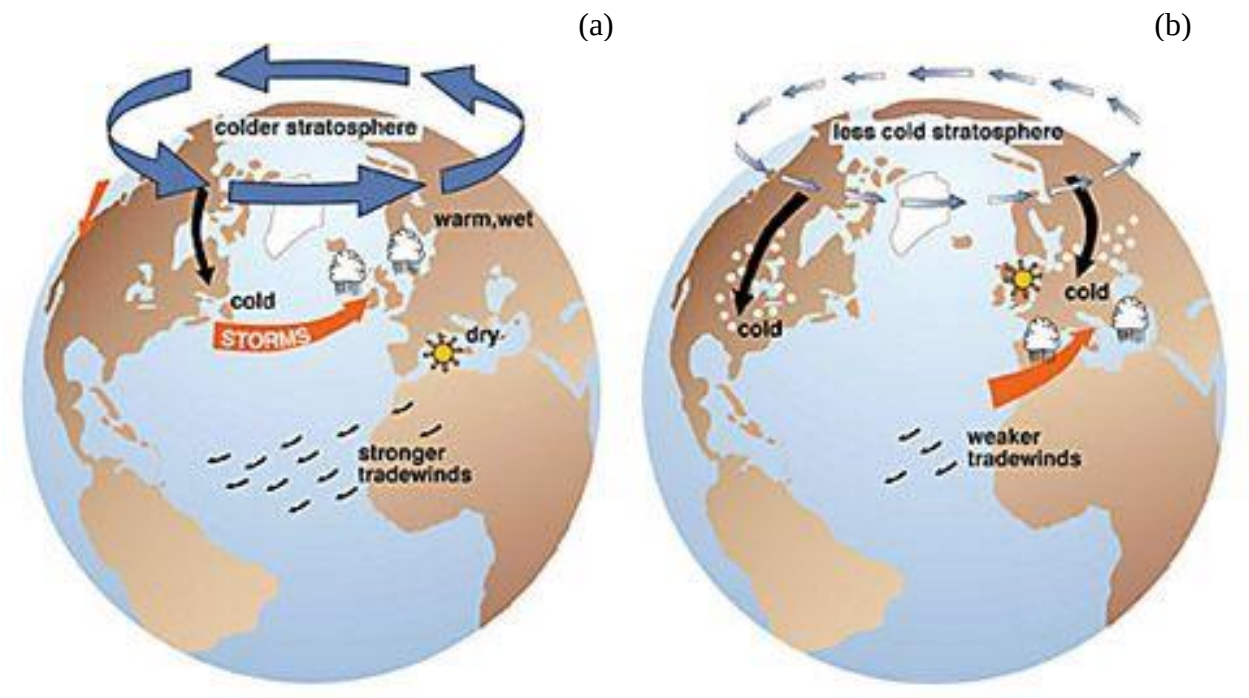

Figure 1.4. Schematic of positive (a) and negative (b) phases of the Arctic Oscillation (from National Snow and Ice Data Center 2012).

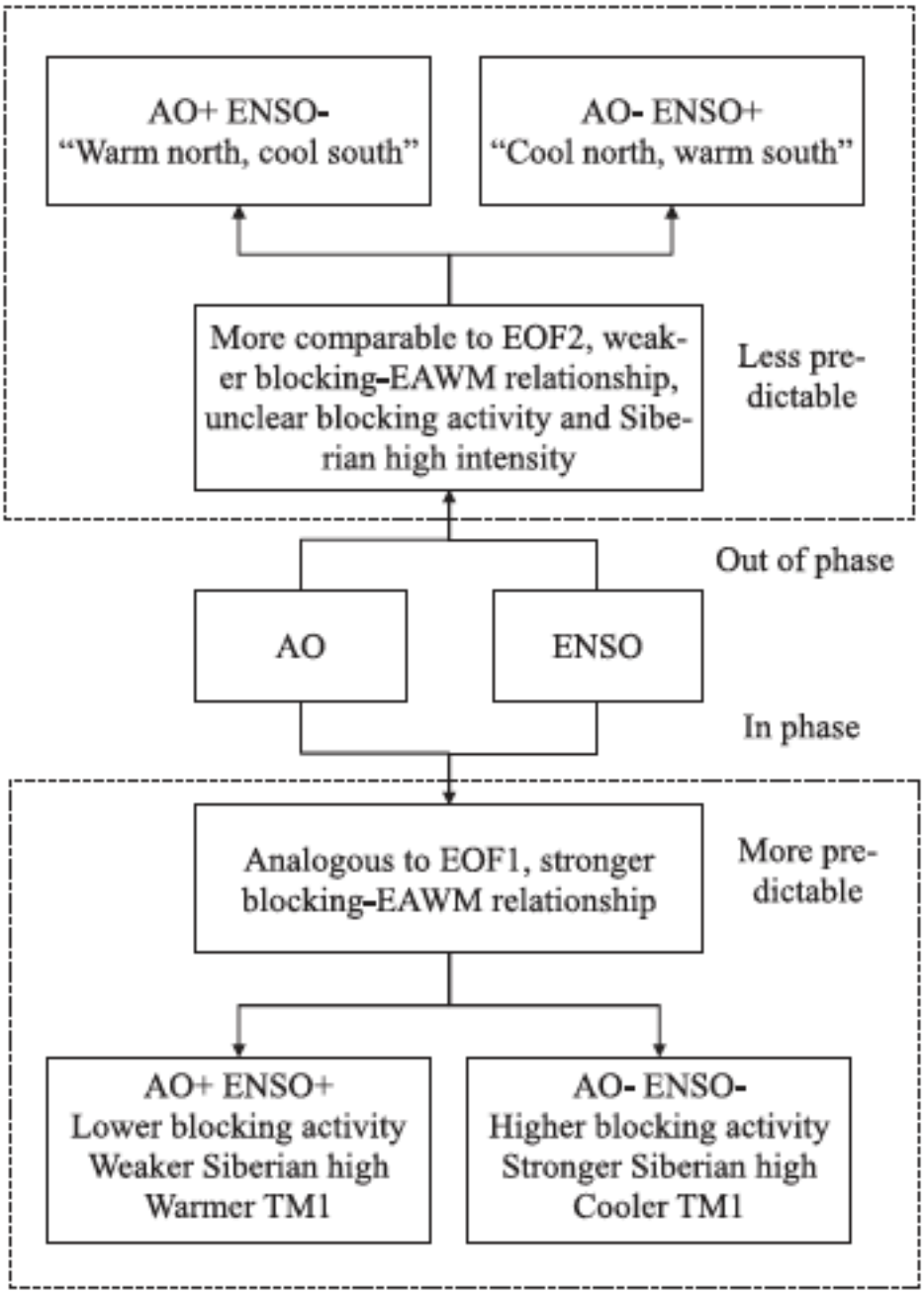

Figure 1.5. Schematic of Ural-Siberian blocking and the East Asian Winter Monsoon with respect to the roles of the AO and the El Niño Southern Oscillation (from Cheung et al. 2012).

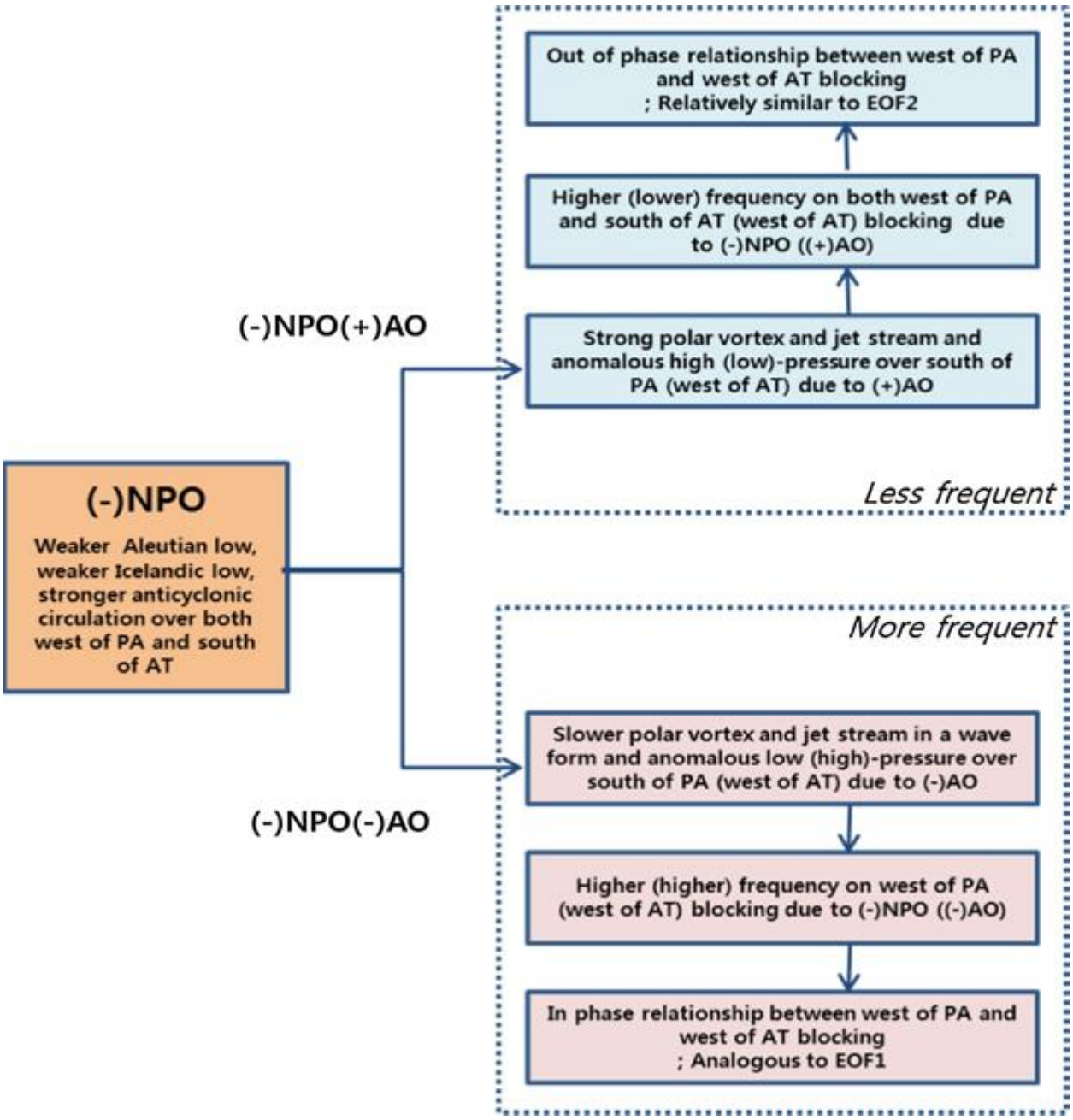

Figure 1.6. Schematic of Pacific and Atlantic blocking frequency with respect to the roles of AO and NPO (from Kim and Ha 2014).

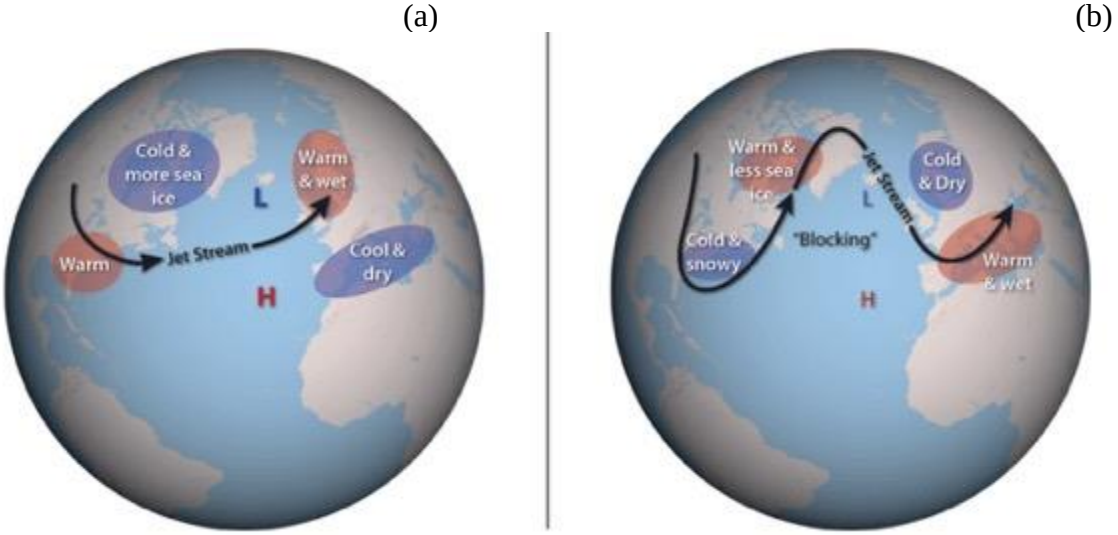

Figure 1.7. Schematic of positive (a) and negative (b) phases of the North Atlantic Oscillation (from Met Office 2018).

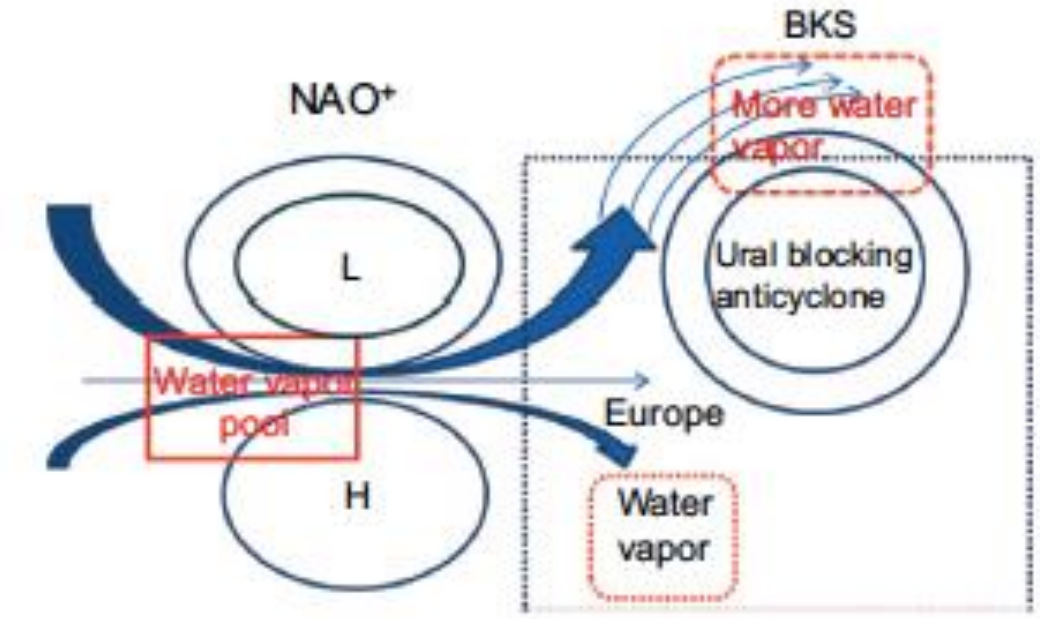

Figure 1.8. Schematic of the enhanced moisture transport from the midlatitude North Atlantic to the Barents and Kara Seas during positive NAO and Ural blocking conditions (from Luo et al. 2017)

CHAPTER 2

DATA AND METHODOLOGY

2.1 Overview

Atmospheric blocking patterns form and persist across the entire Arctic (e.g., TM90; PH03). Many methodological approaches can be used to identify atmospheric blocking patterns; however, no single index is able to effectively describe all stages of the blocking pattern life cycle (Woolings et al. 2018). Additionally, models have consistently struggled to present and capture blocking events (Scaife et al. 2011; Masato et al. 2013; Davini and D'Andrea 2016; Pithan et al. 2016; Hanna et al. 2018b; Woolings et al. 2018). Before scholars can examine possible future changes in blocking, a better understanding of past and present blocking frequency is necessary. This thesis provides a systematic examination of blocking frequency across the Arctic using two different blocking metrics. Unlike similar published work (e.g., Luo et al. 2016a, 2016b), this study examines the Arctic as a whole for all four seasons instead of focusing on only one region during a single season. Furthermore, the relationship between low-frequency teleconnection patterns (i.e. AO and NAO) and blocking frequency in the Arctic, from both seasonal and spatial perspectives, are examined in this thesis. A better understanding of the relationship between low-frequency teleconnections and Arctic blocking frequency is critical due to the impact blocking has on the conditions of the Arctic including sea ice concentration and snow cover (Ogi et al. 2003; García-Herrera and Barriopedro 2006; Matsumura et al. 2010; Xiaoge et al. 2010; Luo et al. 2017) and the Greenland ice sheet surface mass balance (McLeod et al. 2015; McLeod et al. 2016).

2.2 Study Area

The Arctic is divided into four regions similar to the locations discussed in Kim and Ha (2014) based on where atmospheric blocking most frequently occurs: the North Pacific, Greenland, Europe, and Ural-Siberian. The quadrants are divided based on longitude bands, Quadrant I encompasses longitudes from 0° to 90°E; Quadrant II, 90°W to 0°; Quadrant III, 90°W to 180°; and Quadrant IV, 90°E to 180° (Figure 2.1).

2.3 Atmospheric Blocking Climatology

2.3.1 ECMWF Reanalysis (ERA) Interim

The ERA-Interim dataset is used for this study to identify blocking days in the four quadrants of the Arctic. ERA-Interim data are chosen for this study due to the relatively high temporal and spatial resolution and extensive use in earlier Arctic blocking research (e.g. McLeod et al. 2015; McLeod et al. 2016; Luo et al. 2016a; Luo et al. 2016b; Luo et al. 2017; Luo et al. 2018; Valisuo et al. 2018). ERA-Interim has 60 vertical levels (37 pressure levels) with a top level located at 0.1hPa and produces four analyses per day at 00, 06, 12, and 18Z respectively (Dee et al. 2011; https://apps.ecmwf.int/datasets/data/interim-full-daily/). The dataset has a spatial resolution of 0.75° latitude by 0.75° longitude grid beginning in 1979 to the present (Dee et al. 2011). For the purpose of this thesis, blocking events are identified from January 1980 to December 2017. The reanalysis dataset is produced using a "sequential data assimilation scheme" that advances forward in time using 12-hourly analysis cycles. For each cycle, the information from the previous forecast model is combined with available observations to estimate the changing state of the atmosphere and underlying surface, which involves four-dimensional variational analysis of the upper air atmospheric fields (i.e. surface pressure, temperature, wind, humidity) as well as an analysis of near-surface parameters (2m temperature

and humidity) (Dee et al. 2011). A short-range model forecast is initialized by the analyses, so the model can provide the state of the atmosphere estimates for the next cycle (Dee et al. 2011).

Daily 500hPa geopotential height fields are first used to determine the blocking events, similar to the approach of TM90. Daily values of potential temperature on a constant potential vorticity field of 2 PVU are used for the second approach to determine blocking events using the PH03. After determining the blocking events using the daily data, the frequencies are summed monthly to find seasonal totals before converting to a percentage of blocking frequency, which allows for a comparison of the frequency of blocking events during different seasons as well as during different teleconnection phases.

2.3.2 Adjusted Tibaldi and Molteni (1990) Method

Similar to the methodologies of Luo et al. (2016a; 2016b) and Davini et al. (2012a), this thesis uses a modified form of the TM90 method to identify blocking events. Additionally, this work uses the modified PH03, to determine both how the TM90 and PH03 compare at identification of blocking events and the relationship between teleconnections and blocking frequency. Two different methods of atmospheric blocking identification are chosen as a means to address the issues discussed in Woolings et al. (2018), who found that no single index is able to effectively describe all stages of the blocking pattern life cycle.

Blocking events are determined using an approach similar to that of TM90 using the ERA-Interim dataset combining the following steps using the 500hPa geopotential height field, evaluated on a 0.75° by 0.75° latitude-longitude grid. Midlatitude geopotential height gradients (GHGS) and high latitude geopotential height gradients (GHGN) are identified to determine blocking events by:

$$GHGN = \frac{Z(\Phi_n) - Z(\Phi_o)}{(\Phi_n - \Phi_o)} \quad (1)$$

$$GHGS = \frac{Z(\Phi_o) - Z(\Phi_s)}{(\Phi_o - \Phi_s)} \quad (2)$$

Where:
$\phi_n = 80.25°N + \Delta$
$\phi_o = 60°N + \Delta$
$\phi_s = 39.75°N + \Delta$
$\Delta = -4.5°, -3°, -1.5°, 0°, 1.5°, 3°, or\ 4.5°$

Blocking days are determined when the following criteria for GHGS and GHGN are met for at least one Δ value and span 12° of longitude for four or more days:

$$GHGS > 0 \quad (3)$$

$$GHGN < -10\ m/\deg lat \quad (4)$$

2.3.3 Adjusted Pelly and Hoskins (2003) Method

Using an approach similar to that of PH03, blocking events are identified with the ERA-Interim dataset using the potential temperature on a constant potential vorticity field of 2 PVU. The blocking index at a particular longitude ($\mathcal{B}$) is given as:

$$\mathcal{B} = \frac{2}{\Delta\phi}\int_{\phi_0}^{\phi_0+\Delta\phi/2}\theta\, d\phi - \frac{2}{\Delta\phi}\int_{\phi_0-\Delta\phi/2}^{\phi_0}\theta\, d\phi \quad (5)$$

Where:
$\Delta\phi = 30°$
$\phi_0 = \phi_c + \Delta$
$\phi_c = 50.25°$
$\Delta = -4.5°, 0°, or\ 4.5°$

Blocking days are identified when $\mathcal{B}$ spans 15° of longitude for four or more days consecutively, where $\mathcal{B}$ is the blocking index at a particular longitude:

$$\mathcal{B} > 0 \quad (6)$$

Both identification methods compare gradients at different latitudes, with the TM90 method using 500hPa geopotential height gradients and the PH03 method comparing potential temperature gradients on a constant 2PVU surface. Using a single PV field allows provides some simplicity in examining synoptic scale features of the rapidly changing and dynamic Arctic

compared to the use of multiple pressure levels. Compared to the TM90 method, the PH03 method uses the PV framework, which gives a better image of the structure of the atmosphere compared to geopotential height fields. The PH03 method assumes the absence of diabatic processes, which conserves potential temperature on a PV surface (PH03). For this idealized explanation of the atmosphere, the tropopause denotes a discontinuity between the two regions with uniform but different PV (PH03). When this information is inverted with surface potential temperature and total mass information, information about the balanced flow can be inferred (PH03). The PH03 method uses reversals in the meridional gradient of potential temperature to identify blockings events, while the TM90 method identifies blocking by identifying reversals of the zonal wind field using 500hPa geopotential height gradients. Based on the results of PH03, the 500hPa height fields (TM90) identifies little blocking in the Pacific. The PH03 authors state this is possibly due to the fact that Omega blocks are most common in the Pacific, which have weaker easterly flow compared to the Euro-Atlantic dipole blocks, making it difficult to be captured with the TM90 method (PH03). The PH03 method is able to identify more Pacific blocking events, which suggests this more dynamical approach is better suited for identifying Omega blocks.

2.3.4 Statistical Analysis for Trends

Statistical analysis includes an analysis of trends in blocking frequency. The Dickey-Fuller test is conducted in order to determine if there is a trend in the frequency for the four quadrants of the Arctic across the blocking data record (1980–2017). Monthly blocking frequencies for each quadrant are seasonally standardized as a Z score, where X is the monthly frequency, μ is the mean for the corresponding month, and σ is the standard deviation for that month:

$$Z = \frac{x-\mu}{\sigma} \quad (7)$$

After the blocking frequency is standardized, a Dickey-Fuller test is conducted in order to test whether or not the trend-stationarity is present for each of the quadrant (Dickey and Fuller 1979). The Dickey-Fuller test is an approach that determines whether or not the data has a unit root (a stochastic trend in a time series or a "random walk with drift"); if a unit root is present, the data cannot be considered stationary (Dickey and Fuller 1979). This test has been used in time series trend analysis of other climate data (e.g., Estrada et al. 2013). The trends are considered significant for $p \leq 0.10$, $p \leq 0.05$, and $p \leq 0.01$ (90, 95, and 99% confidence intervals). Additionally, autocorrelation plots are developed to determine if there is any relationship outside seasonal variability present for each of the quadrants.

2.4 Assessing the Influence of the AO and the NAO on Arctic Blocking

2.4.1 Teleconnection Indices

Two low-frequency atmospheric teleconnection patterns (i.e., Arctic Oscillation and North Atlantic Oscillation) are chosen for this study as they have been shown to be highly related to blocking patterns in the Arctic (Shabbar et al. 2000; Ogi et al. 2003). The teleconnection indices are divided into positive (index value ≥ 0.5), negative (index value ≤ -0.5), and neutral ($-0.5 <$ index value < 0.5) phases, similar to that of Luo et al. (2016b); a 0.5 division was chosen because it is not as restrictive compared to divisions around 1.0. Luo et al. (2016b) compared the results of their study using the 1.0 and 0.5 divisions of the NAO and found a similar pattern of a more prominent quasi-biweekly winter warm Arctic-cold Eurasian anomalies during positive phase NAO Ural blocks compared to other Ural blocks with the 0.5 division.

2.4.1.1 Arctic Oscillation

Daily index values of AO were obtained from NOAA ESRL (https://www.esrl.noaa.gov/psd/data/correlation/ao.data), which were created by projecting the daily 1000hPa height anomalies north of 20° latitude on to the Empirical Orthogonal Function analysis of monthly mean 1000hPa heights during the time period of 1979-2000 (Higgins et al. 2000; Higgins et al. 2001; Zhou et al. 2001; Higgins et al. 2002; Larson et al. 2004). The daily values are then standardized using the standard deviation of the monthly AO index from 1979-2000 (Higgins et al. 2000; Higgins et al. 2001; Zhou et al. 2001; Higgins et al. 2002; Larson et al. 2004). For the purpose of this thesis, monthly values are obtained from January 1980 to December 2017, however data is available from 1950 to the present.

2.4.1.2 North Atlantic Oscillation

NAO index values were obtained from NOAA ESRL (https://www.esrl.noaa.gov/psd/data/correlation/nao.data) based on Rotated Principal Component Analysis applied to monthly standardized 500hPa height anomalies, which isolates the teleconnection patterns (Barnston & Livezey 1987; van den Dool et al. 2000; Chen and van den Dool 2003). Index values cover the 1950 to the present, however for the purpose of this thesis monthly values from January 1980 to December 2017 are used.

2.4.2 Statistical Analysis of Teleconnections and Blocking

Statistical tests including the Kruskal-Wallis and Conover's post hoc test are conducted to understand the relationship between blocking pattern frequency and low-frequency Arctic atmospheric teleconnections (i.e. AO and NAO).

2.4.2.1 Kruskal-Wallis Test

The Kruskal-Wallis test, a non-parametric analysis of variance (ANOVA), is conducted to determine if there is a significant difference between blocking pattern frequency during

positive, negative, and neutral phases of the AO and NAO (Kruskal and Wallis 1952). This test has been used in climate science research in a variety of subjects such as the spatiotemporal variability of precipitation to the magnitude of uncertainty for different climate change scenarios (e.g., Winkler et al. 2003; Türkeş et al. 2009). Because the Kruskal-Wallis test is non-parametric, it does not assume a normal distribution or equal variances across groups like the one-way ANOVA (Kruskal and Wallis 1952). The Kruskal-Wallis test pools the data for each of the groups and then ranks them. Once the data are ranked, the sum of the ranks and the mean rank for each group is calculated (Kruskal and Wallis 1952). Then, the test statistic is calculated in order to test if there is a significant difference between blocking frequency and teleconnection phase. The relationship between blocking frequency and teleconnection phases are considered significant for $p \leq 0.10$, $p \leq 0.05$, and $p \leq 0.01$ (90, 95, and 99% confidence intervals).

2.4.2.2 Conover's Post Hoc Test

The Kruskal-Wallis test will only determine whether or not at a minimum of two of the three phases of teleconnection patterns are statistically different than one another. Although the Conover test is not a well-known post hoc test, this test is powerful and has been used in climate related research from the influence of climate change on tree phenology as well as changes in precipitation regimes (e.g., Fatichi and Caporali 2009; Vitasse et al. 2018). A Conover's post hoc test is conducted to determine which of the three groups are significantly different than each other (Conover and Iman 1979; Conover 1999). Similar to the Kruskal-Wallis test, the Conover's test does not assume a normal distribution and is based on ranks (Conover and Iman 1979; Conover 1999). The relationship between blocking frequency and teleconnection phases are considered significant for $p \leq 0.10$, $p \leq 0.05$, and $p \leq 0.01$ (90, 95, and 99% confidence intervals).

A climatology from 1980 to 2017 of blocking frequency for four quadrants of the Arctic is constructed using adjusted forms of the TM90 and PH03 blocking identification approaches. Statistical analyses are utilized to quantify both the changes in frequency of blocking over time and to quantify the relationship between phases of teleconnection patterns and blocking frequency seasonally, across the Arctic. The findings of this work are provided in Chapter 3 and conclusions summarized in Chapter 4.

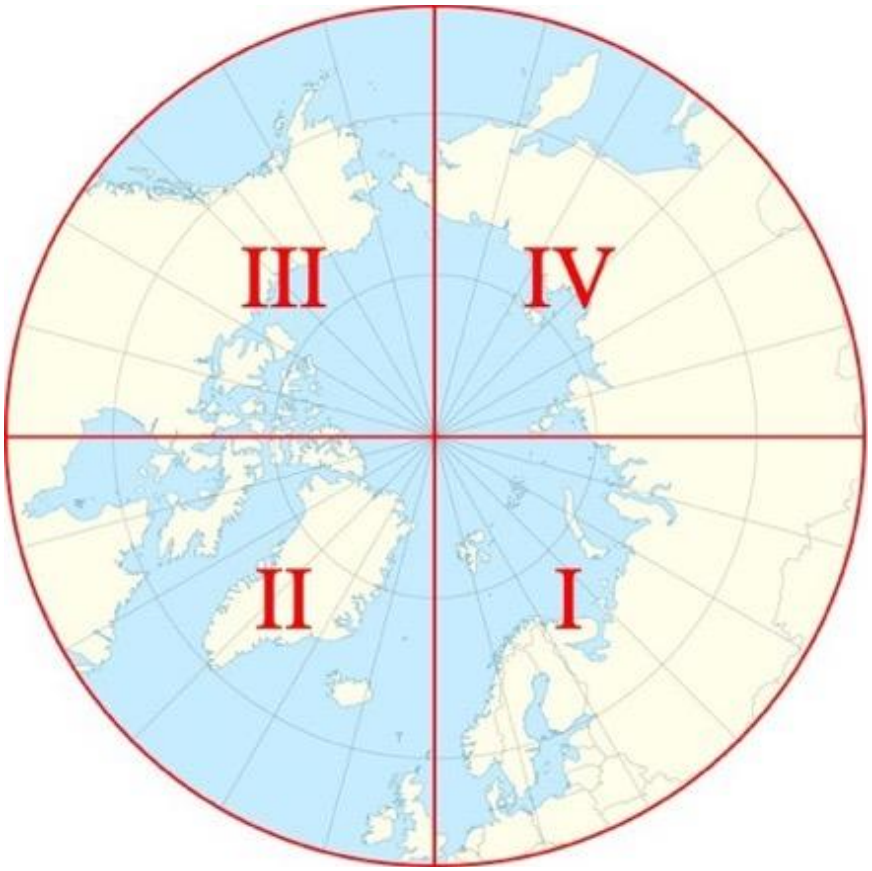

Figure 2.1. Map of the Arctic divided into the four quadrants for use in this study.

CHAPTER 3

RESULTS

3.1 Arctic Blocking Climatology

In order to have a further understanding of possible future changes in blocking, a better understanding of past and present blocking frequency is necessary. This thesis develops a climatology (1980–2017) of blocking frequency for four quadrants of the Arctic, which is constructed using adjusted forms of the TM90 and PH03 methodologies. The quadrants are divided to correspond to the locations discussed in Kim and Ha (2014), where atmospheric blocking most frequently occurs: the North Pacific, Greenland, Europe, and Ural-Siberian. Two different methods of atmospheric blocking identification are compared to address the issues discussed in Woolings et al. (2018), in which no methodological approach is able to effectively describe all stages of the blocking pattern life cycle.

3.1.1 Seasonality

As a means to understand the relationship between Arctic blocking pattern frequency and low-frequency atmospheric teleconnections (i.e. AO and NAO), a blocking pattern climatology is developed for the four quadrants of the Arctic using an adjusted TM90 and adjusted PH03 blocking identification approach. Atmospheric blocking patterns persist across the Arctic, however peak blocking frequency differs between the two blocking identification methods. Blocking frequency using the adjusted TM90, peaks at 180° and 30°E longitude (10–15%), while blocking frequency using the adjusted PH03, peaks at ~130°E longitude (~40%) with two smaller peaks at 180° and 75°W longitude (15–20%) (Figure 3.1). These results differ from the

original TM90 and PH03 approaches, which only utilized five years of data, compared to the three decades of data for this study (Figure 1.2). Similar to the original TM90 and PH03 analysis, both blocking identification methods identify two peaks of annual blocking frequency. However, they differ in location compared to these results where one is located between 30°E and 45°W longitude and one located between 180° and 90°W longitude (Figure 1.2) When comparing the two blocking pattern identification methods, a higher percentage of blocking is identified using the modified PH03 than the TM90 (Figures 3.1 and 3.2). However, the PH03 method identified the most events in Quadrants IV and I, while the TM90 method identified more blocking events for Quadrant I (Figure 3.2). The TM90 method shows less of a difference between quadrants compared to the PH03 method (Figure 3.2). When comparing blocking days seasonally, the adjusted TM90 method identifies more winter (DJF) and spring (MAM) blocking events for Quadrants I, II, and III while more DJF and summer (JJA) events are identified for Quadrant IV (Figure 3.3). Comparatively, the adjusted PH03 method, identifies more JJA and fall (SON) blocking events for Quadrant I (Figure 3.4). Quadrant II has more blocking events identified during DJF and MAM, while Quadrants III and IV blocking events are more evenly distributed over all four seasons (Figure 3.4). Overall, blocking frequency based on TM90 showed less interquadrant variability and has more winter and spring blocking for most of the Arctic (Quadrants I–III); while, blocking frequency based on PH03 showed more interquadrant variability.

3.1.2 Annual Time Series

Figure 3.5 shows the frequency of blocking events for each quadrant using both blocking pattern identification methods during the entire period of record. The interannual variability of blocking frequency among the four quadrants is smaller using the TM90 method compared to the

PH03 method (Figure 3.5). For both identification methodologies, a trend is not easily detected for any of the quadrants (Figure 3.5). However, the two methodologies show similar patterns with a decreasing frequency in blocking recently from 2015–2017 for Quadrants I, II, and III and an increasing frequency from 2015–2017 for Quadrant IV (Figure 3.5). Although, these slight changes and variability in frequency can be detected throughout the data record, it is important to note that there does not appear to be a change in frequency from the beginning to the end of the record (Figure 3.5).

3.1.3 Seasonal Time Series

When blocking events are identified using the adjusted TM90, significant variability persists across all four seasons, however there is less variability among quadrants. In Quadrants I (Europe) and II (Greenland) during DFJ, blocking frequency is increasing since 2013 (Figure 3.6). However, since 2013, a decrease in blocking frequency for Quadrants III (North America/Pacific) and IV (Ural-Siberia) is present (Figure 3.6). For MAM, the frequency of blocking is not as high in DJF, with a decrease in blocking frequency since 2015 for Quadrants I, II, and III and an increase in frequency for Quadrant IV (Figure 3.6). In JJA and SON, fewer blocking events were identified compared the other two seasons across all four quadrants, and since approximately 2013 there has been an overall decrease in blocking frequency (Figure 3.6).

When comparing with the PH03, there is more variability from quadrant to quadrant and the trends differ from the TM90 method. Quadrants I, II, III have similar frequencies of blocking for DJF, with a fairly consistent decrease in blocking frequency since 2013 (Figure 3.7). While Quadrant IV, has an increase in blocking during DJF since 2013 after a long period of fairly consistent blocking frequency since 2000 (Figure 3.7). During MAM, Quadrants I and II have a decreasing trend in blocking frequency since 2015, while Quadrants III and IV have an

increase in blocking frequency (Figure 3.7). For JJA, blocking frequency is greatest for Quadrants I and IV; however, there appears to be an increase in blocking frequency since 2015 for all four quadrants (Figure 3.7). All four quadrants are experiencing an increase in frequency since approximately 2012 during SON (Figure 3.7). When examining the period of record, the sub-decadal variability in seasonal blocking frequency is visible across the four quadrants, however, a trend in seasonal blocking frequency is not present (Figure 3.7).

3.1.4 Monthly Frequency

Through the examination of the monthly means of blocking frequency for each quadrant, the intra-annual variability in blocking is more clearly evident than in the seasonal means and time series. Using the TM90 method, blocking frequency for Quadrant I does not exhibit much variability across the year, with all monthly frequencies around 30% (Figure 3.8). Quadrant II has a peak in blocking frequency in the spring (April–May) and a minimum in the summer (July–August), while Quadrant III is similar to Quadrant I with blocking not changing much throughout the year (Figure 3.8). Quadrant IV has two peaks in blocking frequency in the winter (January–February) and the summer (June), with the minimum frequencies occurring during the fall (September) (Figure 3.8). When comparing the results with the adjusted PH03, the intra-annual variability of frequencies differs. Quadrant I has a strong seasonality present in terms of blocking frequency, with a peak during the summer and early fall (June–September) (Figure 3.9). Quadrant II is not as variable across the year aside from a small peak in late winter (Figure 3.9). Blocking frequency is consistent in Quadrant III through most of the year, however during the summer (August), the frequency reaches a minimum (Figure 3.9). Quadrant IV blocking frequency peaks during the winter months and reaches a minimum during spring and summer (Figure 3.9). The PH03 method uses reversals in the meridional gradient of potential

temperature to identify blockings events, while the TM90 method identifies blocking by identifying reversals of the zonal wind field using 500hPa geopotential height gradients. The differences in the physical processes represented in the two identification methods is a possible explanation for the differences in the seasonal means.

These results differ from previous studies, possibly due to the differences in blocking identification methods. For example, Trigo et al. (2004) found that blocks most typically occur in winter and spring, while both approaches in this thesis found a significant number of blocking events also during the summer. The results of this thesis also differ from that of Tyrlis and Hoskins (2008), who found that blocking activity is largest over Europe and the eastern Atlantic Ocean in the winter, and eastern Europe and central Asia during the summer. The disparities between the adjusted TM90 and PH03 approaches blocking frequency further verifies Woolings et al. (2018) finding that no single index is able to identify all blocking events.

3.2 Relationship between AO, NAO, and Arctic Blocking

The AO and NAO influence Arctic blocking patterns with respect to formation, lifespan, and frequency (Shabbar et al. 2000; Ogi et al. 2003; Cheung et al. 2012; Davini et al. 2012b; Hassanzadeh and Kuang 2015). The seasonal and spatial differences in Arctic blocking frequency during positive, negative, and neutral phases of each teleconnection (i.e., AO and NAO) are explored in this thesis. Understanding the influences of teleconnections on blocking patterns across the Arctic can help improve knowledge on the impact of blocking on the sea ice, ice sheet surface mass balance, and snow cover across regions of the Arctic.

3.2.1 Monthly

Figures 3.10–3.13, demonstrate the significant variability month-to-month in blocking frequency, however the two-year running means show little change in the frequency of blocking

across the period of record. In order to determine if a trend is present, the frequencies are standardized by season (Figures 3.14 and 3.15). The seasonally standardized frequencies indicate the presence of noise once the seasonality is removed, so there is no significant trend in the frequency in blocking across the Arctic using these two methods of identifying blocking (Figures 3.14 and 3.15). The presence of noise once the frequencies are seasonally standardized indicates that the variability in blocking frequency can be completely explained by blocking seasonally. Additionally, the Dickey-Fuller tests the null hypothesis that a unit root is present, which indicates a non-stationary time series, while the alternative hypothesis is trend stationarity. The test statistics shown in Table 3.1 indicate that the null hypothesis is rejected at the 99% confidence level when this test is applied to the seasonal blocking frequency time series for each quadrant. Therefore, one must assume that the time series are stationary and no trends are present. (Table 3.1). The Dickey-Fuller test of the quadrants for both methodological approaches was statistically significant with 99% confidence, which indicates that the data are stationary (Table 3.1). Autocorrelation plots of the seasonally standardized frequencies indicate there is little autocorrelation present once the seasonality is removed, so any variability in blocking frequency can be explained by the differences in blocking seasonally (Figures 3.16 and 3.17). The inability to determine a trend proves to be significant because it is difficult to trust models making predictions on how blocking is possibly changing in the future. Frequency and trends of past blocking events must be better characterized before we can begin to understand future behavior of atmospheric blocking (Scaife et al. 2011; Masato et al. 2013; Davini and D'Andrea 2016; Pithan et al. 2016; Hanna et al. 2018b; Woolings et al. 2018).

Figures 3.18 and 3.19 show the differences in blocking frequency during positive, negative, and neutral phases for both the TM90 and PH03, respectively. The Kruskal-Wallis test

indicates whether samples originate from the same distribution. The test indicates whether one sample – the positive, negative or neutral phase blocking frequency – is significantly different. Table 3.2 shows that the test statistic exceeds the critical value at the 99% confidence interval for Quadrant II (Greenland), indicating a relationship between NAO and AO phases and blocking frequency when examining monthly blocking frequency. For Quadrant III (North America/Pacific) the test statistic exceeds the critical value at the 95% confidence interval indicating a relationship between monthly blocking frequency and AO phases. The Conover's post hoc test confirms the relationship between Quadrant II blocking frequency and AO and NAO phases in which increased blocking is associated with negative phases of both NAO and AO (Table 3.3; Figure 3.18). For Quadrant III, the Conover's post hoc confirms the relationship between AO phases and blocking frequency where increased blocking activity is associated with the negative phase of the AO (Table 3.3; Figure 3.18). Using the PH03 method, there are more significant relationships present between teleconnection phase and blocking frequency for all Quadrants (Tables 3.4 and 3.5). Table 3.4 shows that the test statistic exceeds the critical value at the 99% confidence interval for all quadrants, indicating a relationship between AO phases and blocking frequency when examining monthly blocking frequency. Additionally, the test statistic exceeded the critical value at the 99% confidence interval for Quadrant II indicating a relationship between NAO phases and monthly blocking frequency (Table 3.4). The Conover's post hoc test confirms at the 99% confidence interval the result of increased Quadrant II blocking frequency during the negative phases of AO and NAO (Table 3.5; Figure 3.19). The Conover's post hoc test results indicate the presence of a relationship between monthly blocking frequency and phases of the AO at the 99% confidence interval for Quadrants I–III and the 95% confidence interval for Quadrant IV (Table 3.5).

3.2.2 Seasonal

The groups of blocking frequencies are divided by teleconnection phase in order to better understand the relationship between AO and NAO and seasonal blocking frequency. The Kruskal-Wallis and Conover's post hoc tests are used to determine if a relationship is present. The Kruskal-Wallis test statistic exceeds the critical value at the 99% confidence interval for Quadrant II for all seasons indicating a relationship between AO phases and seasonal blocking frequency (Table 3.6). The Conover's post hoc test confirms this relationship with the test statistic exceeding the critical value at the 95% confidence interval of increased Quadrant II blocking frequency during negative phases of AO in all seasons (Table 3.7; Figure 3.20), Although not as strong, the Kruskal-Wallis test statistic exceeds the critical value at the 99% confidence interval for DJF and SON Quadrant III blocking frequency (Table 3.6). The Conover's post hoc test indicates the relationship between increased DJF and SON blocking frequency for Quadrant III (Table 3.7; Figure 3.20). Additionally, the Kruskal-Wallis statistic exceeds the critical value at the 99% confidence interval for Quadrant IV only during DJF (Table 3.6). The Conover's post hoc test confirms the claim of greater DJF blocking frequency for Quadrant IV during the negative phase of the AO (Table 3.7; Figure 3.20). Overall, the relationship between greater blocking frequency and the negative phase of the AO is stronger in winter for all quadrants, but Quadrant II (Greenland) has the strongest relationship throughout the year.

A similar pattern is present, although not as strong, when comparing phases of NAO to Arctic blocking frequency using the TM90 approach. Unlike the relationship between Quadrant I blocking frequency and the AO, Quadrant I blocking frequency is related to the NAO. In JJA, the test statistic for both the Kruskal-Wallis and Conover's post hoc test exceeds the 95%

confidence interval indicating a relationship between blocking frequency and NAO phases (Table 3.8 and 3.9; Figure 3.21). For Quadrant II, the Kruskal-Wallis test statistic exceeds the 99% confidence interval for DJF, MAM, and SON (Table 3.8). The Conover's post hoc test confirms the relationship of increased blocking frequency during the negative phase of the NAO (Table 3.9; Figure 3.21). The Kruskal-Wallis and Conover's post hoc test indicated a relationship between Quadrant III DJF blocking frequency and phases of NAO (Table 3.8 and 3.9; Figure 3.21).

When using blocking frequencies identified using the modified PH03 approach, the relationship between AO and NAO appears stronger. The Kruskal-Wallis test statistic exceeds the critical value at the 90% confidence interval for Quadrant I during DJF and JJA indicating a relationship between AO phases and blocking frequency (Table 3.10). The Conover's post hoc test confirms the relationship between increased blocking frequency and the negative phases of the AO (Table 3.11; Figure 3.22). The Kruskal-Wallis test statistic exceeds the critical value at the 99% confidence interval for Quadrant II for all seasons indicating a relationship between AO phases and seasonal blocking frequency (Table 3.10). The Conover's post hoc test confirms this relationship with the test statistic exceeding the critical value at the 99% confidence interval of increased Quadrant II blocking frequency during negative phases of AO in all seasons (Table 3.11; Figure 3.22). The test statistics of the Kruskal-Wallis and Conover's post hoc test exceed the 99% confidence interval, indicating a relationship between SON blocking frequency for Quadrant III and phases of the AO (Tables 3.10 and 3.11; Figure 3.22). Additionally, a relationship between MAM blocking frequency for Quadrant IV and phases of the AO was indicated based on the results of the Kruskal-Wallis and Conover's post hoc tests (Tables 3.10 and 3.11; Figure 3.22).

The relationship between blocking frequencies and NAO using the adjusted PH03 shows a similar relationship when using the modified TM90 with Quadrant II showing the strongest relationships with the NAO pattern. The Kruskal-Wallis test statistic exceeds the critical value at the 99% confidence interval for Quadrant II for all seasons indicating a relationship between AO phases and seasonal blocking frequency (Table 3.12). The Conover's post hoc test confirms this relationship with the test statistic exceeding the critical value at the 99% confidence interval of increased Quadrant II blocking frequency during negative phases of AO in all seasons (Table 3.13; Figure 3.23). The Kruskal-Wallis test statistic exceeds the critical value at the 90% confidence interval for Quadrant I during DJF and JJA indicating a relationship between AO phases and blocking frequency (Table 3.12). The Conover's post hoc test confirms the relationship between increased blocking frequency and the negative phases of the NAO (Table 3.13; Figure 3.23). The test statistics of the Kruskal-Wallis and Conover's post hoc test exceed the 99% confidence interval indicating a relationship between SON blocking frequency for Quadrant III and phases of the AO (Tables 3.12 and 3.13; Figure 3.23). Additionally, a relationship between MAM blocking frequency for Quadrant IV and phases of the AO was indicated based on the results of the Kruskal-Wallis and Conover's post hoc tests (Tables 3.12 and 3.13; Figure 3.23).

Despite the vast differences in the blocking frequencies for the two methods, using these two methodological approaches to identifying atmospheric blocking, there is no significant trend present over the period of record. This is an important finding because it further demonstrates the inconsistency among studies on the changes in blocking frequency currently and in the future. Overland et al. (2012) found an increase in blocking since 2007; while the cause of increased blocking is not completely understood, they stated that it may be related to an earlier

seasonal snowmelt and Arctic sea ice loss. Previous studies have found that the decline in sea ice has led to an increase in atmospheric blocking frequency for North America and Europe in winter, summer, and fall (Liu et al. 2012; Francis and Vavrus 2012; Tang et al. 2013). Additionally, there is low confidence in model projections of atmospheric blocking, despite good agreement among models on an overall decline in blocking in the future (Woolings et al. 2018). Hanna et al. (2018b), found that models predict a decrease in atmospheric blocking frequency in the future possibly associated with an increase in NAO. Before definitive statements on changes in atmospheric blocking can be made, methods of identifying blocking must converge on the similar results. The results of this thesis found similar results to previous studies in which, atmospheric blocking frequency is associated with both the AO and NAO across the Arctic. More specifically, blocking frequency during negative phases of both teleconnections is associated with higher blocking frequencies. Similarly, previous studies including Davini et al. (2012a, 2012b) and Woolings et al. (2010) found the strongest relationships between blocking frequency and teleconnection patterns over Greenland (Quadrant II), which proved to have the strongest relationships as well in the findings presented in this thesis. Through this further understanding of the influences of teleconnections on blocking patterns, improvements on understanding the impact blocking on the conditions of the Arctic can be fully addressed.

Table 3.1. Results from a Dickey-Fuller test between blocking pattern frequencies determined using the adjusted TM90 and adjusted PH03 for each quadrant, including T-statistic, and p-value. P-values ≤ 0.10 are in italic; p ≤ 0.05 are in bold; p ≤ 0.01 are bolded and italicized.

	Quadrant I		Quadrant II		Quadrant III		Quadrant IV	
	T	p	T	p	T	p	T	p
TM90	-6.861	***<0.001***	-21.233	***<0.001***	-19.432	***<0.001***	-14.452	***<0.001***
PH03	-14.935	***<0.001***	-18.221	***<0.001***	-19.952	***<0.001***	-18.744	***<0.001***

Table 3.2. Results from a Kruskal-Wallis test between blocking pattern frequencies determined using the adjusted TM90 for each quadrant, including H-statistic, and p-value for both the AO and NAO. P-values ≤ 0.10 are in italic; p ≤ 0.05 are in bold; p ≤ 0.01 are bolded and italicized.

	Quadrant I		Quadrant II		Quadrant III		Quadrant IV	
	H	p	H	p	H	p	H	p
AO	0.133	0.935	58.919	***<0.001***	7.765	**0.018**	3.384	0.173
NAO	2.956	0.225	66.910	***<0.001***	2.064	0.345	2.585	0.262

Table 3.3. Results from a Conover's post hoc test between blocking pattern frequencies determined using the adjusted TM90 for each quadrant, including H-statistic, and p-value for both the AO and NAO. P-values ≤ 0.10 are in italic; p ≤ 0.05 are in bold; p ≤ 0.01 are bolded and italicized.

			Quadrant I		Quadrant II		Quadrant III		Quadrant IV	
	Group I	Group II	t	p	t	p	t	p	t	p
AO	NEG	NEU	0.243	0.808	5.917	***<0.001***	2.391	**0.017**	1.558	0.120
	NEG	POS	0.085	0.933	7.396	***<0.001***	2.541	**0.011**	1.693	*0.091*
	NEU	POS	0.344	0.731	2.248	**0.025**	0.405	0.686	0.308	0.758
NAO	NEG	NEU	0.034	0.973	4.863	***<0.001***	1.409	0.159	0.005	0.996
	NEG	POS	1.484	0.139	8.150	***<0.001***	0.974	0.331	1.375	0.170
	NEU	POS	1.489	0.137	3.414	***0.001***	0.436	0.663	1.406	0.160

Table 3.4. Results from a Kruskal-Wallis test between blocking pattern frequencies determined using the adjusted PH03 for each quadrant, including H-statistic, and p-value for both the AO and NAO. P-values ≤ 0.10 are in italic; p ≤ 0.05 are in bold; p ≤ 0.01 are bolded and italicized.

	Quadrant I		Quadrant II		Quadrant III		Quadrant IV	
	H	p	H	p	H	p	H	p
AO	23.109	***<0.001***	45.299	***<0.001***	18.966	***<0.001***	10.309	***0.006***
NAO	1.807	0.405	50.608	***<0.001***	0.480	0.787	1.524	0.467

Table 3.5. Results from a Conover's post hoc test between blocking pattern frequencies determined using the adjusted PH03 for each quadrant, including H-statistic, and p-value for both the AO and NAO. P-values ≤ 0.10 are in italic; p ≤ 0.05 are in bold; p ≤ 0.01 are bolded and italicized.

			Quadrant I		Quadrant II		Quadrant III		Quadrant IV	
	Group I	Group II	t	p	t	p	t	p	t	p
AO	NEG	NEU	3.810	***<0.001***	6.170	***<0.001***	4.170	***<0.001***	3.123	***0.002***
	NEG	POS	0.220	0.826	5.679	***<0.001***	3.399	***<0.001***	2.378	**0.018**
	NEU	POS	4.161	***<0.001***	0.054	0.957	0.457	0.648	0.531	0.596
NAO	NEG	NEU	1.035	0.301	4.514	***<0.001***	0.243	0.808	0.645	0.519
	NEG	POS	1.271	0.205	7.016	***<0.001***	0.679	0.497	1.233	0.218
	NEU	POS	0.251	0.802	2.605	***0.009***	0.450	0.653	0.609	0.543

Table 3.6. Results from a Kruskal-Wallis test between blocking pattern frequencies determined using the adjusted TM90 for each quadrant by season, including H-statistic, and p-value for the AO. P-values ≤ 0.10 are in italic; p ≤ 0.05 are in bold; p ≤ 0.01 are bolded and italicized.

	AO							
	Quadrant I		Quadrant II		Quadrant III		Quadrant IV	
	H	p	H	p	H	p	H	p
DJF	1.806	0.401	33.315	***<0.001***	8.299	**0.015**	4.592	***0.010***
MAM	1.125	0.569	22.370	***<0.001***	1.591	0.449	1.357	0.498
JJA	0.433	0.803	9.534	**0.003**	1.239	0.526	1.843	0.392
SON	0.918	0.623	9.527	**0.007**	10.908	***0.001***	3.156	0.109

Table 3.7. Results from a Conover's post hoc test between blocking pattern frequencies determined using the adjusted TM90 for each quadrant by season, including H-statistic, and p-value for the AO. P-values ≤ 0.10 are in italic; p ≤ 0.05 are in bold; p ≤ 0.01 are bolded and italicized.

			AO							
			Quadrant I		Quadrant II		Quadrant III		Quadrant IV	
	Group I	Group II	t	p	t	p	t	p	t	p
DJF	NEG	NEU	0.348	0.728	3.849	***<0.001***	0.170	0.866	1.547	0.125
	NEG	POS	1.008	0.316	5.574	***<0.001***	2.652	***0.009***	2.017	**0.046**
	NEU	POS	1.265	0.209	1.342	0.182	2.265	**0.026**	0.335	0.738
MAM	NEG	NEU	0.173	0.862	3.157	***0.002***	0.475	0.636	0.397	0.692
	NEG	POS	0.712	0.478	4.726	***<0.001***	0.620	0.536	0.611	0.542
	NEU	POS	1.033	0.304	2.056	**0.042**	1.261	0.210	1.164	0.247
JJA	NEG	NEU	0.658	0.512	2.760	***0.007***	0.501	0.617	0.427	0.671
	NEG	POS	0.400	0.690	2.780	***0.006***	0.483	0.630	1.282	0.203
	NEU	POS	0.137	0.891	0.780	0.437	1.077	0.284	1.172	0.244
SON	NEG	NEU	0.170	0.865	1.565	0.120	3.227	***0.002***	0.163	0.870
	NEG	POS	0.881	0.380	3.084	***0.003***	2.368	**0.020**	1.393	0.166
	NEU	POS	0.799	0.426	1.827	*0.070*	0.622	0.535	1.692	*0.093*

Table 3.8. Results from a Kruskal-Wallis test between blocking pattern frequencies determined using the adjusted TM90 for each quadrant by season, including H-statistic, and p-value for the NAO. P-values ≤ 0.10 are in italic; p ≤ 0.05 are in bold; p ≤ 0.01 are bolded and italicized.

	NAO							
	Quadrant I		Quadrant II		Quadrant III		Quadrant IV	
	H	p	H	p	H	p	H	p
DJF	2.667	0.259	59.937	***<0.001***	7.042	**0.029**	2.505	0.284
MAM	0.728	0.694	30.761	***<0.001***	0.874	0.644	0.124	0.938
JJA	8.360	**0.014**	2.796	0.187	3.009	0.211	1.128	0.564
SON	3.360	0.178	11.480	***0.002***	1.794	0.331	5.327	**0.024**

Table 3.9. Results from a Conover's post hoc test between blocking pattern frequencies determined using the adjusted TM90 for each quadrant by season, including H-statistic, and p-value for the NAO. P-values ≤ 0.10 are in italic; p ≤ 0.05 are in bold; p ≤ 0.01 are bolded and italicized.

			NAO							
			Quadrant I		Quadrant II		Quadrant III		Quadrant IV	
	Group I	Group II	t	p	t	p	t	p	t	p
DJF	NEG	NEU	0.173	0.863	1.344	0.182	1.630	0.106	1.434	0.155
	NEG	POS	0.187	0.852	1.692	*0.094*	2.198	**0.030**	1.358	0.177
	NEU	POS	0.000	1.000	0.224	0.824	0.406	0.685	0.122	0.903
MAM	NEG	NEU	0.257	0.798	3.945	**<0.001**	0.935	0.352	0.282	0.778
	NEG	POS	0.825	0.411	5.415	***<0.001***	0.476	0.635	0.330	0.742
	NEU	POS	0.606	0.546	1.669	*0.098*	0.455	0.650	0.059	0.953
JJA	NEG	NEU	0.654	0.514	0.999	0.320	0.610	0.220	0.395	0.694
	NEG	POS	2.145	**0.034**	1.657	*0.100*	0.786	*0.099*	0.670	0.504
	NEU	POS	2.811	***0.006***	0.750	0.455	0.375	0.594	1.0558	0.292
SON	NEG	NEU	0.203	0.839	2.175	**0.032**	1.033	0.304	0.488	0.626
	NEG	POS	1.668	*0.098*	3.348	***0.001***	1.262	0.210	2.187	**0.031**
	NEU	POS	1.460	0.147	1.116	0.267	0.203	0.840	1.686	*0.095*

Table 3.10. Results from a Kruskal-Wallis test between blocking pattern frequencies determined using the adjusted PH03 for each quadrant by season, including H-statistic, and p-value for the AO. P-values ≤ 0.10 are in italic; p ≤ 0.05 are in bold; p ≤ 0.01 are bolded and italicized.

	AO							
	Quadrant I		Quadrant II		Quadrant III		Quadrant IV	
	H	p	H	p	H	p	H	p
DJF	5.283	*0.071*	21.080	***<0.001***	2.213	0.331	1.982	0.371
MAM	0.866	0.649	6.479	**0.039**	2.765	0.251	10.515	***0.005***
JJA	6.609	**0.037**	23.342	***<0.001***	1.416	0.493	0.636	0.727
SON	0.446	0.800	8.511	**0.014**	13.476	***0.001***	1.251	0.535

Table 3.11. Results from a Conover's post hoc test between blocking pattern frequencies determined using the adjusted PH03 for each quadrant by season, including H-statistic, and p-value for the AO. P-values ≤ 0.10 are in italic; p ≤ 0.05 are in bold; p ≤ 0.01 are bolded and italicized.

			AO							
			Quadrant I		Quadrant II		Quadrant III		Quadrant IV	
	Group I	Group II	t	p	t	p	t	p	t	p
DJF	NEG	NEU	0.563	0.574	3.997	***<0.001***	0.866	0.388	0.763	0.447
	NEG	POS	1.719	*0.088*	3.835	***<0.001***	1.470	0.144	1.394	0.166
	NEU	POS	2.146	**0.034**	0.439	0.661	0.495	0.622	0.527	0.599
MAM	NEG	NEU	0.917	0.361	2.534	**0.013**	1.366	0.175	3.212	**0.002**
	NEG	POS	0.473	0.637	1.553	0.123	1.597	0.113	1.713	*0.090*
	NEU	POS	0.477	0.634	1.026	0.307	0.356	0.722	1.607	0.111
JJA	NEG	NEU	2.534	**0.013**	2.873	***0.005***	1.104	0.272	0.562	0.575
	NEG	POS	1.274	0.205	4.797	***<0.001***	0.326	0.745	0.107	0.915
	NEU	POS	0.871	0.386	3.135	***0.002***	0.661	0.510	0.672	0.503
SON	NEG	NEU	0.665	0.508	1.162	0.248	3.097	***0.002***	0.031	0.975
	NEG	POS	0.327	0.744	2.844	***0.005***	3.348	***0.001***	0.911	0.364
	NEU	POS	0.311	0.756	1.961	*0.052*	0.562	0.575	1.035	0.303

Table 3.12. Results from a Kruskal-Wallis test between blocking pattern frequencies determined using the adjusted PH03 for each quadrant by season, including H-statistic, and p-value for the NAO. P-values ≤ 0.10 are in italic; p ≤ 0.05 are in bold; p ≤ 0.01 are bolded and italicized.

	NAO							
	Quadrant I		Quadrant II		Quadrant III		Quadrant IV	
	H	p	H	p	H	p	H	p
DJF	2.539	0.281	9.951	***0.007***	0.533	0.766	0.271	0.873
MAM	1.02	0.601	24.776	***<0.001***	1.347	0.510	1.469	0.480
JJA	6.394	**0.041**	28.650	***<0.001***	0.785	0.675	2.826	0.243
SON	6.986	**0.030**	12.030	***0.002***	1.606	0.448	2.252	0.324

Table 3.13. Results from a Conover's post hoc test between blocking pattern frequencies determined using the adjusted PH03 for each quadrant by season, including H-statistic, and p-value for the NAO. P-values ≤ 0.10 are in italic; p ≤ 0.05 are in bold; p ≤ 0.01 are bolded and italicized.

			NAO							
			Quadrant I		Quadrant II		Quadrant III		Quadrant IV	
	Group I	Group II	t	p	t	p	t	p	t	p
DJF	NEG	NEU	1.267	0.208	1.348	0.181	0.469	0.640	0.433	0.666
	NEG	POS	0.116	0.908	3.123	***0.002***	0.213	0.832	0.474	0.636
	NEU	POS	1.459	0.147	1.820	*0.072*	0.717	0.475	0.034	0.973
MAM	NEG	NEU	0.513	0.609	3.502	***0.001***	0.524	0.601	1.175	0.243
	NEG	POS	1.006	0.317	4.848	***<0.001***	1.153	0.251	0.880	0.381
	NEU	POS	0.531	0.596	1.504	0.135	0.676	0.500	0.283	0.778
JJA	NEG	NEU	2.390	**0.019**	3.832	***<0.001***	0.602	0.549	1.391	0.167
	NEG	POS	1.839	*0.069*	5.078	***<0.001***	0.857	0.393	1.496	0.138
	NEU	POS	0.396	0.693	1.530	0.129	0.301	0.764	0.202	0.841
SON	NEG	NEU	1.894	*0.061*	1.824	*0.071*	1.138	0.258	1.319	0.190
	NEG	POS	2.545	**0.012**	3.433	***0.001***	1.054	0.294	1.281	0.203
	NEU	POS	0.585	0.559	1.539	0.127	0.119	0.905	0.080	0.937

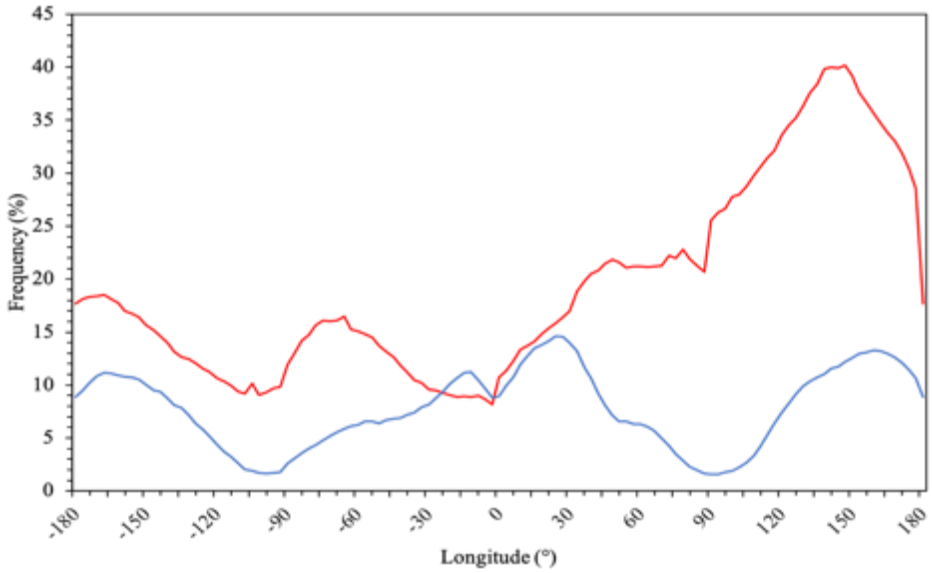

Figure 3.1. Annual blocking frequency against longitude between January 1980 and December 2017 using the adjusted TM90 (blue trace) and using the adjusted PH03 (red trace).

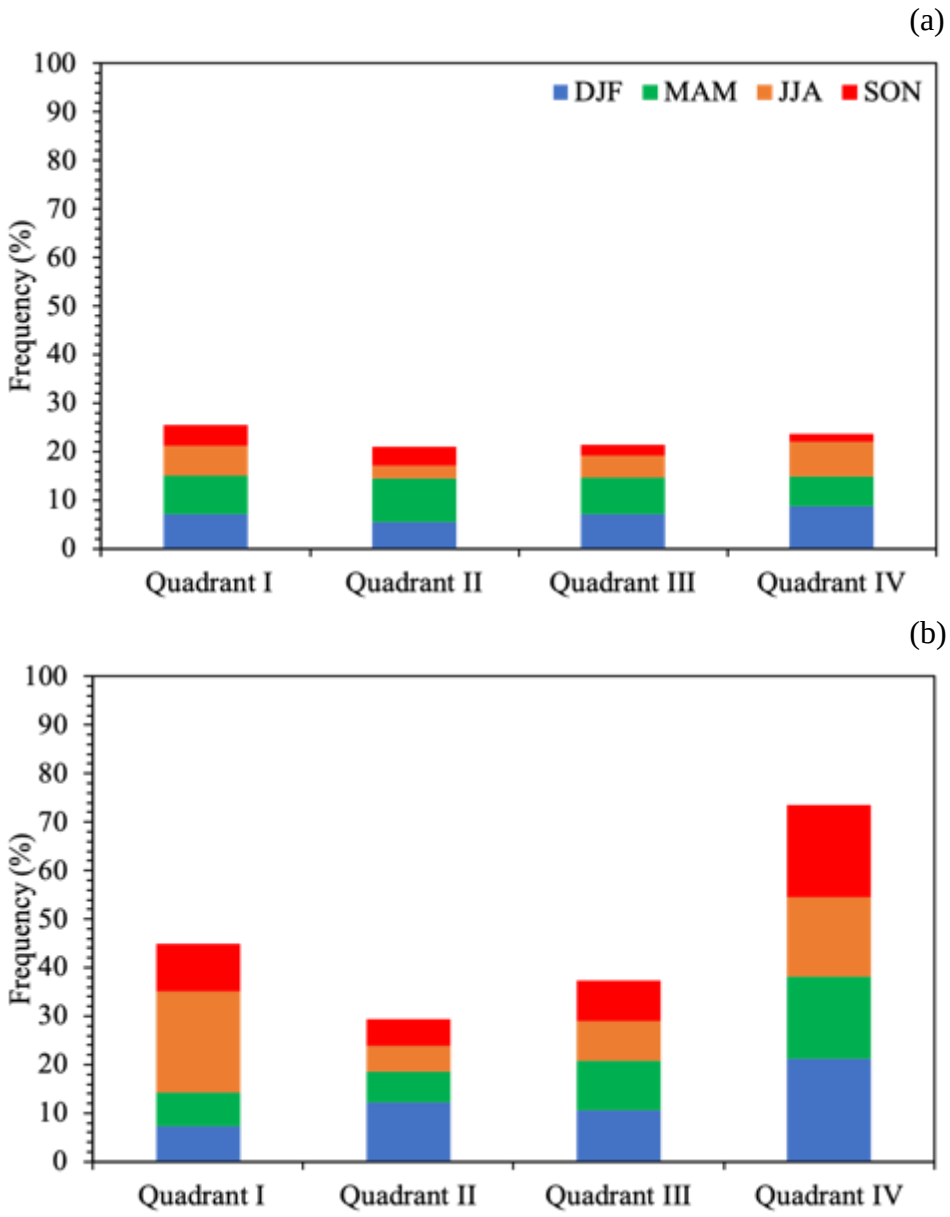

Figure 3.2. Blocking frequency from January 1980 to December 2017 by season for each quadrant of the Arctic using (a) the adjusted TM90 and (b) the adjusted PH03.

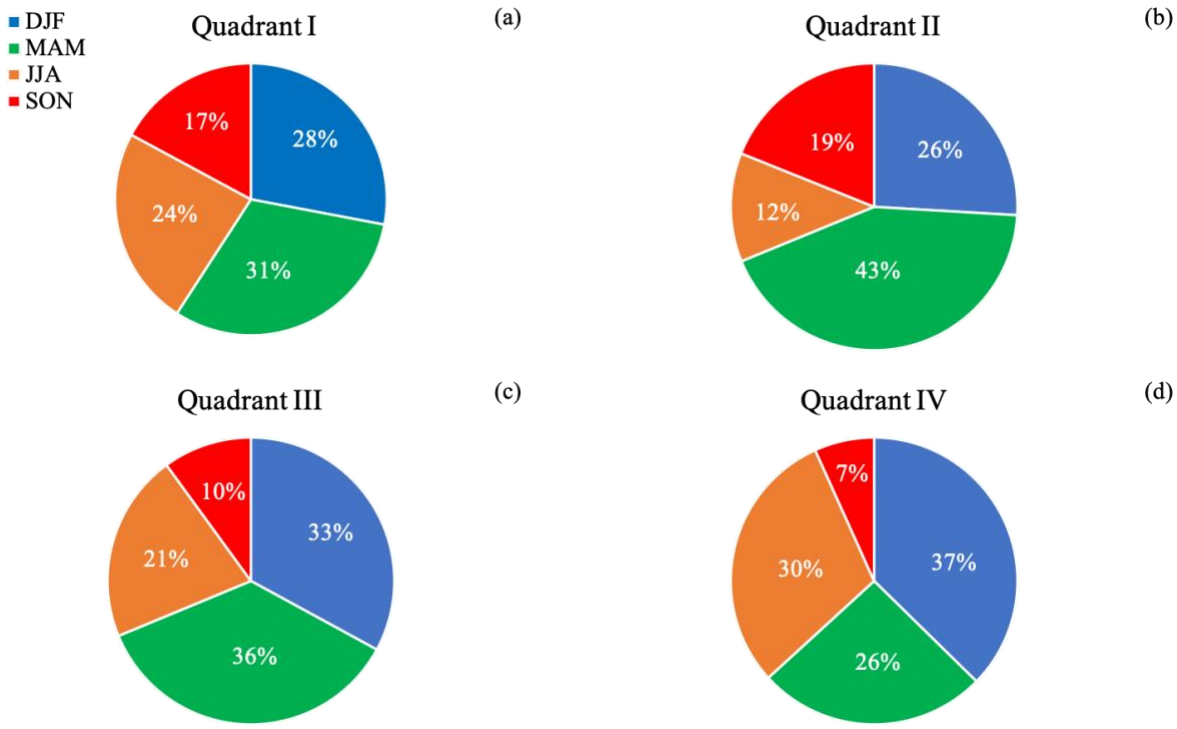

Figure 3.3. Seasonal blocking frequency for each quadrant of the Arctic from January 1980 to December 2017 using the adjusted TM90, Quadrant (a) I, (b) II, (c) III, (d) IV.

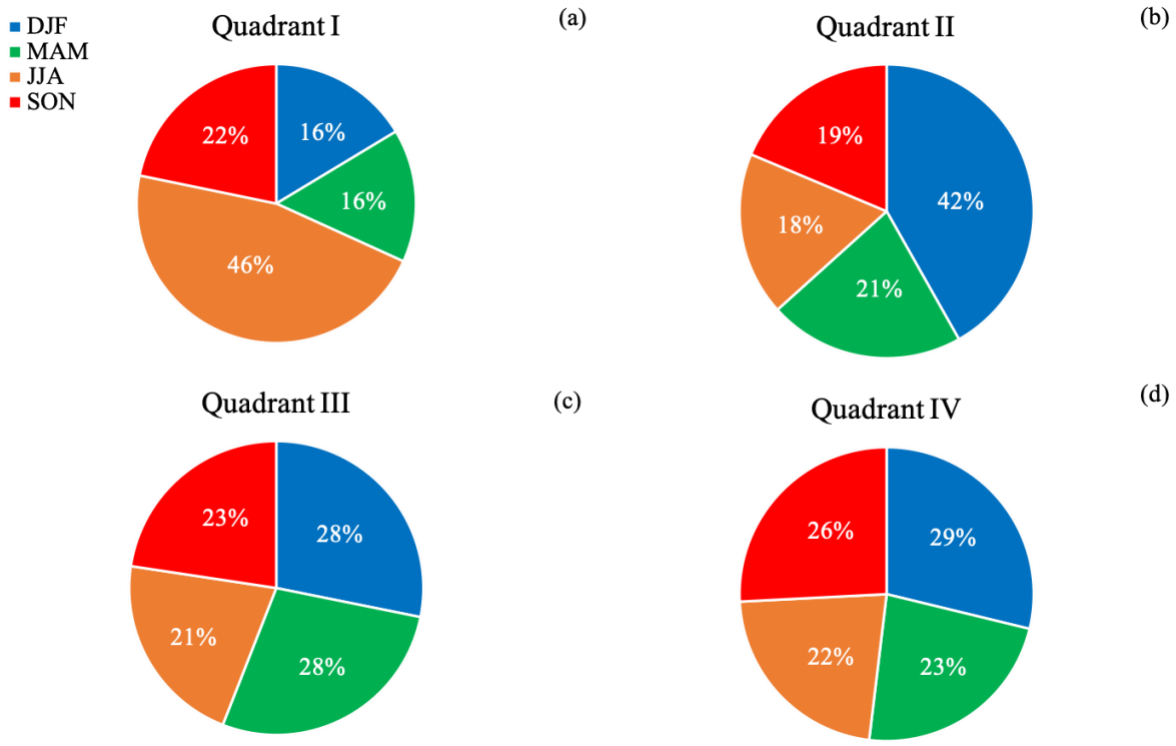

Figure 3.4. Seasonal blocking frequency for each quadrant of the Arctic from January 1980 to December 2017 using the adjusted PH03, Quadrant (a) I, (b) II, (c) III, (d) IV.

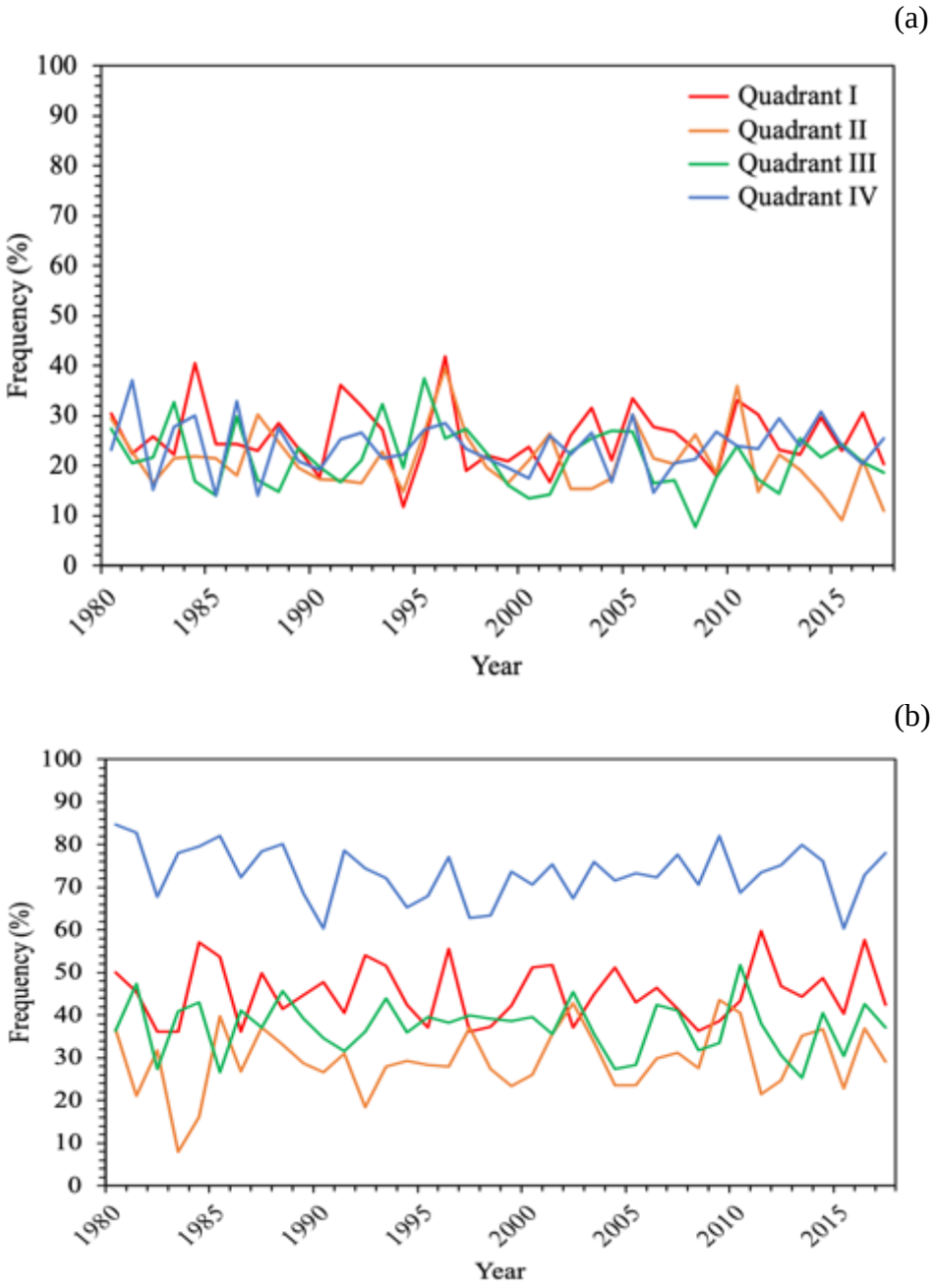

Figure 3.5. Annual blocking frequency from 1980 to 2017 for each quadrant of the Arctic using (a) the adjusted TM90 and (b) the adjusted PH03.

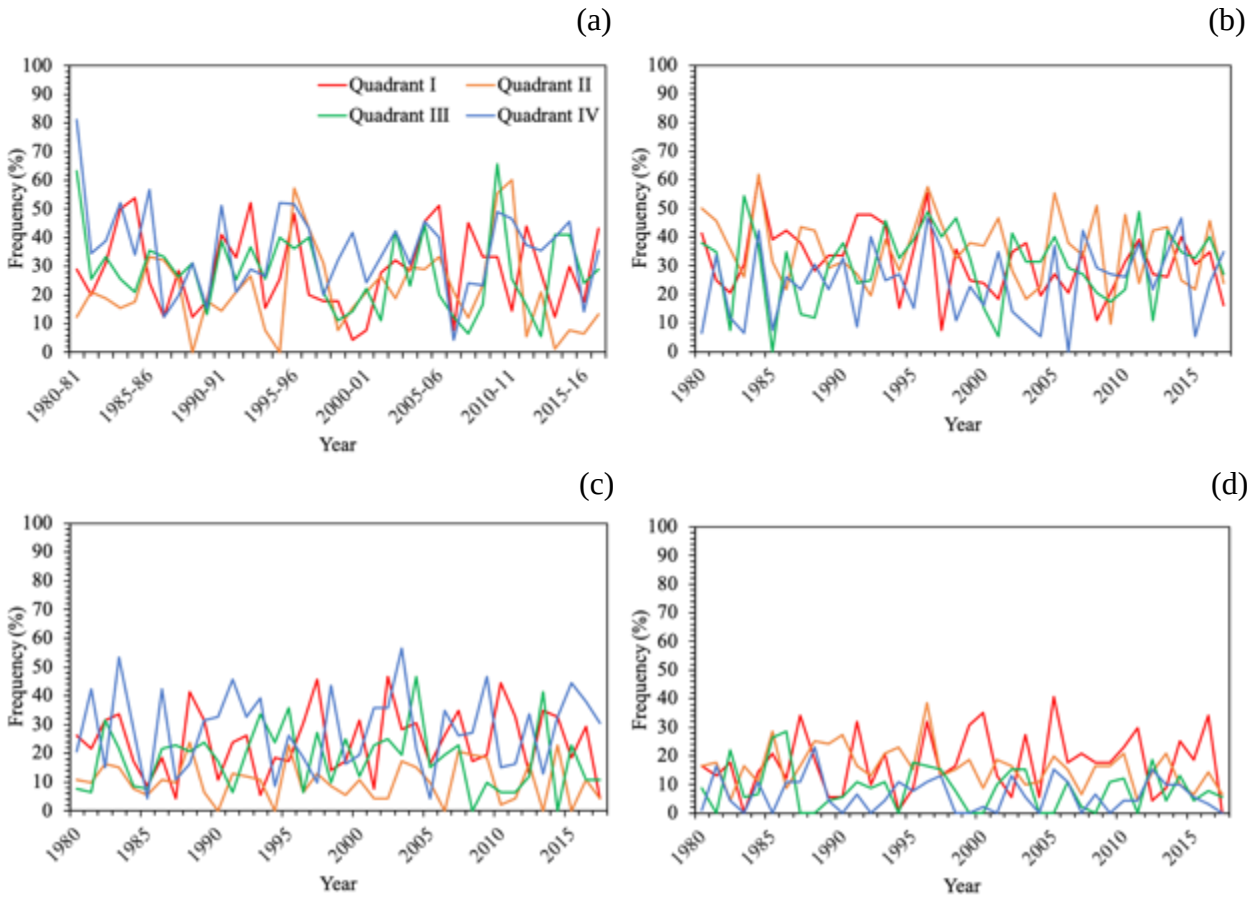

Figure 3.6. Seasonal blocking frequency in terms of number of blocking days for each quadrant of the Arctic using the adjusted TM90, (a) DJF, (b) MAM, (c) JJA, (d) SON, where the traces represent Quadrant I (red), II (orange), III (green) and IV (blue).

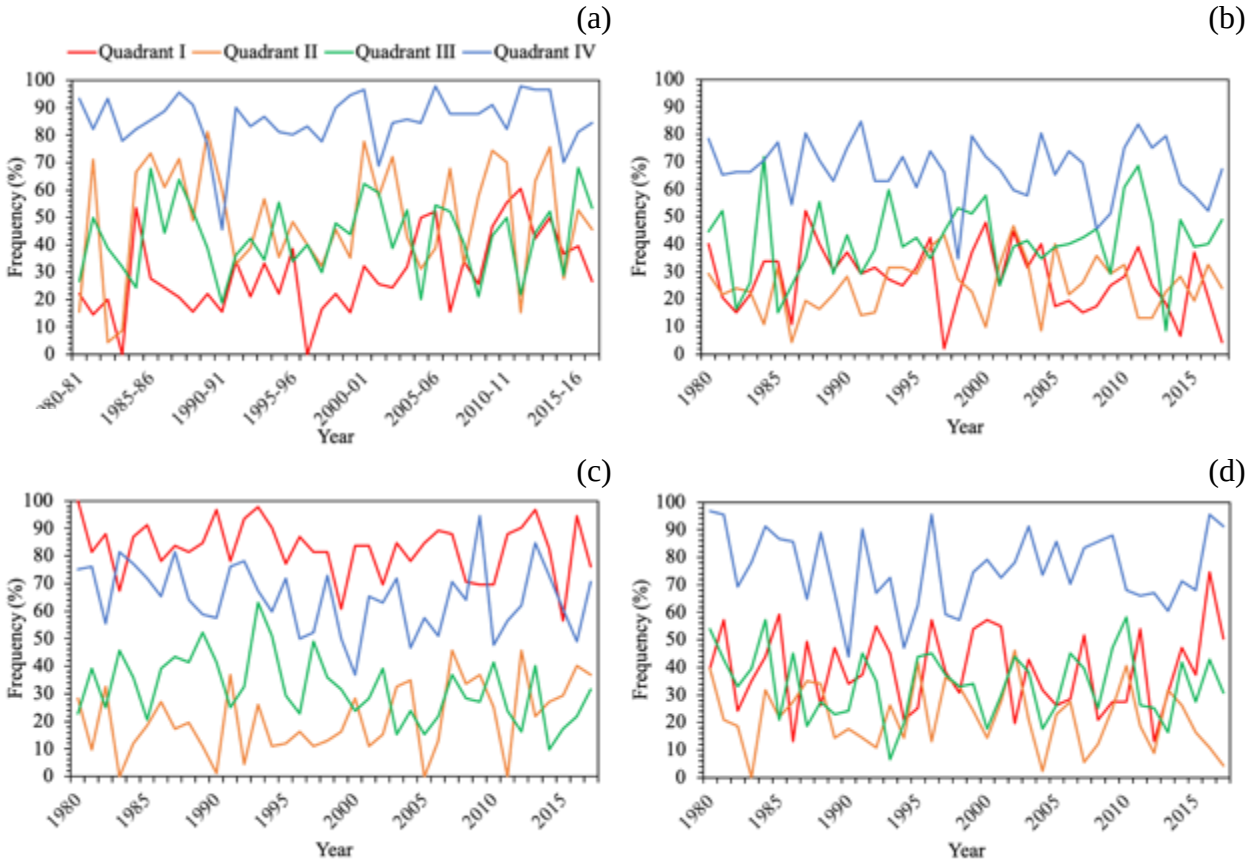

Figure 3.7. Seasonal blocking frequency in terms of number of blocking days for each quadrant of the Arctic using the adjusted PH03, (a) DJF, (b) MAM, (c) JJA, (d) SON, where the traces represent Quadrant I (red), II (orange), III (green) and IV (blue).

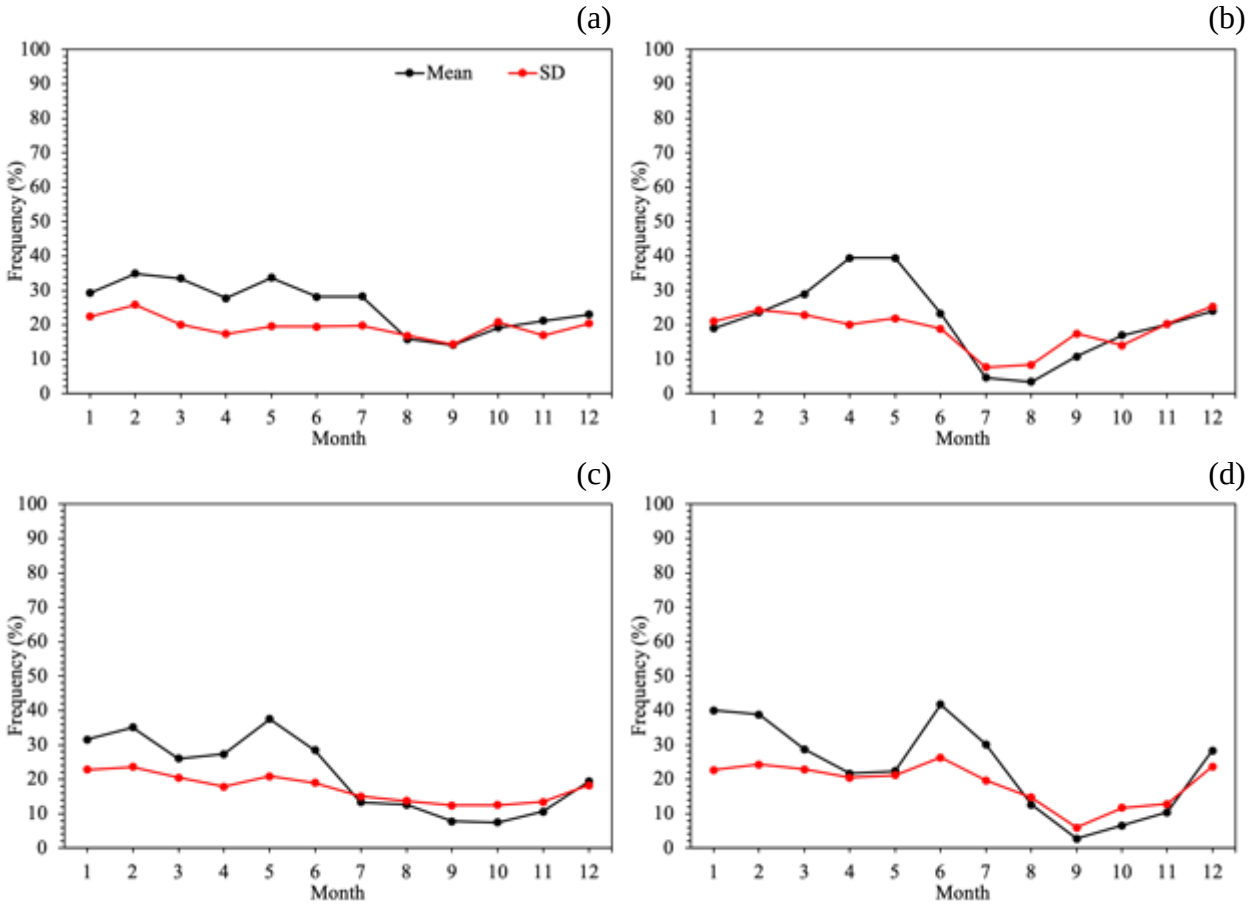

Figure 3.8. Monthly mean (black) and standard deviation (red) of blocking frequency for each quadrant of the Arctic, Quadrant (a) I, (b) II, (c) III, and (d) IV using the adjusted TM90 method.

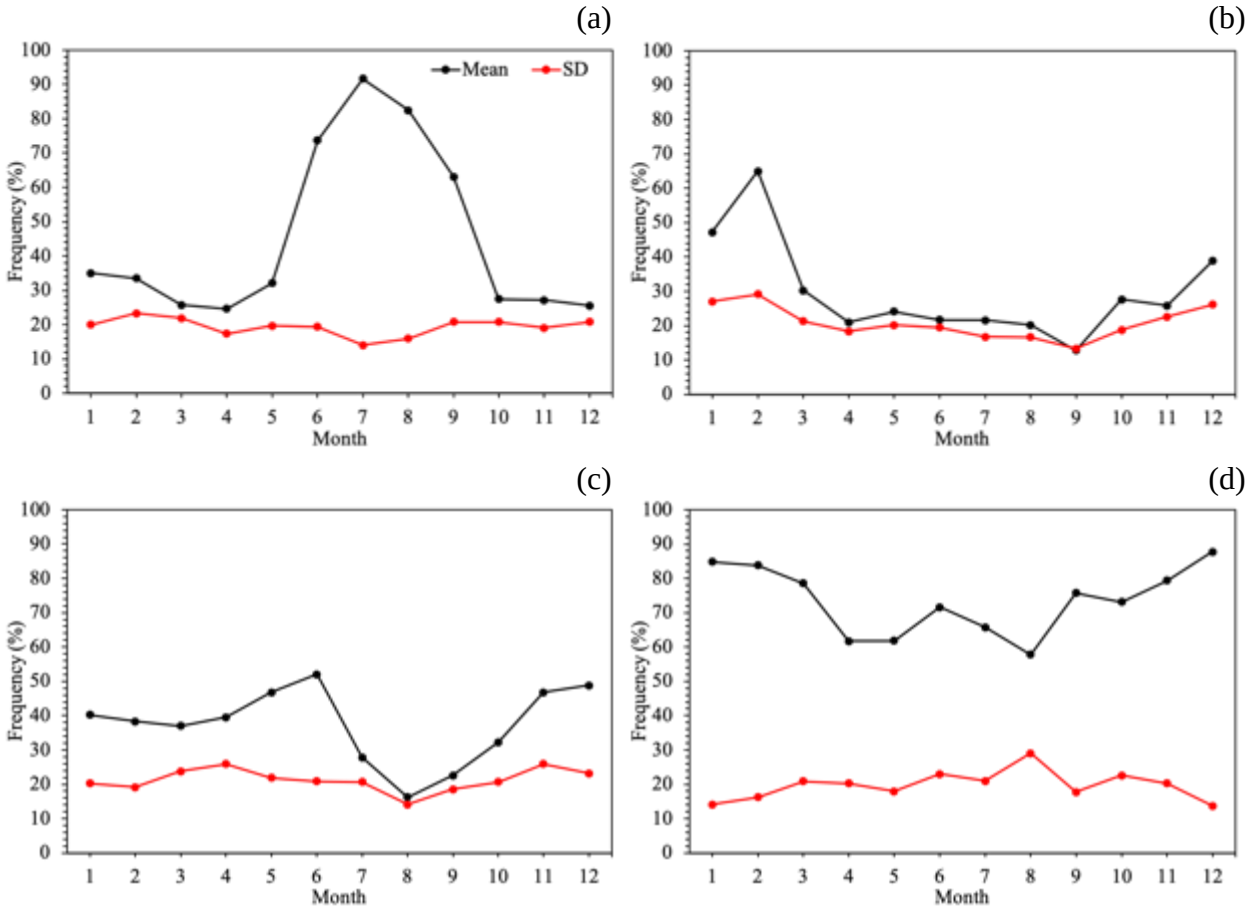

Figure 3.9. Monthly mean (black) and standard deviation (red) of blocking frequency for each quadrant of the Arctic, Quadrant (a) I, (b) II, (c) III, and (d) IV using the adjusted PH03 method.

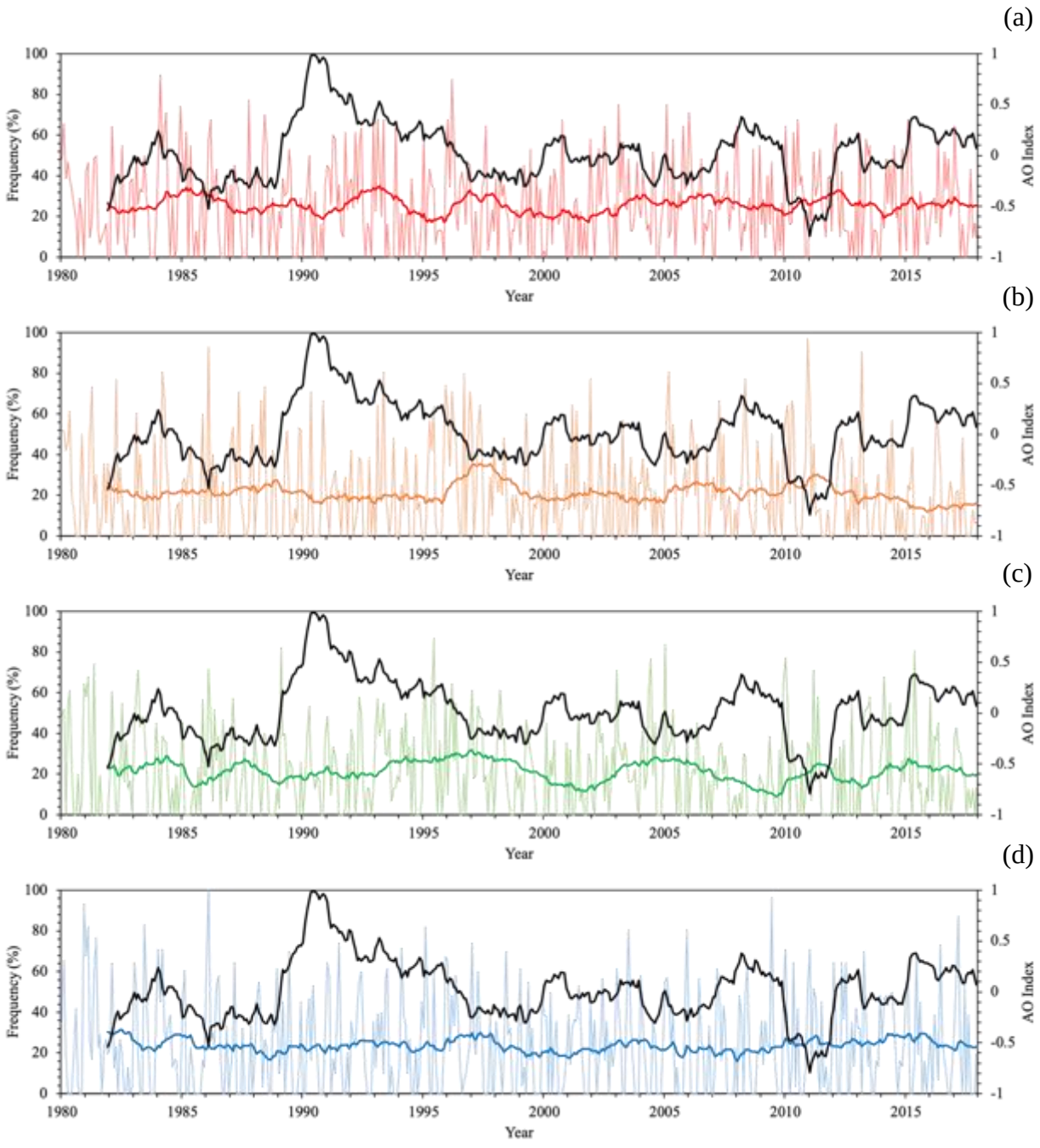

Figure 3.10. Monthly blocking frequency and a two-year running mean of blocking frequency for each quadrant of the Arctic using the adjusted TM90, Quadrant (a) I (red), (b) II (orange), (c) III (green), (d) IV (blue), and a two-year running mean of AO Index Values (black).

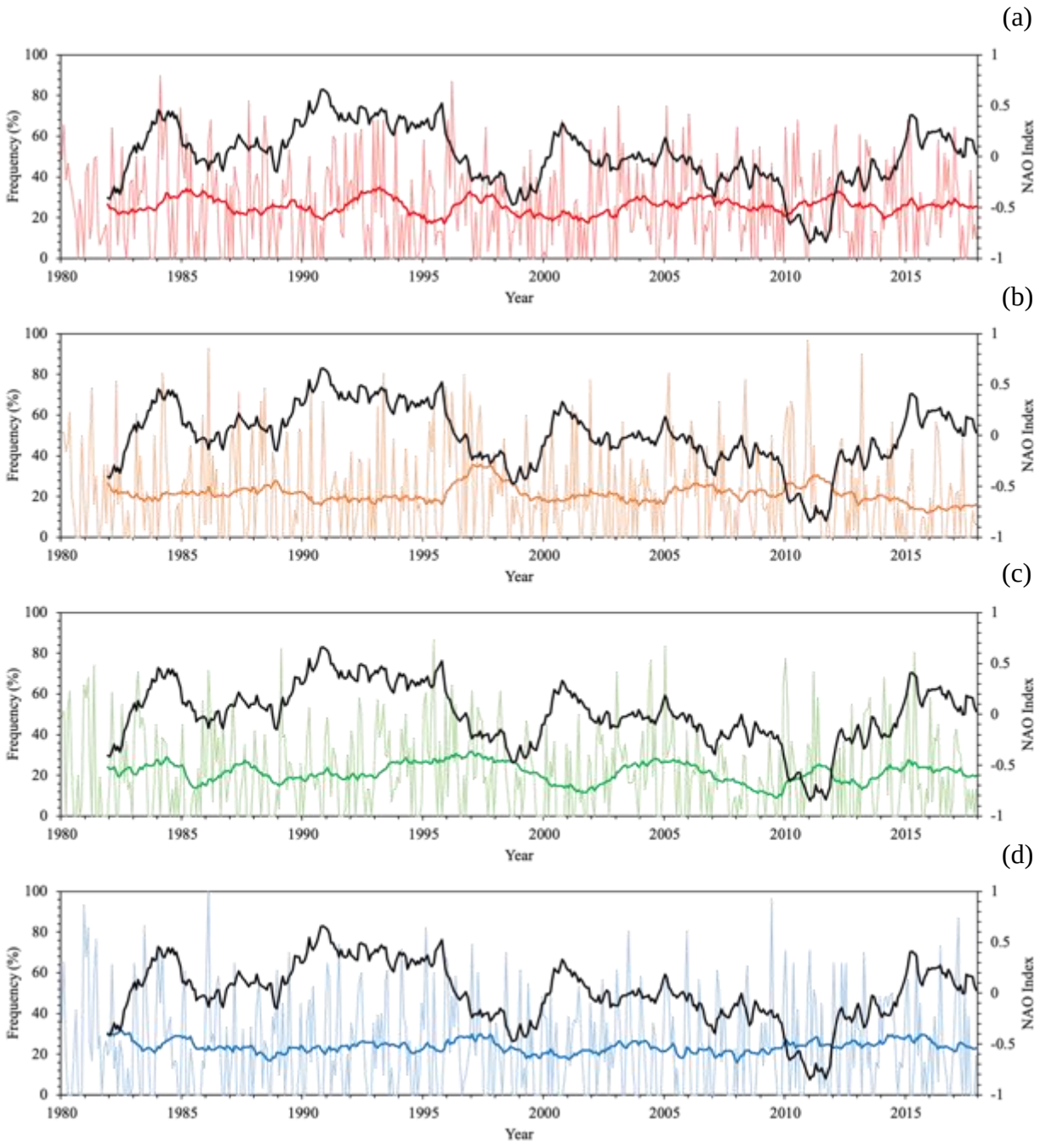

Figure 3.11. Monthly blocking frequency and a two-year running mean of blocking frequency for each quadrant of the Arctic using the adjusted TM90, Quadrant (a) I (red), (b) II (orange), (c) III (green), (d) IV (blue), and a two-year running mean of NAO Index Values (black).

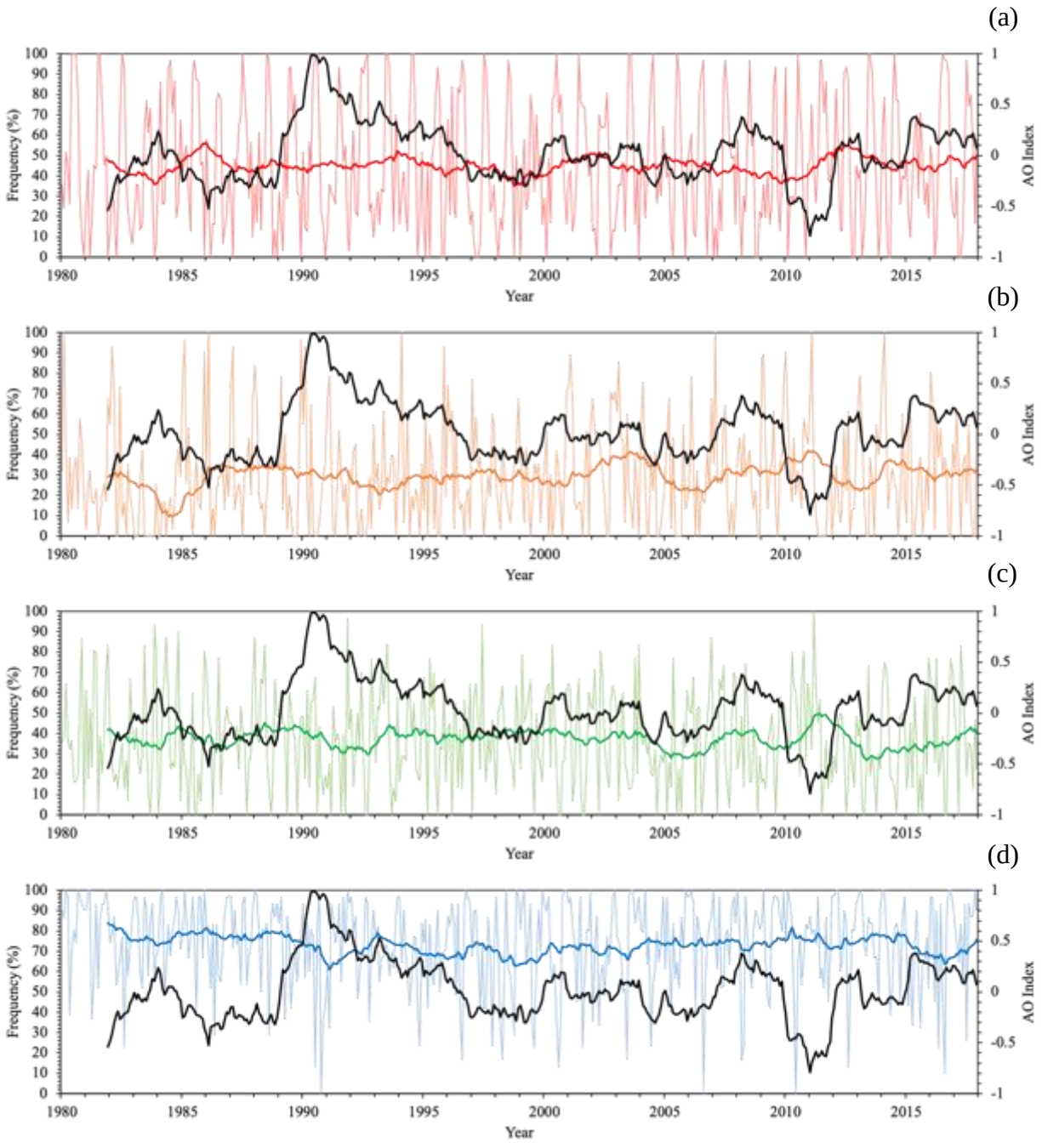

Figure 3.12. Monthly blocking frequency and a two-year running mean of blocking frequency for each quadrant of the Arctic using the adjusted PH03, Quadrant (a) I (red), (b) II (orange), (c) III (green), (d) IV (blue), and a two-year running mean of AO Index Values (black).

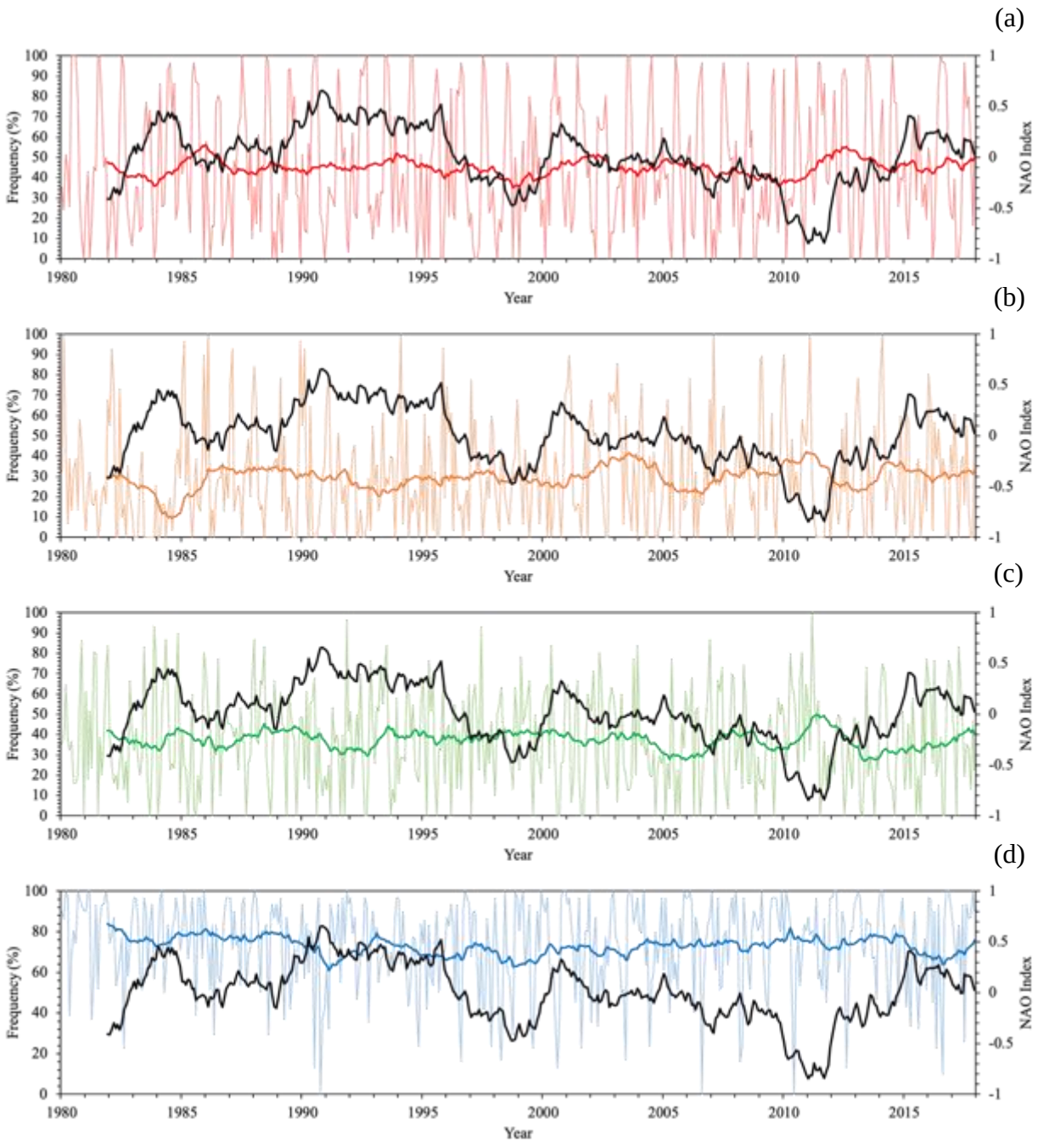

Figure 3.13. Monthly blocking frequency and a two-year running mean of blocking frequency for each quadrant of the Arctic using the adjusted PH03, Quadrant (a) I (red), (b) II (orange), (c) III (green), (d) IV (blue), and a two-year running mean of NAO Index Values (black).

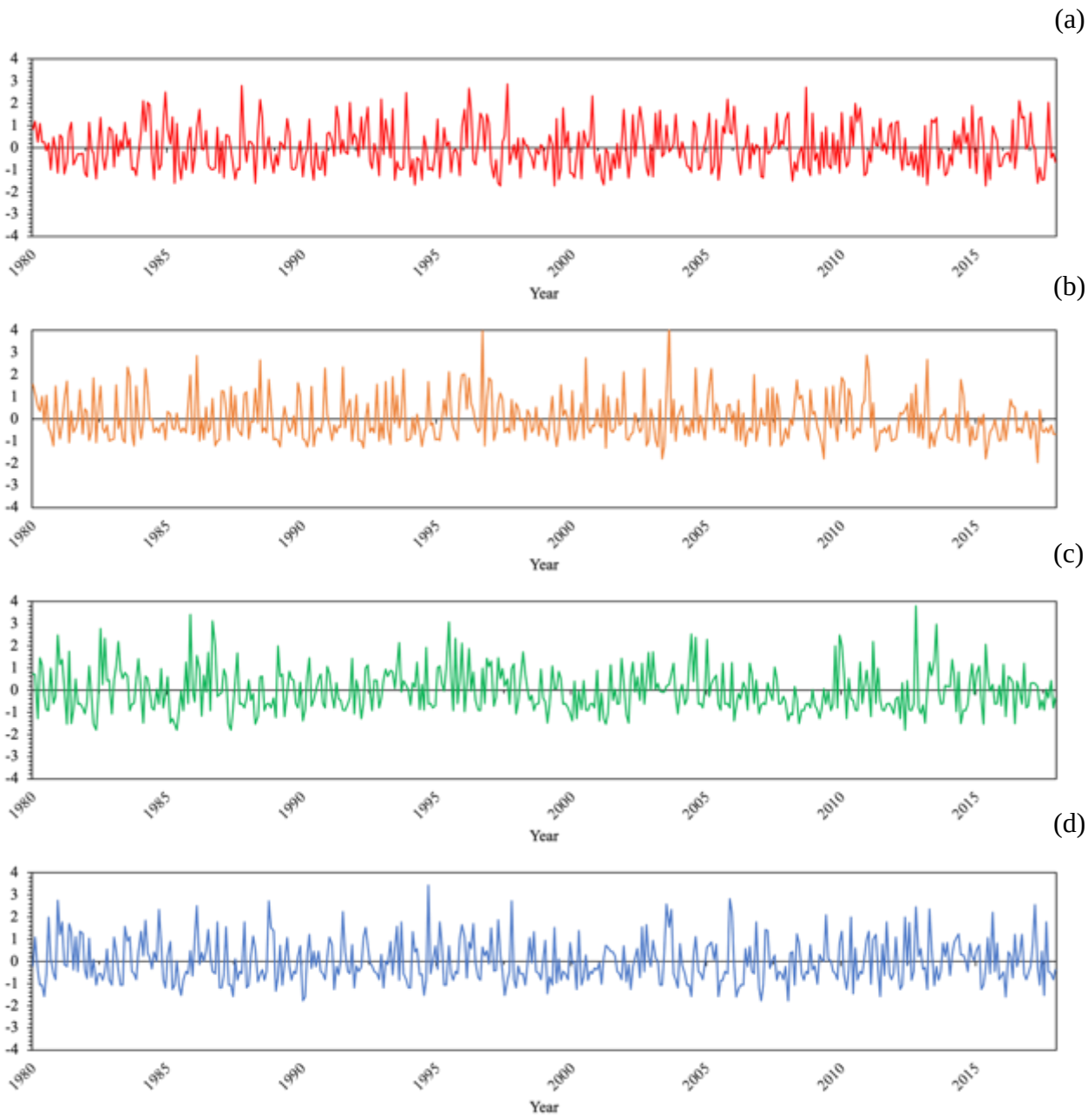

Figure 3.14. Seasonally standardized monthly blocking frequency or each quadrant of the Arctic using the adjusted TM90, Quadrant (a) I (red), (b) II (orange), (c) III (green), (d) IV (blue).

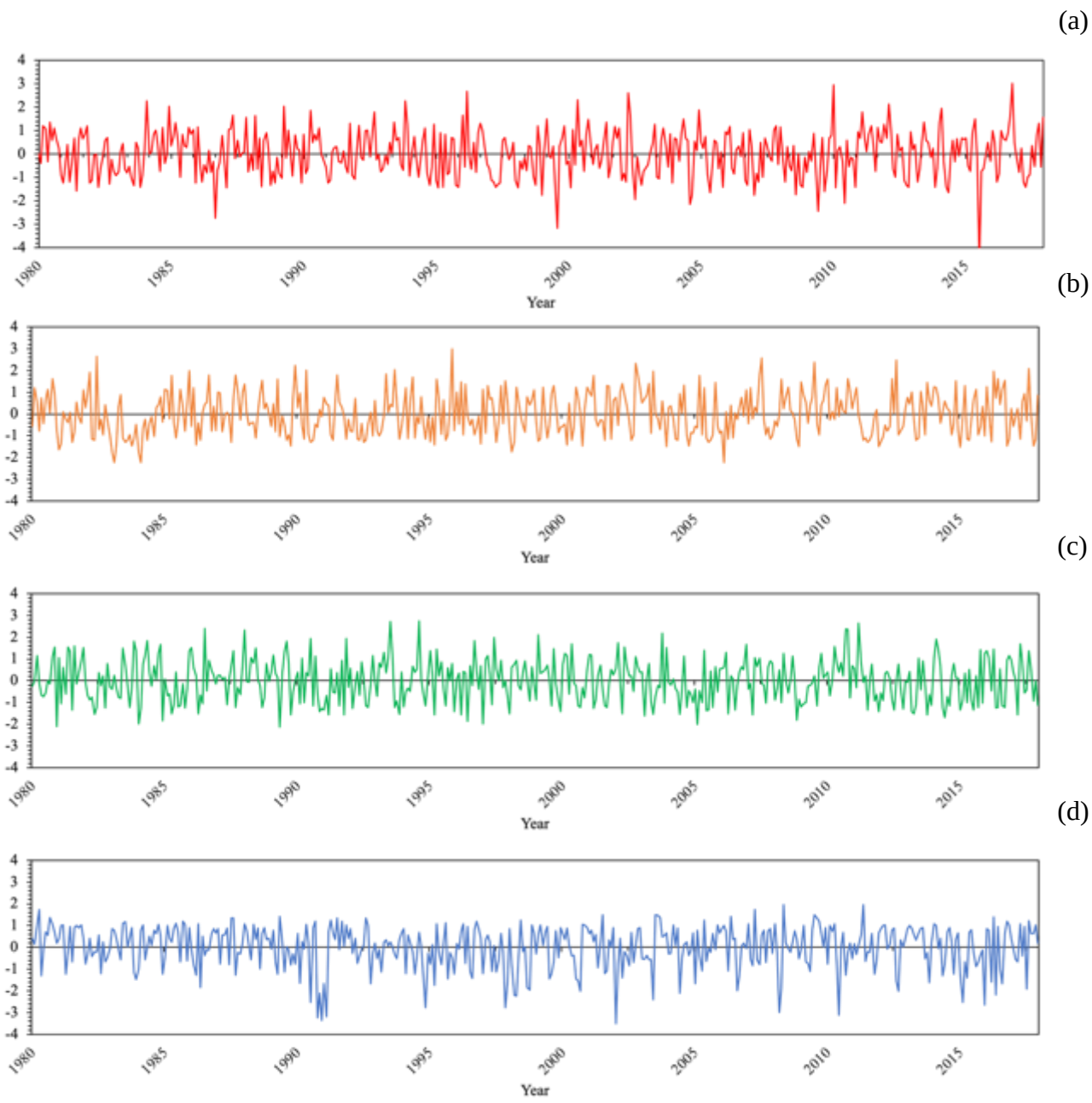

Figure 3.15. Seasonally standardized monthly blocking frequency or each quadrant of the Arctic using the adjusted PH03, Quadrant (a) I (red), (b) II (orange), (c) III (green), (d) IV (blue).

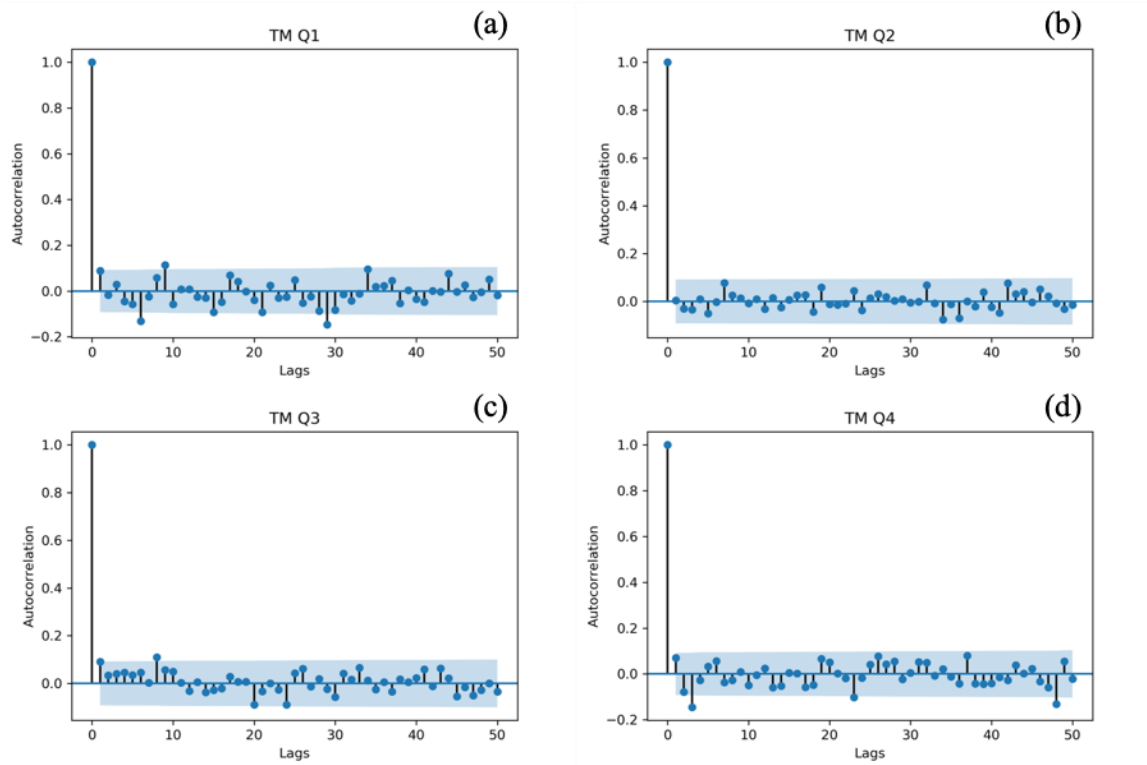

Figure 3.16. Autocorrelation for each quadrant of the Arctic using the adjusted TM90, Quadrant (a) I, (b) II, (c) III, and (d) IV.

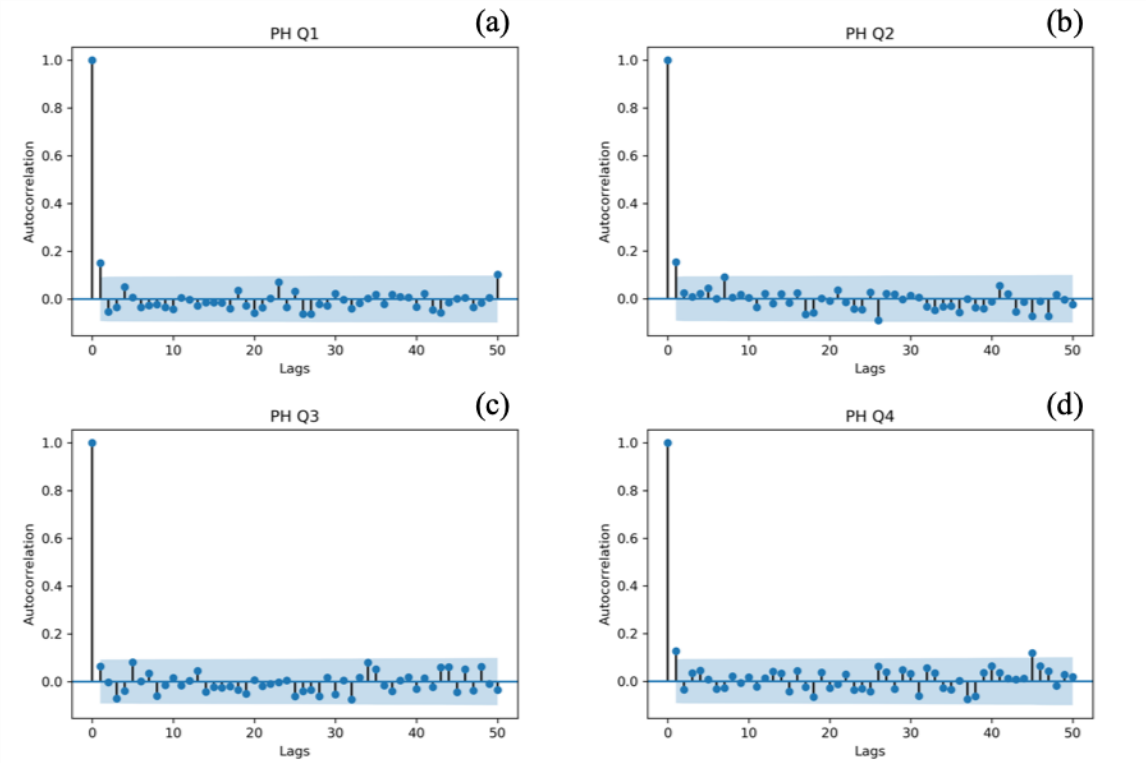

Figure 3.17. Autocorrelation for each quadrant of the Arctic using the adjusted PH03, Quadrant (a) I, (b) II, (c) III, and (d) IV.

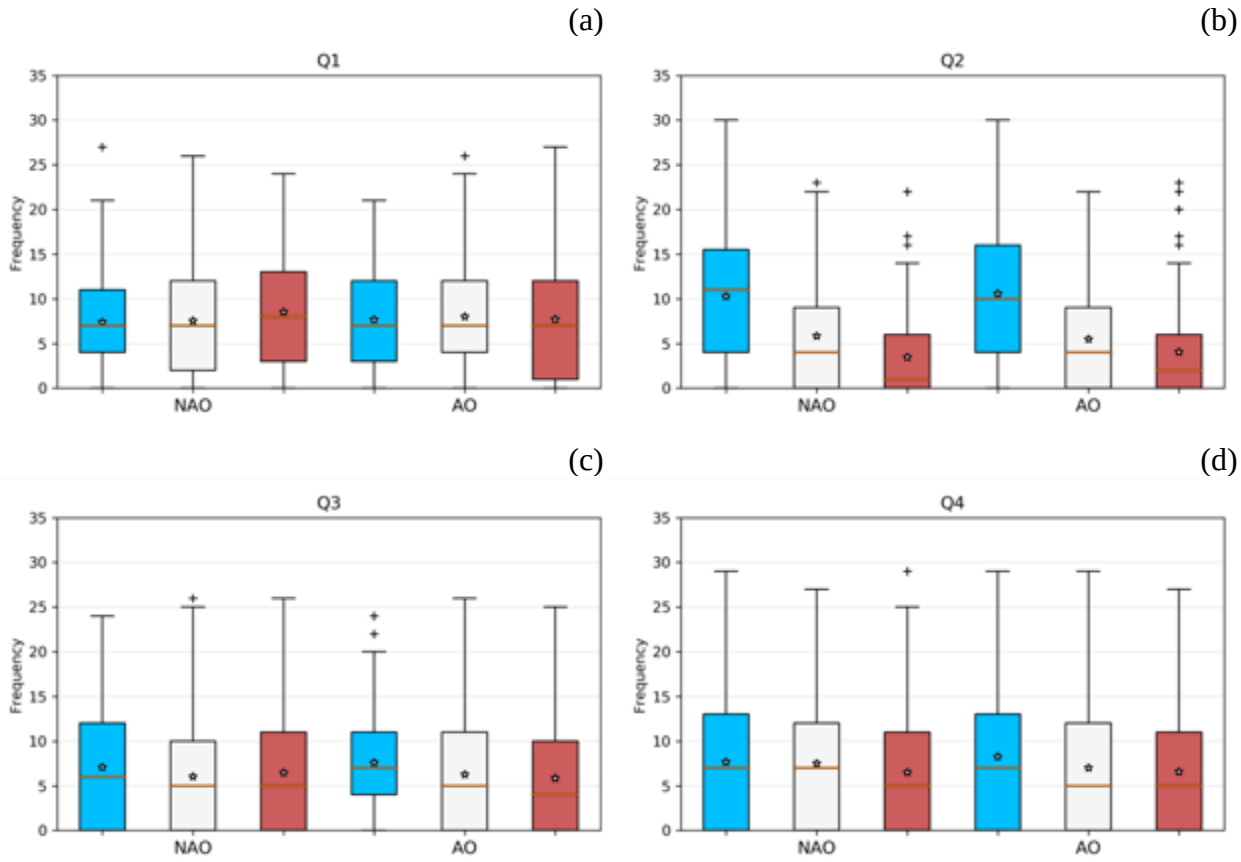

Figure 3.18. Annual blocking frequency using the adjusted TM90 during negative (blue), neutral (grey), and positive (red) phases of both NAO and AO for Quadrant (a) I, (b) II, (c) III, and (d) IV. The star indicates the mean, and the red line indicates the median of the sample.

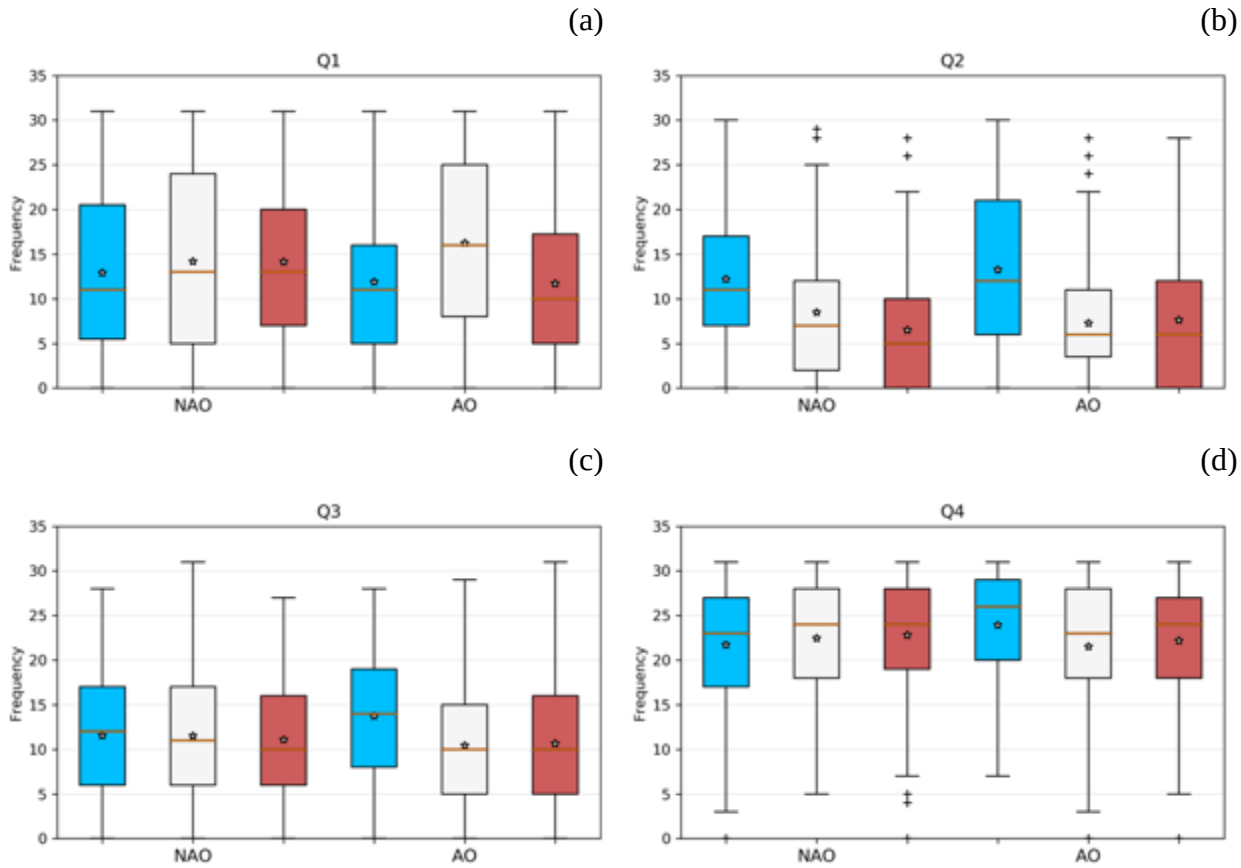

Figure 3.19. Annual blocking frequency using the adjusted PH03 during negative (blue), neutral (grey), and positive (red) phases of both NAO and AO for Quadrant (a) I, (b) II, (c) III, and (d) IV. The star indicates the mean, and the red line indicates the median of the sample.

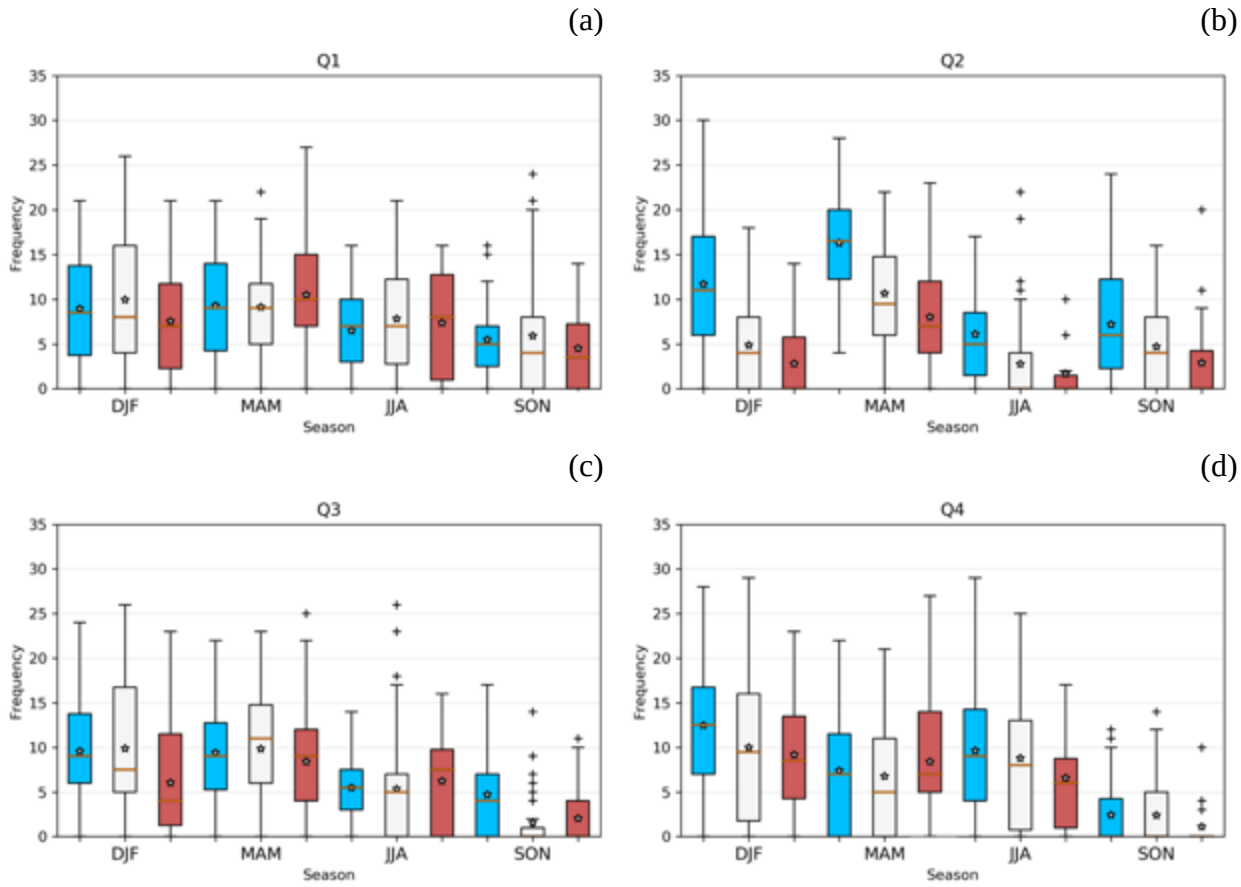

Figure 3.20. Seasonal blocking frequency using the adjusted TM90 during negative (blue), neutral (grey), and positive (red) phases of the AO for Quadrant (a) I, (b) II, (c) III, and (d) IV. The star indicates the mean, and the red line indicates the median of the sample.

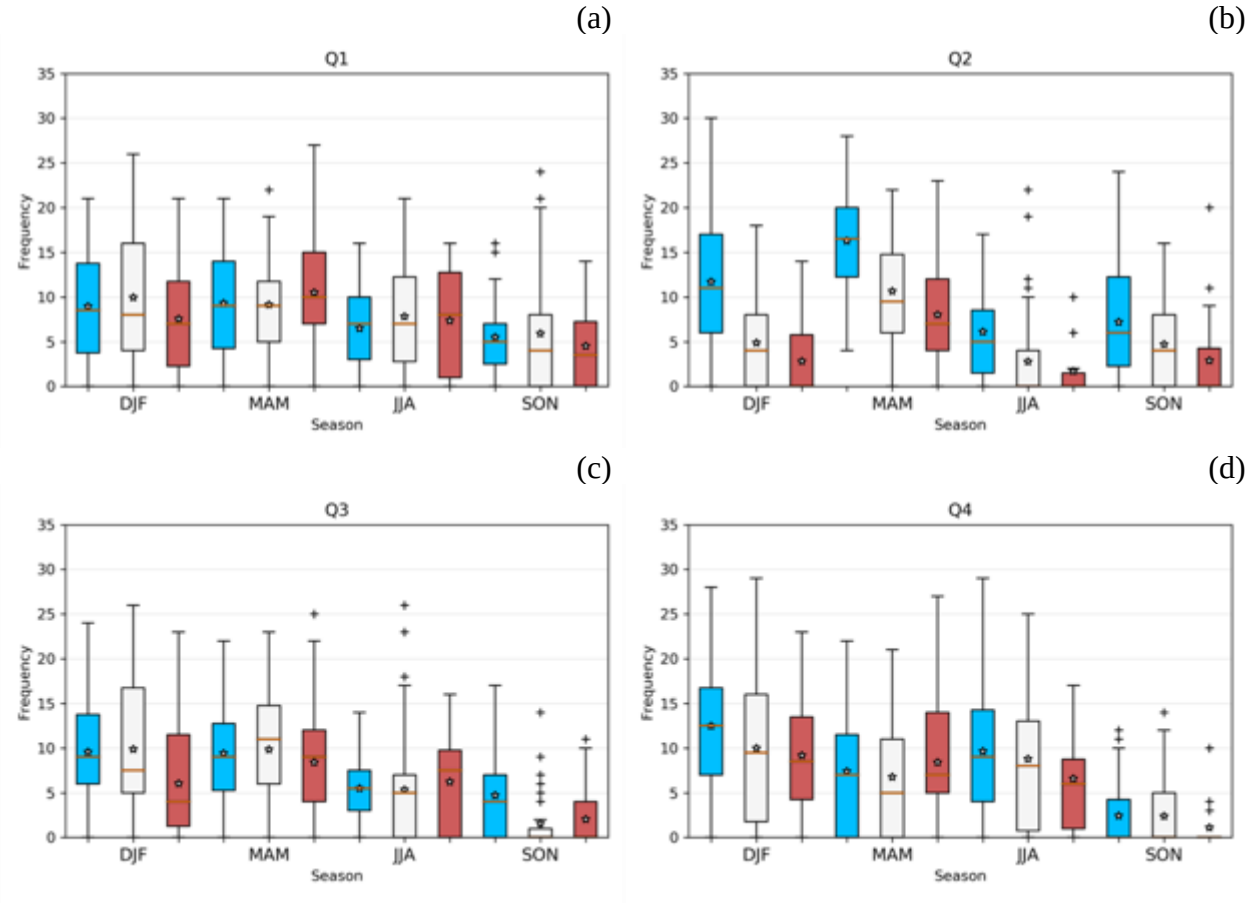

Figure 3.21. Seasonal blocking frequency using the adjusted TM90 during negative (blue), neutral (grey), and positive (red) phases of the NAO for Quadrant (a) I, (b) II, (c) III, and (d) IV. The star indicates the mean, and the red line indicates the median of the sample.

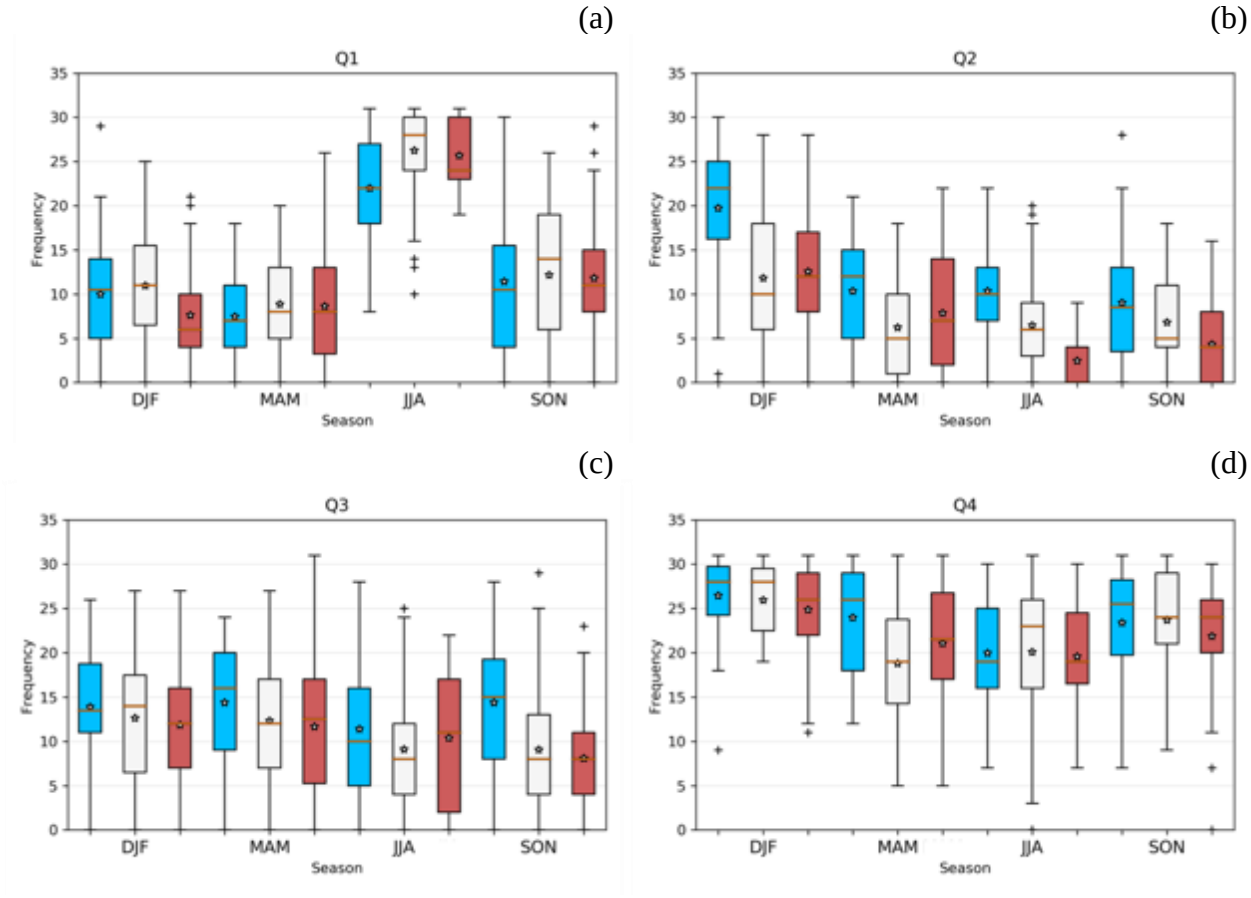

Figure 3.22. Seasonal blocking frequency using the adjusted PH03 during negative (blue), neutral (grey), and positive (red) phases of the AO for Quadrant (a) I, (b) II, (c) III, and (d) IV. The star indicates the mean, and the red line indicates the median of the sample.

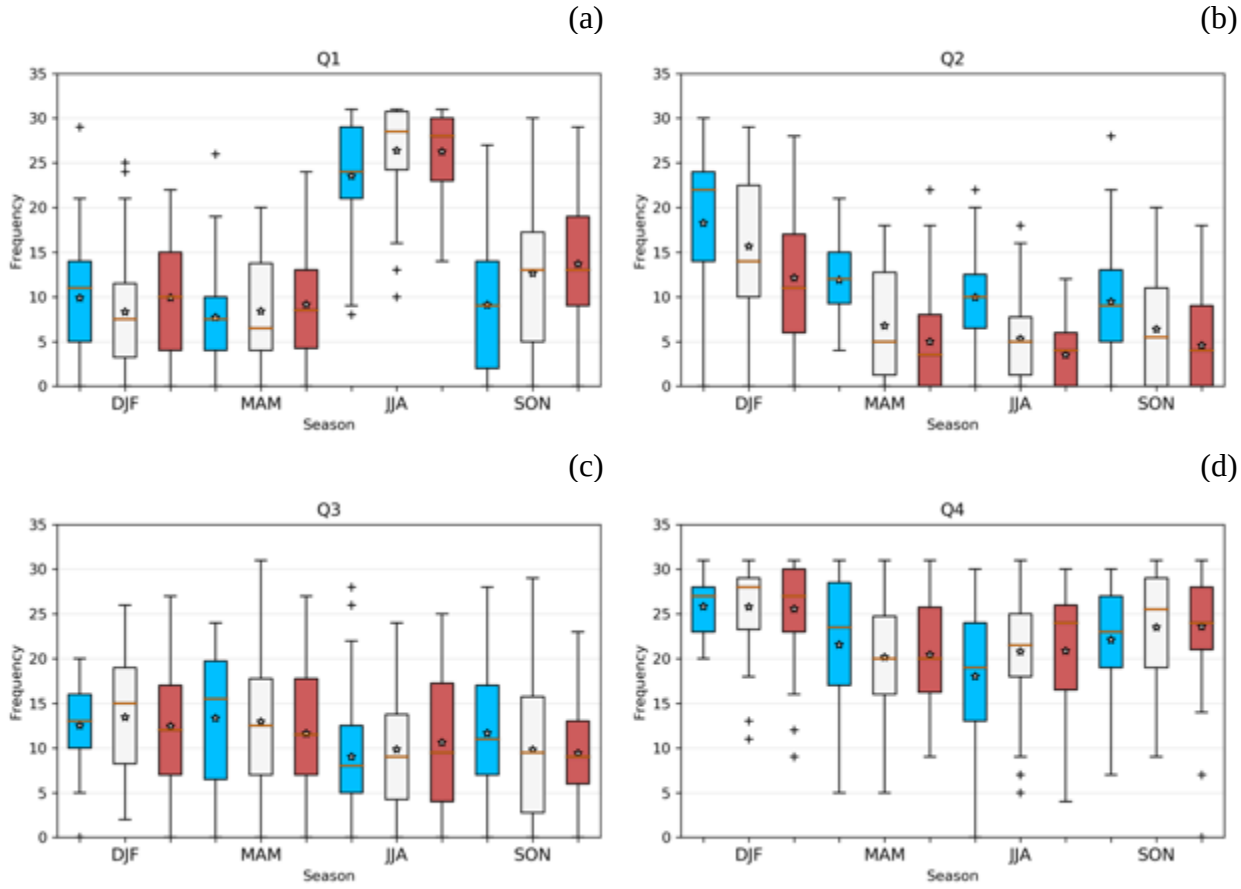

Figure 3.23. Seasonal blocking frequency using the adjusted PH03 during negative (blue), neutral (grey), and positive (red) phases of the NAO for Quadrant (a) I, (b) II, (c) III, and (d) IV. The star indicates the mean, and the red line indicates the median of the sample.

CHAPTER 4

CONCLUSION

Atmospheric blocking has major implications in the Arctic as the resulting sensible and latent head advection and effects of cloud cover on radiative processes alter the surface energy budget. The surface energy budget, in turn, affects patterns of temperature and precipitation, leading to changes in snow accumulation and ice melt that drive sea ice distribution and ice sheet surface mass balance. Furthermore, it is important to better understand atmospheric blocking in relation to low, frequency, large-scale atmospheric variability (i.e., atmospheric teleconnections). The effects of atmospheric blocking across the Arctic are myriad. For example, Ural-Siberian blocking promotes a cold East Asian winter monsoon, where a block positioned upstream of Siberia during the winter is associated with enhanced northerly cold air advection that increases mass convergences in the upper troposphere (Ding 1990; Cheung et al. 2012). This in turn intensifies the surface Siberian high and leads to a cold air outbreak in East Asia (Ding 1990; Cheung et al. 2012). Additionally, the advection of relatively warm subtropical airmasses as a result of increased blocking are contributing to the further acceleration of Greenland Ice Sheet surface melt (Fettweis et al. 2013; Hanna et al. 2014; Delhasse et al. 2018; Hofer et al. 2019). Diabatic latent heat release associated with extreme moisture transport may develop and strengthen blocking patterns even further (Pfahl et al. 2015; Grams and Archambault 2016; O'Reilly et al. 2016; Mattingly et al. 2018). The physical mechanisms associated with moisture transport, including the formation of low-level clouds and an enhanced water vapor greenhouse

effect, influence the melt of the ice sheet as well as sea-ice (Luo et al. 2016a; Binder et al. 2017; Mattingly et al. 2018).

Unlike previous research, this thesis created an overarching examination of atmospheric blocking in the Arctic rather than focus on a single region like Greenland or the Ural-Siberian Mountains (McLeod and Mote 2016; Luo et al. 2016a; Luo et al. 2016b). Winter and summer are most commonly the focus of similar studies; however, few examine the entire year especially the transitional seasons (Kim and Ha 2014; Luo et al. 2016a). This thesis examined how blocking and teleconnections are related during all four seasons.

The modified PH03 method identified far more atmospheric blocking events compared to the adjusted TM90, just as the original PH03 identified more events than the original TM90; the PH03 was able to capture additional blocking pattern types that were not identified with the original TM90 method (Pelly and Hoskins 2003). Comparing these two methods of blocking identification aided in further addressing the vast differences in blocking indices discussed in Woolings et al. (2018), who found that no single method is able to identify all blocking pattern types. As a result, no one index can be portrayed as an example of a completely accurate representation of atmospheric blocking pattern frequency of the Arctic. Compared to the TM90 method, the PH03 method is able to identify more types of blocking events because the reversal of the meridional gradient of potential temperature is a more robust indicator of blocking compared to changes to the easterly flow pattern, especially when identifying Omega blocks in the Pacific (PH03), as discussed in Chapter 2. However, before any statements on the most effective method are made future work needs to compare the approaches to other methodologies as well as which types of blocking events are being captured by each method.

The PH03 method not only identified more blocking events than the TM90 method, but also had significant differences in blocking locations across all seasons. The PH03 method identified the most events in Quadrant IV (Ural-Siberia) and I (Europe) compared to the other two quadrants, while the TM90 method identified more blocking events for Quadrant I. The TM90 method showed less spatial variability in blocking frequency then the PH03 method. When comparing seasonally, the adjusted TM90 method identifies more winter (DJF) and spring (MAM) blocking events for Quadrants I, II, and III while more DJF and summer (JJA) events are identified for Quadrant IV. The adjusted PH03 method, identifies more JJA and fall (SON) blocking events for Quadrant I. Quadrant II has more blocking events identified during DJF and MAM, while Quadrants III and IV blocking events are more evenly distributed over all four seasons. However, these findings differ slightly from the results of previous studies. For example, Tyrlis and Hoskins (2008) found that blocking activity is largest over Europe and the eastern Atlantic Ocean in the winter, and eastern Europe and central Asia during the summer. Additionally, Trigo et al. (2004) found that blocks most typically occur in winter and spring, while both approaches in this thesis found a significant number of blocking events also during the summer. Using the original form of the PH03, Euro-Atlantic blocking activity is high in the summer before peaking in autumn, followed by significantly lower activity in winter and spring (Pelly and Hoskins 2003); the results of this thesis differ from this possibly due to the fact that the original work only used five years of data. In the Pacific, autumn is the most inactive season while blocking frequency remains approximately constant in the winter and spring before peaking in the summer over the central Pacific and decreasing along the west coast of North America, so results differ slightly with the adjusted form (Pelly and Hoskins 2003). The

disparities between the adjusted TM90 and PH03 approaches blocking frequency further verifies Woolings et al. (2018) finding that no single index is able to identify all blocking events.

Based on the approaches of blocking identification used for this thesis, no significant trends in atmospheric blocking can be determined because all of the variability across the data record can be explained by the seasonality of blocking frequency across the Arctic. Thus, it is difficult to make any statements regarding how blocking will change in the future if the climate community is unable to determine how blocking has changed to date. This possibly has to do with the methodological approaches used to identify blocking, so until models are able to better capture atmospheric blocking it is difficult to make any inference regarding future blocking changes (Woolings et al. 2018). Additionally, the length of the record and statistical tests used in previous studies may explain the differences in results presented here compared to previous studies. Compared to previous studies, this thesis examined the trend in blocking frequency over a much longer period of record, while many examined seasonal trends in blocking (e.g., Francis and Vavrus 2012; Tang et al. 2013), which is a possible explanation for the differences in results. Despite the large differences in frequency and location between the two blocking identification approaches, neither approach identified a trend in blocking frequency, which lend additional credence to this finding. Based on the results of this thesis and previous studies, there is significant inconsistency in regard to trends in blocking frequency. The results of this thesis show no evidence for an increasing in blocking frequency in the Arctic, which contradicts earlier studies. For example, Overland et al. (2012) found an increase in blocking after 2007; while they stated that the cause of increased blocking is not completely understood. Previous studies also have found that the decline in sea ice has led to an increase in atmospheric blocking frequency for North America and Europe in winter, summer, and fall (e.g., Liu et al. 2012;

Francis and Vavrus 2012; Tang et al. 2013). However, there is good agreement among models on an overall decline in blocking in the future (Hanna et al. 2018a, 2018b; Woolings et al. 2018). One could therefore question whether any previous increase in blocking, as identified in earlier studies, has since been mitigated by the anticipated decrease in blocking associated with anthropogenic warming. This thesis is unable to address that question, but it presents an important hypothesis that should be the basis for future research.

In addition to the seasonal distribution of blocking frequency across the Arctic, the relationship between the AO and NAO were explored. Similar to previous studies, this thesis found increased blocking frequency is related to the negative phases of both teleconnection patterns (e.g. Shabbar et al. 2000; Woolings et al. 2010; Davini et al. 2012; Kim and Ha 2014; Hassanzadeh and Kuang 2015). The few differences in these relationships identified in this thesis and previous work largely point to the immense difficulty to determine the accurate frequencies in blocking across the Arctic. No single index alone can be taken as a completely accurate representation of atmospheric blocking frequency.

This thesis serves as a form of exploratory data analysis to create an overarching understanding of the frequency of atmospheric blocking across the Arctic during the past four decades and to better understand how blocking is further influenced by low-frequency teleconnections like the AO and NAO. It important to understand the distribution of the seasonality of Arctic blocking frequency in order to understand changes in local climate. Additionally, understanding how the frequency of blocking is changing over time should allow climate scientists to better predict how it could change in the future.

REFERENCES

Altenhoff, A.M., O. Martius, M. Croci-Maspoli, C. Schwierz, and H.C. Davies, 2008: Linkage of atmospheric blocks and synoptic-scale Rossby waves: A climatological analysis. *Tellus A: Dynamic Meteorology and Oceanography*, **60**, 1053–1063. doi:10.1111/j.1600-0870.2008.00354.x.

Ballinger, T.J., E. Hanna, R.J. Hall, J. Miller, M.H. Ribergaard, and J.L. Høyer, 2018: Greenland coastal air temperatures linked to Baffin Bay and Greenland Sea ice conditions during autumn through regional blocking patterns. *Climate Dynamics*, **50**, 83–100. doi: 10.1007/s0038/2-017-3583-3.

Barnston, A.G., and R.E. Livezey, 1987: Classification, seasonality and persistence of low-frequency atmospheric circulation patterns. *Monthly Weather Review*, **115**, 1083–1126. doi: 10.1175/`520-0493(1987)115<1083:CSAPOL>2.0.CO;2.

Barriopedro, D., R. García-Herrera, A.R. Lupo, and E. Hernández, 2006: A climatology of Northern Hemisphere blocking. *Journal of Climate*, **19**, 1042–1063. doi: 10.1175/JCLI3678.1.

Benedict, J.J., S. Lee, and S.B. Feldstein, 2004: Synoptic view of the North Atlantic Oscillation. *Journal of Atmospheric Science*, **61**, 121–144. doi: 10.1175/1520-0469(2004)061<0121:SVOTNA>2.0CO;2.

Berggren, R., B. Bolin, and C.G. Rossby, 1949: An aerological study of zonal motion, its perturbations and break-down. *Tellus*, **1**, 14–37. doi: 10.1111/j.2153-3490.1949.tb01257.x.

Binder, H., M. Boettcher, C.M. Grams, H. Joos, S. Pfahl, and H. Wernli, 2017: Exceptional air mass transport and dynamical drivers of an extreme wintertime Arctic warm event. *Geophysical Research Letters*, **44**, 12028–12036. doi: 10.1002/2017GL075841.

Buehler, T., C.C. Raible, and T.F. Stocker, 2011: The relationship of winter season North Atlantic blocking frequencies to extreme cold or dry spells in the ERA-40. *Tellus*, **63**, 212–222. doi: 10.1111/j.1600-0870.2010.00492.x.

Charney, J.G., J. Shukla, and K.C. Mo, 1981: Comparison of a barotropic blocking theory with observation. *Journal of the Atmospheric Sciences*, **38**, 762–779. doi: 10.1175/1520-0469(1981)038<0762:COABBT>2.0.CO;2.

Chen, W.Y., and H. van den Dool, 2003: Sensitivity of teleconnection patterns to the sign of their primary action center. *Monthly Weather Review*, **131**, 2885–2899. doi: 10.1175/1520-0493(2003)131<2885:SOTPTT>2.0.CO;2

Cheung, H.N., W. Zhou, H.Y. Mok, and M.C. Wu, 2012: Relationship between Ural–Siberian blocking and the East Asian winter monsoon in relation to the Arctic Oscillation and the El Niño–Southern Oscillation. *Journal of Climate*, **25**, 4242–4257. doi: 10.1175/JCLI-D-11-00225.1

Cheung, H.N., W. Zhou, H.Y. Mok, M.C. Wu, and Y. Shao, 2013a: Revisiting the climatology of atmospheric blocking in the Northern Hemisphere. *Advances in Atmospheric Sciences*, **30**, 397–410. doi: 10.1007/s00376-012-2006-y.

Cheung, H.N., W. Zhou, Y. Shao, W. Chen, H.Y. Mok, and M.C. Wu, 2013b: Observational climatology and characteristics of wintertime atmospheric blocking over Ural–Siberia. *Climate Dynamics*, **41**, 63–79. doi: 10.1007/s00382-012-1587-6

Conover, W. J., 1999: *Practical Nonparametric Statistics*. John Wiley & Sons Inc., 592 pp.

Conover, W. J., and R.L. Iman, 1979: On multiple-comparisons procedures. *NM, USA: Los Alamos Scientific Lab*, 1–17.

Croci-Maspoli, M., C. Schwierz, and H.C. Davies, 2007: Atmospheric blocking: space-time links to the NAO and PNA. *Climate Dynamics*, **29**, 713–725. doi: 10.1007/s00382-007-0259-4.

Davini, P., C. Cagnazzo, S. Gualdi, and A. Navarr, 2012a: Bidimensional diagnostics, variability, and trends of Northern Hemisphere blocking. *Journal of Climate*, **25**, 6496–6509. doi: 10.1175/JCLI-D-12-00032.1.

Davini, P., C. Cagnazzo, R. Neale, and J. Tribbia, 2012b: Coupling between Greenland blocking and the North Atlantic Oscillation pattern. *Geophysical Research Letters*, **39**. doi: 10.1029/2012GL052315.

Davini, P., and F. D'Andrea, 2016: Northern hemisphere atmospheric blocking representation in global climate models: Twenty years of improvements? *Journal of Climate*, **29**, 8823–8840. doi: 10.1175/JCLI-D-16-0242.1.

Dee, D.P., S.M. Uppala, A.J. Simmons, P. Berrisford, P. Poli, S. Kobayashi, U. Andrae, M.A Balmaseda, G. Balsamo, P. Bauer, P. Bechtold, A.C.M Beljaars, L. van de Berg, J. Bidlot, N. Bormann, C. Delsol, R. Dragani, M. Fuentes, A.J. Geer, L. Haimberger, S.B. Healy, H. Hersbach, E.V. Hólm, L. Isaksen, P. Kållberg, M. Köhler, M. Matricardi, A.P. McNally, B.M. Monge-Sanz, J.J. Morcrette, B.K. Park, C. Peubey, P. de Rosnay, C. Tavolato, J.N. Thépaut, and F. Vitart, 2011: The ERA-Interim reanalysis: Configuration and performance of the data assimilation system. *Quarterly Journal of the Royal Meteorological Society*, **137**, 553–597. doi: 10.1002/qj.828.

Delhasse, A., X. Fettweis, C. Kittel, C. Amory, and C. Agosta, 2018: Brief communication: Impact of the recent atmospheric circulation change in summer on the future surface

mass balance of the Greenland Ice Sheet. *Cryosphere*, **12**, 3409–3418. doi:10.5194/tc-2018-65.

Diao, Y., J. Li, and D. Luo, 2006: A new blocking index and its application: Blocking action in the Northern Hemisphere. *Journal of Climate*, **19**, 4819–4839. doi: 10.1175/JCLI3886.1.

Dickey, D.A., and W.A. Fuller. 1979: Distribution of the estimators for autoregressive time series with a unit root. *Journal of the American Statistical Association*, **74**, 427–431. doi: 10.1080/01621459.1979.10482531.

Ding, Y., 1990: Buildup, air-mass transformation and propagating of Siberian high and its relations to cold surge in East Asia. *Meteorology and Atmospheric Physic*s, **44**, 281–292. doi: 10.1007/BF01026822.

Dole, R.M., and N.D. Gordon, 1983: Persistent anomalies of the extratropical Northern Hemisphere wintertime circulation: Geographical distribution and regional persistence characteristics. *Monthly Weather Review*, **111**, 1567–1586. doi: 10.1175/1520-0493(1983)111<1567:PAOTEN>2.0.C);2.

Drouard, M., and T. Woollings, 2018: Contrasting mechanisms of summer blocking over western Eurasia. *Geophysical Research Letters*, **45**, 12040–12048. doi: 10.1029/2018GL079894.

Estrada, F., P. Perron, C. Gay-García, and B. Martínez-López, 2013: A time-series analysis of the 20th Century climate simulations produced for the IPCC's Fourth Assessment Report. *PLoS One*, **8**, 60017. doi: 10.1371/journal.pone.0060017.

Fang, Z.F., 2004: Statistical relationship between the northern hemisphere sea ice and atmospheric circulation during wintertime. *In Observation, Theory and Modeling of*

Atmospheric Variability: *Selected Papers of Nanjing Institute of Meteorology Alumni in Commemoration of Professor Jijia Zhang*, 131–141. doi: 10.1142/9789812791139_0006.

Fatichi, S., and E. Caporali, 2009: A comprehensive analysis of changes in precipitation regime in Tuscany. *International Journal of Climatology*, **29**, 1883–1893. doi: 10.1002/joc.1921.

Fettweis, X., E. Hanna, C. Lang, A. Belleflamme, M. Erpicum, and H. Gallée, 2013: Brief communication: Important role of the midtropospheric atmospheric circulation in the recent surface melt increase over the Greenland ice sheet. *The Cryosphere*, **7**, 241–248. doi: 10.5194/tc-7-241-2013.

Francis, J.A., and S.J. Vavrus, 2012: Evidence linking Arctic amplification to extreme weather in mid-latitudes. *Geophysical Research Letters*, **39**, LO6801. doi: 10.1029/2012GL051000.

Gabriel, A., and D. Peters, 2008: A diagnostic study of different types of Rossby wave breaking events in the northern extratropics. *Journal of the Meteorological Society of Japan*, **86**, 613–631. doi: 10.2151/jmsj.86.613.

García-Herrera, R., and D. Barriopedro, 2006: Northern Hemisphere snow cover and atmospheric blocking variability. *Journal of Geophysical Research: Atmospheres*, **111**, D21104. doi: 10.1029/2005JD006975.

Geb, M., 1966: Synoptic-statistical investigations into the initiation of blocking action over the North Atlantic and Europe. *Meteorologishe Abhandlungen,* **69**, 89.

Grams, C.M., and H.M. Archambault, 2016: The key role of diabatic outflow in amplifying the midlatitude flow: A representative case study of weather systems surrounding western North Pacific extratropical transition. *Monthly Weather Review*, **144**, 3847–3869. doi: 10.1175/MWR-D-15-0419.1.

Hanna, E., T.E. Cropper, R.J. Hall, and J. Cappelen, 2016: Greenland Blocking Index 1851–2015: A regional climate change signal. *International Journal of Climatology*, **36**, 4847–4861. doi: 10.1002/joc.4673.

Hanna, E., T.E. Cropper, P.D Jones, A.A. Scaife, and R. Allan, 2015: Recent seasonal asymmetric changes in the NAO (a marked summer decline and increased winter variability) and associated changes in the AO and Greenland Blocking Index. *International Journal of Climatology*, **35**, 2540–2554. doi: 10.1002joc.4157.

Hanna, E., R.J. Hall, T.E. Cropper, T.J. Ballinger, L. Wake, T. Mote, and J. Cappelen, 2018a: Greenland blocking index daily series 1851–2015: Analysis of changes in extremes and links with North Atlantic and UK climate variability and change. *International Journal of Climatology*, **38**, 3546-3564. doi: 10.1002joc.5516.

Hanna, E., X. Fettweis, and R.J. Hall, 2018b: Brief communication: Recent changes in summer Greenland blocking captured by none of the CMIP5 models. *The Cryosphere*, **12**, 3287–3292. doi: 10.5194/tc-12-3287-2018.

Hanna, E., X. Fettweis, S.H. Mernild, J. Cappelen, M.H. Ribergaard, C.A. Shuman, K. Steffen, L. Wood, and T.L. Mote, 2014: Atmospheric and oceanic climate forcing of the exceptional Greenland ice sheet surface melt in summer 2012. *International Journal of Climatology*, **34**, 1022–1037. doi: 10.1002/joc.3743.

Hanna, E., J.M. Jones, J. Cappelen, S.H. Mernild, L. Wood, K. Steffen, and P. Huybrechts, 2013: The influence of North Atlantic atmospheric and oceanic forcing effects on 1900–2010 Greenland summer climate and ice melt/runoff. *International Journal of Climatology*, **33**, 862–880. doi: 10.1002/joc.3475.

Hassanzadeh, P., and Z. Kuang, 2015: Blocking variability: Arctic amplification versus Arctic Oscillation. *Geophysical Research Letters*, **42**, 8586–8595. doi: 10.1002/2015GL065923.

Higgins, R.W., A. Leetmaa, and V.E. Kousky, 2002: Relationships between climate variability and winter temperature extremes in the United States. *Journal of Climate*, **15**, 1555–1572. doi: 10.1175/1520-0442(2002)015<1555:RBCVAW>2.0.CO;2.

Higgins, R.W., A. Leetmaa, Y. Xue, and A. Barnston, 2000: Dominant factors influencing the seasonal predictability of U.S. precipitation and surface air temperature. *Journal of Climate*, **13**, 3994–4017. doi: 10.1175/1520-0442(2000)013<3994:DFITSP>2.0.CO;2.

Higgins, R.W., Y. Zhou, and H.K. Kim, 2001: Relationships between El Niño-Southern Oscillation and the Arctic Oscillation: A climate-weather link. NCEP/Climate Prediction Center ATLAS No. 8, accessed 3 September 2018, https://www.cpc.ncep.noaa.gov/research_papers/ncep_cpc_atlas/8/toc.html.

He, Y., J. Huang, and M. Ji, 2014: Impact of land–sea thermal contrast on interdecadal variation in circulation and blocking. *Climate Dynamics*, **43**, 3267–3279. doi: 10.1007/s00382-014-2103-y.

He, Y., J. Huang, D. Li, Y. Xie, G. Zhang, Y. Qi, S. Wang, and S. Totz, 2018: Comparison of the effect of land-sea thermal contrast on interdecadal variations in winter and summer blockings. *Climate Dynamics*, **51**, 1275–1294. doi: 10.1007/s00382-017-3954-9.

Hofer, S., A.J. Tedstone, X. Fettweis, and J.L. Bamber, 2019: Cloud microphysics and circulation anomalies control differences in future Greenland melt. *Nature Climate Change*, **9**, 523–528. doi: 10.1038/s41558-019-0507-8.

Hoskins, B.J., M.E. McIntyre, and A.W. Robertson, 1985: On the use and significance of isentropic potential vorticity maps. *Quarterly Journal of the Royal Meteorological Society*, **111**, 877–946. doi: 10.1002/qj.49711147002.

Kim, S.H., and K.J. Ha, 2015: Two leading modes of Northern Hemisphere blocking variability in the boreal wintertime and their relationship with teleconnection patterns. *Climate Dynamics*, **44**, 2479–2491. doi: 10.1007/s00382-014-2304-4.

Kruskal, W.H., and W.A. Wallis, 1952: Use of ranks in one-criterion variance analysis. *Journal of the American Statistical Association*, **47**, 583–621 and errata, ibid. **48**, 907–911.

Larson, J., Y. Zhou, and R.W. Higgins, 2004: Characteristics of landfalling tropical cyclones in the United States and Mexico: Climatology and interannual variability. *Journal of Climate*, **18**, 1247–1262. doi: 10.1175/JCLI3317.1.

Lejenäs, H., and H. Øakland, 1983: Characteristics of northern hemisphere blocking as determined from long time series of observational data. *Tellus*, **35**, 350–362. doi: 10.1111/j.1600-0870.1983.tb00210.x.

Liu, C., and E.A. Barnes, 2015: Extreme moisture transport into the Arctic linked to Rossby wave breaking. *Journal of Geophysical Research: Atmospheres*, **120**, 3774–3788. doi: 10.1002/2014JD022796.

Liu, J., J. Curry, and H. Wang, 2012: Impact of declining Arctic sea ice on winter snowfall. *Proceedings of the National Academy of Sciences*, **109**, 4074–4079. doi: 10.1073/pnas.1114910109.

Liu, Q., 1994: On the definition and persistence of blocking. *Tellus*, **46**, 286–290. doi: 10.1034/j.1600-0870.1994.t01-2-00004.x.

Luo, B., D. Luo, L. Wu, L. Zhong, and I. Simmonds, 2017: Atmospheric circulation patterns which promote winter Arctic sea ice decline. *Environmental Research Letters*, **12**, 054017. doi: 10.1088/1748-9326/aa69d0.

Luo, D., X. Chen, A. Dai, and I. Simmonds, 2018: Changes in atmospheric blocking circulations linked with winter Arctic warming: A new perspective. *Journal of Climate*, **31**, 7661–7678. doi: 10.1175/JCLI-D-18-0040.1.

Luo, D., Y. Xiao, Y. Yao, A. Dai, I. Simmonds, and C.L. Franzke, 2016a: Impact of Ural blocking on winter warm Arctic–cold Eurasian anomalies. Part I: Blocking-induced amplification. *Journal of Climate*, **29**, 3925–3947. doi: 10.1175/JCLI-D-15-0611.1.

Luo, D., Y. Xiao, Y. Diao, A. Dai, C.L. Franzke, and I. Simmonds, 2016b: Impact of Ural blocking on winter warm Arctic–cold Eurasian anomalies. Part II: The link to the North Atlantic Oscillation. *Journal of Climate*, **29**, 3949–3971. doi: 10.1175/JCLI-D-15-0612.1.

Lupo, A.R., A.D. Jensen, I.I. Mokhov, A.V. Timazhev, T. Eichler, and B. Efe, 2019: Changes in global blocking character in recent decades. *Atmosphere*, **10**, 92. doi: 10.3390/atmos10020092.

Lupo, A.R., and P.J. Smith, 1995: Climatological features of blocking anticyclones in the Northern Hemisphere. *Tellus*, **47**, 439–456. doi: 10.1034/j.1600-0870.1995.t01-3-00004.x.

Masato, G., B.J. Hoskins, and T.J. Woollings, 2012: Wave-breaking characteristics of midlatitude blocking. *Quarterly Journal of the Royal Meteorological Society*, **138**, 1285–1296. doi: 10.1002/qj.990.

Masato, G., B.J. Hoskins, and T.J. Woollings, 2013: Winter and summer Northern Hemisphere blocking in CMIP5 models. *Journal of Climate*, **26**, 7044–7059. doi: 10.1175/JCLI-D-12-00466.1.

Matsumura, S., K. Yamazaki, K., and T. Tokioka, 2010: Summertime land-atmosphere interactions in response to anomalous springtime snow cover in northern Eurasia. *Journal of Geophysical Research: Atmospheres*. **115**, D20107. doi: 10.1029/2009JD012342.

Mattingly, K.S., T.L. Mote, and X. Fettweis, 2018: Atmospheric river impacts on Greenland Ice Sheet surface mass balance. *Journal of Geophysical Research*, *Atmospheres*, **123**, 8538–8560. doi: 10.1029/2009JD012342.

McLeod, J.T. and T. Mote, 2015: Assessing the role of precursor cyclones on the formation of extreme Greenland blocking episodes and their impact on summer melting across the Greenland ice sheet. *Journal of Geophysical Research*, **120**, 12357–12377. doi: 10.1002/2015JD023945.

McLeod, J.T., and T.L. Mote, 2016: Linking interannual variability in extreme Greenland blocking episodes to the recent increase in summer melting across the Greenland ice sheet. *International Journal of Climatology*, **36**, 1484–1499. doi: 10.1002/joc.4440.

Mokhov, I.I., A.V. Timazhev, and A.R. Lupo, 2014: Changes in atmospheric blocking characteristics within Euro-Atlantic region and Northern Hemisphere as a whole in the 21st Century from model simulations using RCP anthropogenic scenarios. *Global and Planetary Change*, **122**, 265–270. doi: 10.1016/j.gloplacha.2014.09.004.

National Snow and Ice Data Center, 2012: Positive and Negative Phases of AO. Accessed 1 October 2018, https://nsidc.org/cryosphere/icelights/2012/02/arctic-oscillation-winter-storms-and-sea-ice.

Ogi, M., Y. Tachibana, and K. Yamazaki, 2003: Impact of the wintertime North Atlantic Oscillation (NAO) on the summertime atmospheric circulation. *Geophysical Research Letters*, **30**, 88–96. doi: 10.1029/2003GL017280.

O'Reilly, C.H., S. Minobe, and A. Kuwano-Yoshida, 2016: The influence of the Gulf stream on wintertime European blocking. *Climate Dynamics*, **47**, 1545–1567. doi: 10.1007/s00382-015-2919-0.

Overland, J.E., J. Francis, E. Hanna, and M. Wang, 2012: The recent shift in early summer arctic atmospheric circulation. *Geophysical Research Letters*, **3**, 19804. doi: 10.1029/2012GL053268.

Pelly, J.L., and B.J. Hoskins, 2003: A new perspective on blocking. *Journal of the Atmospheric Sciences*, **60**, 743–755. doi: 10.1175/1520-0469(2003)060<0743:ANPOB>2.0.CO;2.

Peters, D., and D.W. Waugh, 1996: Influence of barotropic shear on the poleward advection of upper-tropospheric air. *Journal of the Atmospheric Sciences*, **53**, 3013–3031. doi: 10.1175/1520-0469(1996)053<3013:IOBSOT>2.0.CO;2.

Pfahl, S., C. Schwierz, M. Croci-Maspoli, C. Grams, and H. Wernli, 2015: Importance of latent heat release in ascending air streams for atmospheric blocking. *Nature Geoscience*, **8**, 610–614. doi: 10.1038/ngeo2487.

Pithan, F., T.G. Shepherd, G. Zappa, and I. Sandu, 2016: Missing orographic drag leads to climate model biases in jet streams, blocking and storm tracks. *Geophysical Research Letters*, **43**, 7231–7240. doi: 10.1002/2016GL069551.

Rajewicz, J., and S.J. Marshall, 2014: Variability and trends in anticyclonic circulation over the Greenland ice sheet, 1948–2013. *Geophysical Research Letters*, **41**, 2842–2850. doi: 10.1002/2014GL059255.

Renwick, J.A., and J.M. Wallace, 1996: Relationships between North Pacific wintertime blocking, El Niño, and the PNA pattern. *Monthly Weather Review*, **124**, 2071–2076. doi: 10.1175/1520-0493(1996)124<2071:RBNPWB>2.0.CO;2.

Rex, D.F., 1950: Blocking action in the middle troposphere and its effect upon regional climate: I. An aerological study of blocking action. *Tellus*, **2**, 196–211. doi: 10.1111/j.2153-3490.1950.tb00331.x.

Rimbu, N., and G. Lohmann, 2011: Winter and summer blocking variability in the North Atlantic region–evidence from long-term observational and proxy data from southwestern Greenland. *Climate of the Past*, **7**, 543–555. doi: 10.5194/cp-7-543-2011.

Scaife, A.A., D. Copsey, C. Gordon, C. Harris, T. Hinton, S. Keeley, A. O'Neil, M. Roberts, and K. Williams, 2011: Improved Atlantic winter blocking in a climate model. *Geophysical Research Letters*, **38**, L23703. doi: 10.1029/2011GL049573.

Scherrer, S.C., M. Croci-Maspoli, C. Schwierz, and C. Appenzeller, 2006: Two-dimensional indices of atmospheric blocking and their statistical relationship with winter climate patterns in the Euro-Atlantic region. *International Journal of Climatology*, **26**, 233–249. doi: 10.1002/joc.1250.

Schwierz, C., M. Croci-Maspoli, and H.C. Davies, 2004: Perspicacious indicators of atmospheric blocking. *Geophysical Research Letters*, **31**, L06125. doi:10.1029/2003GL019341.

Shabbar, A., J. Huang, and K. Higuchi, 2001: The relationship between the wintertime North Atlantic Oscillation and blocking episodes in the North Atlantic. *International Journal of Climatology*, **21**, 355–369. doi: 10.1002/joc.612.

Shukla, J., and K.C. Mo, 1983: Seasonal and geographical variation of blocking. *Monthly Weather Review*, **111**, 388–402. doi: 10.1175/1520-0493(1983)111<0388:SAGVOB>2.0CO;2.

Sillmann, J., and M. Croci-Maspoli, 2009: Present and future atmospheric blocking and its impact on European mean and extreme climate. *Geophysical Research Letters*, **36**, L10702. doi:10.1029/2009GL038259.

Sillmann, J., M. Croci-Maspoli, M. Kallache, and R.W. Katz, 2011: Extreme cold winter temperatures in Europe under the influence of North Atlantic atmospheric blocking. *Journal of Climate*, **24**, 5899–5913. doi: 10.1175/2011JCLI4075.1.

Sousa, P.M., R.M. Trigo, D. Barriopedro, P.M. Soares, A.M. Ramos, and M.L. Liberato, 2017: Responses of European precipitation distributions and regimes to different blocking locations. *Climate Dynamics*, **48**, 1141–1160. doi: 10.1007/s00382-016-3132-5.

Sumner, E.J., 1954: A study of blocking in the Atlantic-European of the northern hemisphere. *Quarterly Journal of the Royal Meteorological Society*, **80**, 402–416. doi: 10.1002/qj.49708034510.

Tang, Q., X. Zhang, X. Yang, and J.A. Francis, 2013: Cold winter extremes in northern continents linked to Arctic sea ice loss. *Environmental Research Letters*, **8**, 14–36. doi: 10.1088/1748-9326/8/1/014036.

Thompson, D.W., and J.M. Wallace, 1998: The Arctic Oscillation signature in the wintertime geopotential height and temperature fields. *Geophysical Research Letters*, **25**, 1297–1300. doi: 10.1029/98GL00950.

Thorncroft, C.D., B.J. Hoskins, and M.E. McIntyre, 1993: Two paradigms of baroclinic wave life cycle behaviour. *Quarterly Journal of the Royal Meteorological Society*, **119**, 17–55. doi: 10.1002/qj.711950903.

Tibaldi, S., F. d'Andrea, E. Tosi, and E. Roeckner, 1997: Climatology of Northern Hemisphere blocking in the ECHAM model. *Climate Dynamics*, **13**, 649–666. doi: 10.1007/s003820050188.

Tibaldi, S., and F. Molteni, 1990: On the operational predictability of blocking. *Tellus A: Dynamic Meteorology and Oceanography*, **42**, 343–365. doi: 10.1034/j.1600-0870.1990.t01-2-00003.x.

Treidl, R.A., E.C. Birch, and P. Sajecki, 1981: Blocking action in the Northern Hemisphere: A climatological study. *Atmosphere–Ocean*, **19**, 1–23. doi: 10.1080/07055900.1981.9649096.

Trigo, R.M., I.F. Trigo, C.C. DaCamara, and T.J. Osborn, 2004: Climate impact of the European winter blocking episodes from the NCEP/NCAR Reanalysis. *Climate Dynamics*, **23**, 17–28. doi: 10.1007/s00382-004-0410-4.

Türkeş, M., T. Koç, and F. Sariş, 2009: Spatiotemporal variability of precipitation total series over Turkey. *International Journal of Climatology: A Journal of the Royal Meteorological Society*, **29**, 1056–1074. doi: 10.1002/joc.1768.

Tyrlis, E., and B.J. Hoskins, 2008: Aspects of a Northern Hemisphere atmospheric blocking climatology. *Journal of the Atmospheric Sciences*, **65**, 1638–1652.

U.K. Met Office, 2018: Positive and Negative Phases of NAO. Accessed 1 October 2018, https://www.metoffice.gov.uk/learning/atmosphere/north-atlantic-oscillation.

Välisuo, I., T. Vihma, R. Pirazzini, and M. Schäfer, 2018: Interannual variability of atmospheric conditions and surface melt in Greenland in 2000–2014. *Journal of Geophysical Research: Atmospheres*, **123**, 10443–10463. doi: 10.1029/2018JD028445.

van den Dool, H.M., S. Saha, and Å. Johansson, 2000: Empirical orthogonal teleconnections. *Journal of Climate*, **13**, 1421–1435. doi: 10.1175/1520-0442(2000)013<1421:EOT>2.0.CO;2.

Vitasse, Y., C. Signarbieux, and Y.H. Fu, 2018: Global warming leads to more uniform spring phenology across elevations. *Proceedings of the National Academy of Sciences*, **115**, 1004–1008. doi: 10.1073/pnas.1717342115.

Wiedenmann, J.M., A.R. Lupo, I.I. Mokhov, and E.A. Tikhonova, 2002: The climatology of blocking anticyclones for the Northern and Southern Hemispheres: Block intensity as a diagnostic. *Journal of Climate*, **15**, 3459–3473. doi: 10.1175/1520-0442(2002)015<3459:TCOBAF>2.0.CO;2.

Winkler, J.A., J.A. Andresen, G. Guentchev, E.A. Waller, and J.T. Brown, 2003: Using ANOVA to estimate the relative magnitude of uncertainty in a suite of climate change scenarios. *14th Symposium on Global Change and Climate Variations*, Long Beach, CA, American Meteorological Society, 2.7, https://ams.confex.com/ams/annual2003/techprogram/paper_55250.htm.

Woollings, T., D. Barriopedro, J. Methven, S.W. Son, O. Martius, B. Harvey, J. Sillmann, A.R. Lupo, and S. Seneviratne, 2018: Blocking and its response to climate change. *Current Climate Change Reports*, **4**, 287–300. doi: 10.1007/s40641-018-0108-z.

Woollings, T., A. Hannachi, B. Hoskins, and A. Turner, 2010: A regime view of the North Atlantic Oscillation and its response to anthropogenic forcing. *Journal of Climate,* **23**, 1291–1307. doi: 10.1175/2009JCLI3087.1.

Woollings, T., B. Hoskins, M. Blackburn, and P. Berrisford, 2008: A new Rossby wave-breaking interpretation of the North Atlantic Oscillation. *Journal of Atmospheric Science*, **65**, 609–626. doi: 10.1175/2007JAS2347.1.

Xiaoge, X., T. Zhou, and R. Yu, 2010: Increased Tibetan Plateau snow depth: An indicator of the connection between enhanced winter NAO and late-spring tropospheric cooling over East Asia. *Advances in Atmospheric Sciences*, **27**, 788–794. doi: 10.1007/s00376-009-9071-x.

Zhou S., A.J. Miller, J. Wang, and J.K. Angell, 2001: Trends of NAO and AO and their associations with stratospheric processes. *Geophysical Research Letters*, **28**, 4107–4110. doi: 10.1029/2001GL013660.